IN VITRO BONE TISSUE ENGINEERING ON PATTERNED BIODEGRADABLE POLYESTER BLENDS

A THESIS SUBMITTED TO
THE GRADUATE SCHOOL OF NATURAL AND APPLIED SCIENCES
OF
THE MIDDLE EAST TECHNICAL UNIVERSITY

BY

HALİME KENAR

IN PARTIAL FULFILLMENT OF THE REQUIREMENTS FOR THE DEGREE OF
MASTER OF SCIENCE
IN
THE DEPARTMENT OF BIOTECHNOLOGY

SEPTEMBER, 2003

ABSTRACT

IN VITRO BONE TISSUE ENGINEERING ON PATTERNED BIODEGRADABLE POLYESTER BLENDS

Kenar, Halime

M. Sc., Department of Biotechnology

Supervisor: Prof. Dr. Vasıf Hasırcı

Co-Supervisor: Prof. Dr. Mehmet Toner

September 2003, 130 pages

This study aimed at guiding osteoblast cells on biodegradable polymer carriers with well-defined surface microtopography and chemistry, and investigating the effect of cell alignment on osteoblast phenotype expression. A blend of two different polyesters, one being natural in origin (PHBV) and the other synthetic (P(L/DL)LA), was used to form a film with parallel macro- (250 μm wide) or microgrooves (27 μm wide) on its surface, by solvent casting on patterned templates. The micropatterned Si template was produced by photolithography, while the Teflon

macropatterned template was lathe cut. Fibrinogen (Fb) was adsorbed or immobilized via epichlorohydrin spacer/crosslinker on the film surfaces to enhance cell attachment by increasing the surface hydrophilicity and by providing RGD amino acid sequence for integrin binding. Surface hydrophilicity was assessed by water contact angle measurements. Adsorption of Fb caused an increase in hydrophilicity, while the opposite was achieved with its covalent immobilization. Fb was homogeneously immobilized throughout the whole micropatterned film surface with amount of 153.1 ± 42.4 g Fb/cm^2, determined with the Bradford assay, while it was adsorbed within the grooves of the micropattern. Surface characteristics of the films were studied with Scanning Electron (SEM) and Light microscopy.

Osteoblast cells derived from rat bone marrow were seeded on the polymeric films with different surface topography and chemistry and were grown for one and three weeks. Osteoblast proliferation on the films was determined with Cell Titer 96 ^{TM} Non-Radioactive Cell Proliferation (MTS) test. Alkaline Phosphatase (ALP) assay and tetracycline labelling of mineralized matrix were carried out to determine osteoblast phenotype expression on different surfaces. SEM and fluorescence microscopy were used to evaluate the cell alignment. Osteoblasts on the micropatterned films with adsorbed Fb aligned along the groove axis with a mean deviation angle of 13.1^o, while on the unpatterned films deviation from horizontal axis was 63.2^o and cells were randomly distributed. Cell alignment did not affect cell proliferation. However, the highest ALP specific activity and the most homogeneous mineral distribution were obtained on the Fb adsorbed micropatterned films.

Keywords: Bone tissue engineering, patterned surfaces, biodegradable, polymer films, osteoblast giudance, osteoblast phenotype expression

ÖZ

DESENLİ, BİYOBOZUNUR POLYESTER BLENDLER ÜZERİNDE İN VİTRO KEMİK DOKU MÜHENDİSLİĞİ

Kenar, Halime

Yüksek Lisans, Biyoteknoloji Bölümü

Tez Yöneticisi: Prof. Dr. Vasıf Hasırcı

Ortak Tez Yöneticisi: Prof. Dr. Mehmet Toner

Eylül 2003, 130 sayfa

Bu çalışmada, osteoblast hücrelerinin yüzey topografisi ve kimyası kontrol edilen biyobozunur polimer taşıyıcılar üzerinde yönlendirilmesi ve hücre yöneliminin osteoblast fenotip ifadesi üzerindeki etkisinin araştırılması amaçlanmıştır. Doğal ve yapay polyesterler olan PHBV ve P(L/DL)LA blendlerinden, topografik desene sahip şablonlar üzerinde çözücü uçurma yöntemiyle yüzeyinde makro- (250 μm genişlikte) veya mikrokanallara (27 μm genişlikte) sahip filmler oluşturulmuştur. Mikrodesenli Silisyum şablon fotolitografi yöntemi ile, makrodesenli Teflon şablon ise torna tezgahında üretilmiştir. Hücrelerin film

yüzeyine tutunma oranlarını arttırmak amacıyla, Fibrinojen (Fb) yüzeye ya adzorplanmayla ya da epiklorohidrinle kovalent bağlanarak tutuklanmıştır. Fibrinojenin yüzey hidrofilikliğini arttırarak veya hücre integrin reseptörlerine bağlanan RGD amino asit dizilimini sağlayarak bu amaca hizmet edeceği düşünülmüştür. Temas açısı su kullanılarak ölçülmüş, adzorplanmış Fb'nin yüzey hidrofilikliğini arttırdığı, fakat kovalent tutuklanmış Fb'nin hidrofilikliği azalttığı saptanmıştır. Bradford testi ile yüzeye 153.1 ± 42.4 g/cm^2 Fb tutuklandığı belirlenmiştir. Fb tüm desenli film yüzeyinde dengeli bir dağılımla tutuklanırken, adzorpsiyon durumunda bu dağılım sadece kanallara yoğunlaşmıştır. Oluşturulan filmlerin yüzey özellikleri Tarama Elektron (SEM) ve Işık mikroskopisiyle incelenmiştir.

Sıçan kemik iliğinden elde edilen osteoblast hücreleri, farklı yüzey topografisine ve kimyasına sahip olan polimerik filmler üzerinde bir ve üç hafta süre ile büyütülmüştür. Film yüzeyinde hücre çoğalması MTS testi ile belirlenmiştir. Farklı yüzeylerdeki osteoblastların fenotip ifadesi Alkalen Fosfataz (ALP) miktar tayini ve oluşan mineralizasyonun tetrasiklin ile işaretlenmesi yoluyla belirlenmiştir. Hücre yönelimi SEM ve Floresan mikroskopisi ile değerlendirilmiştir. Osteoblast hücrelerinin, üzerinde adzorplanmış Fb bulunduran filmler üzerinde yönlendiği ve 13.1 derecelik bir açıyla kanal ekseninden saptığı gözlenmiştir. Desensiz yüzeylerde ise yatay eksenle yapılan bu açı 63.2 derece olmuş ve hücreler çok farklı açılarla yüzeye yayılmışlardır. Hücre yöneliminin hücre çoğalmasına bir etkisinin olmadığı belirlenmiştir. Buna karşın, en yüksek ALP aktivitesi ve en homojen mineralizasyon oluşumu Fb adzorplanmış mikrodesenli filmler üzerinde saptanmıştır.

Anahtar Kelimeler: Kemik doku mühendisliği, desenli yüzeyler, biyobozunur, polimerik filmler, osteoblast yönlendirilmesi, osteoblast fenotip ifadesi

Dedicated to my family

ACKNOWLEDGEMENTS

I wish to express my most sincere gratitude to Prof. Dr. Vasıf HASIRCI and Asst. Prof. Dr. Gamze TORUN KÖSE for their invaluable advice, guidance and continuous encouragement and support throughout this study.

I would like to extend my deep appreciation to Prof. Dr. Atilla AYDINLI and Ömer SALİHOĞLU for providing the micropatterned template, the indispensible component of this study, and to Assoc. Prof. Dr. Nuhan PURALİ for his kind and valuable support in confocal microscopy studies and providing the fluorescent dyes.

I am grateful to Prof. Dr. Nesrin HASIRCI and Aysel KIZILTAY for contact angle measurements of the carriers, to Prof. Dr. Hikmet ALTUNAY for his help in morphological cell identification, and Prof. Dr. Feza KORKUSUZ and Dr. Nusret TAHERİ for providing the ALP kit used in this study.

I would like to thank Dr. Ayşen TEZCANER, Dr. Dilek KESKİN, Dr. Türker BARAN and Dr. Fatma KÖK for their valuable support in various parts of this study and their encouragement.

I am grateful to my lab partner Suzan BER for her friendship and support during the long hours we spent working hard together to achieve a common goal.

I wish to thank my brother Necmettin KENAR for his continuous encouragement and his technical support in drawing nice 3D objects.

I am very grateful much to all my other friends, Deniz YÜCEL, Sibel ÇINAR,

Süleyman COŞKUN, Şerife AYAZ, Şule ŞEHİRLİ, Hayriye ÖZÇELİK, Zeynep TOKÇAER, Dr. Reşat ÜNAL, Zagit GAYMALOV, Elif KARAGÖZ, Oya TAĞIT, Burcu KASAPOĞLU and to our technician Zeynel AKIN for their support in this study, and to Hakan ŞEN for his kind help in animal care during the experiments.

Finally, I would like to express my deepest gratitude to my parents, Nesibe KENAR and Ahmet KENAR, for their understanding, patience and continuous support and trust in me, without which it would not be possible to succeed.

TABLE OF CONTENTS

LIST OF TABLES

TABLES

LIST OF FIGURES

FIGURES

LIST OF ABBREVIATIONS

ALP:	Alkaline phosphatase
BCECF-AM:	2′,7′-bis-(2-carboxyethyl)-5-(6)-carboxyfluorescein, tetrakis-(acetoxymethyl)ester
BSA:	Bovine serum albumin
CBB:	Coomassie Brilliant Blue
DMEM:	Dulbecco's Modified Eagle Medium
ECM:	Extracellular matrix
EPI:	Epichlorohydrin
Fb:	Fibrinogen
Fb_a:	Adsorbed fibrinogen
Fb_i:	Covalently immobilized fibrinogen
FCS:	Fetal calf serum
HA:	Hydroxyapatite
IGF:	Insulin-like growth factor
Mac P:	Macropatterned film
Mac P Fb_a:	Macropatterned fibrinogen adsorbed film
MP:	Micropatterned film
MP Fb_a:	Micropatterned fibrinogen adsorbed film
MP Fb_i:	Micropatterned fibrinogen immobilized film
MSCs:	Mesenchymal stem cells

MTS:	3-(4,5-dimethylthiazol-2-yl)-5-(3-corboxymethoxyphenyl)-2-(4-sulfophenyl)-2H-tetrazolium, (Owen's reagent)
PBS:	Phosphate buffer saline
PDMS:	Poly(dimethylsiloxane)
PEG:	Polyethylene glycol
PGA:	Poly(glycolic acid)
PHA:	Poly(hydroxyalkanoate)
PHB:	Poly(hydroxybutyrate)
PHBV:	Poly(3-hydroxybutyrate-co-3-hydroxyvalerate)
PLA:	Poly(lactic acid)
P(L/DL)LA:	Poly(L-lactide-co-D,L-lactide)
PLGA:	Poly(lactic-co-glycolic acid)
PMS:	Phenazine methosulfate
RGD:	Arginine-Glycine-Aspartic acid
SAMs:	Self assembled monolayers
SEM:	Scanning electron microscope
TCP:	Tissue culture grade polystyrene
TGF-β:	Tranforming growth factor-beta
Trypsin-EDTA:	Trypsin-ethylenediamine tetraacetic acid
UNP:	Unpatterned film
UNP Fb_a:	Unpatterned fibrinogen adsorbed film

CHAPTER 1

INTRODUCTION

1.1. Tissue Engineering

Tissue engineering is an interdisciplinary field that aims at the development of biological substitutes, which can be used to replace, restore or improve complex human tissue function in case of tissue loss or organ failure (Langer and Vacanti, 1993). Principles of life sciences and engineering are applied to combine supportive carrier materials, which may contain bioactive molecules, and living components in appropriate configurations and environmental conditions. The general approach involves harvesting of a small tissue via biopsy, expansion of isolated cells *in vitro*, seeding the cells on exogeneous extracellular matrices, usually biodegradable polymers, and generation of a substantial amount of tissue that can be reimplanted into the patient (Fig. 1.1, Kim et al., 1998). By this way, the main limitations of conventional therapies, such as limited supply of donor tissues and limited function of synthetic prostheses or mechanical devices, can be eliminated. The matrix component of the engineered tissue serves as a three-dimensional template for the directed organization of cells, provides specific signals to guide the gene expression of the cells and regulate cellular function, and gives the necessary mechanical support to the construct until the cells lay down their own extracellular matrices.

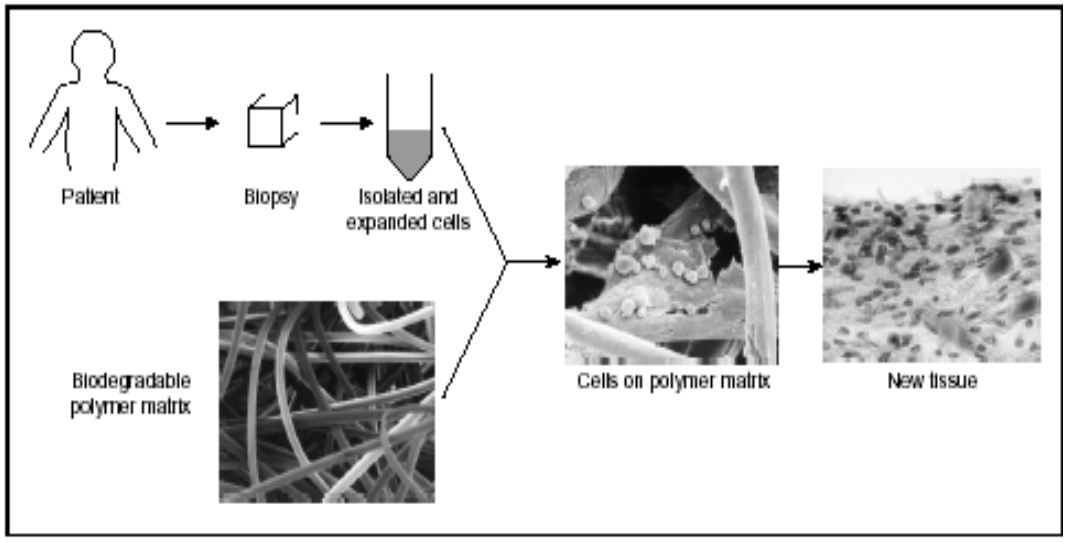

Figure 1.1. A scheme of tissue engineering approach to development of organ replacements using cultured autologous cells (Kim et al., 1998)

Tissue engineering involves the permanent implantation of the engineered construct into the body with no further surgical manipulation, and requires the reformation of natural extracellular matrix while the exogeneous matrix is either degraded or metabolized, by the living component of the construct, the cells, for complete tissue regeneration.

1.1.1. Components of the Tissue Engineered Construct

1.1.1.1.Carrier Material

Generally, three classes of biomaterials are used as a cell carrier material in tissue engineering: naturally derived materials, which include extracellular matrix (ECM) proteins (e.g., collagen and hyaluronate), decellularized biological matrices

produced via enzymatic or detergent treatment (Kim et al., 2000) (e.g., bladder submucosa and small-intestinal submucosa), and synthetic polymers (e.g., polyglycolic acid and polylactic acid). Since it is the ECM that promotes cell adhesion, affects cell migration, growth and differentiation, modulates the activities of cytokines and growth factors, and participates directly in activating intracellular signaling through cell-matrix interactions (Green, 1997), the design and selection of the biomaterial is very critical in the development of engineered tissues. The ideal biomaterial should be biodegradable and bioresorbable to permit the reconstruction of a normal tissue, and its degradation products should not provoke inflammation or toxicity (Kim et al., 2000). It should be able to regulate cell behavior, which includes cell adhesion, growth and differentiation, in order to promote development of a functional new tissue. In addition, the final configuration of the biomaterial should have a large surface area-to-volume ratio for better cell-polymer interactions, ECM regeneration, and for minimal nutrient and waste diffusion constraints. Finally it should be reproducibly processable with appropriate mechanical properties, and its degradation rate should be adjustable to match the rate of tissue regeneration by the cells.

1.1.1.1.1. Natural Biomaterials

Naturally derived macromolecules have potential advantages of biocompatibility, cell controlled degradability, and intrinsic cellular interaction (biological recognition). However, they may exhibit batch-to-batch variations and generally exhibit a narrow and limited range of mechanical properties (Lee and

Mooney, 2001). They can be obtained from various sources: ECM (collagen, hyaluronic acid) or plasma (fibrin) of mammalian tissues, crustaceans and seaweeds (chitin and alginate, respectively), microorganisms (polyhydroxyalkanoates).

1.1.1.1.1.1. Collagen

Collagen is the most widely used tissue-derived natural polymer, and it is a main component of mammalian tissues including skin, bone, cartilage, tendon and ligament (Lee and Mooney, 2001). Collagen has long been known to elicit minimal imflammatory and antigenic responses and has been approved by FDA for many types of medical applications, including wound dressings and artificial skin (Pachene, 1996). Collagen implants degrade through sequential attacks by lysosomal enzymes. The *in vivo* resorption rate can be regulated by control of the density of the implant and the extent of intermolecular crosslinking, which can be accomplished by various physical (e.g., dehydrothermal treatment) or chemical (e.g., glutaraldehyde and carbodiimide) techniques (Hendren, 1986). Collagen contains cell-adhesion domain sequences (e.g., RGD) that elicit specific cellular interactions, which may assist in retention of the phenotype and activity of many types of cells including fibroblasts (Silver et al., 1992) and chondrocytes (Sam et al., 1995). It can be processed into fibers, films and sponges and exhibits high tensile strength and flexibility that can be further enhanced by crosslinking. However the mechanical strength of collagen may not be suitable for use in hard tissue regenerations.

1.1.1.1.1.2. Fibrin

Fibrin plays an important role in natural wound healing and has been used as a sealant and an adhesive in surgery. Fibrin gels can be produced from the patient's own blood and can be used as an autologous scaffold for tissue engineering. No toxic degradation or inflammatory reactions are expected from this natural component of the body. Fibrin forms gels by the enzymatic polymerization of fibrinogen at room temperature in the presence of thrombin (Perka et al., 2000). Fibrin gels have been utilized to engineer tissues with skeletal muscle cells (Ye et al., 2000), smooth muscle cells (Ikary et al., 2000), and chondrocytes (Meinhart et al., 1999). However, fibrin gels are limited in mechanical strength.

1.1.1.1.1.3. Chitosan

Chitosan is a biosynthetic polysaccharide that is the deacetylated derivative of chitin. Chitin is a naturally occuring polysaccharide that can be extracted from crustacean exoskeletons or generated via fungal fermentation processes (Pachence and Kohn, 1997). It is hypothesized that the major path for chitin and chitosan breakdown *in vivo* is through lysozyme, which acts slowly to depolymerize the polysaccharide. The biodegradation rate of the polymer is determined by the amount of residual acetyl content, a parameter that can easily be varied. Chemical modification of chitosan produces materials with a variety of physical and mechanical properties. Like hyaluronic acid, chitosan is not antigenic and is a well tolerated implant material (Khor and Lim, 2003). Chitosan gels, powders, films and

fibers have been formed and tested for such applications as encapsulation (Gupta et al., 1993), adhesion reducing membrane barriers (Vlahos et al., 2001), cell culture (Zhang et al., 2003), and inhibitors of blood coagulations (Vongchan et al.,2002).

1.1.1.1.1.4. Polyhydroxyalkanoates

Polyhydroxyalkanoate (PHA) polyesters are degradable, biocompatible, thermoplastic materials made by many microorganisms as intracellular storage polymers whose function is to provide a reserve of carbon and energy (Pachence and Kohn, 1997). The most extensively studied PHA is the simplest: poly(3-hydroxybutyrate) (PHB). PHB homopolymer is highly crystalline, extremely brittle, and hydrophobic, and has an *in vivo* degradation time of 1-2 years. In contrast, the copolymers of PHB with 3-hydroxyvaleric acid (HV) are less crystalline, more flexible, and more readily processible. It was found previously that a copolymer of 3-HB and 3-HV, with a 3-HV content of about 11%, may have an optimum balance of strength and toughness for a wide range of possible applications (Holmes, 1985). Degradation of these natural polyesters is by hydrolysis. PHB has been found to have low toxicity, in part due to the fact that it degrades in vivo to D-3-hydroxybutyric acid, a normal constituent of human blood (Pachence and Kohn, 1997). Applications of these polymers include controlled drug release systems, sutures, and tissue engineering carriers (Sendil et al., 1999, Williams et al., 1999, Zinn et al., 2001). Poly(3HB-co-3HV) has been processed into vascular grafts and artificial heart valves (Williams et al., 1999). Surface of the PHAs can be modified to improve cellular attachment by introduction of new functional groups through the use of gas plasma

or by attaching bioactive molecules covalently or non-covalently. Blends of PHB and poly(hydroxybutyrate-co-hydroxyhexanoate) that had better flexibility and biocompatibility than PHB alone were used as scaffolds for chondrocyte cells by Zhao et al. (2003). PHB has been claimed to have piezo-electric properties similar to those of natural bone, giving it potential as biodegradable fixative plates that could actually stimulate bone formation and thus promote bone healing (van der Walle et al., 2001).

1.1.1.1.2. Synthetic Biomaterials

In contrast to natural macromolecules, synthetic polymers can be prepared to have more precisely controlled structures and properties (Lee and Mooney, 2001). They can be produced reproducibly on a large scale with relatively controlled strength, degradation rate and microstructure, like porosity, by either altering the ingredients employed or polymer-processing methods (Marler et al., 1998). Properties of synthetic polymers can be altered by varying functional groups (backbone or side chain), polymer architecture (linear, branched, comb or star) and polymer combinations (polymer blends, interpenetrating networks or chemically bonded copolymers) (Wong et al., 1997). Poly (α-hydroxy acids) such as poly lactic acid and its copolymers with glycolic acid are the most commonly used polymers in medicine (Goldstein et al. 2001, Yang et al. 2002, Patel et al. 1998, Chen et al. 2001) besides other synthetic polymers like poly(anhydrides) (Rosen et al. 1983, Domb et al. 1994) and poly(ortho-esters) (Heller et al. 1990, Peppas and Langer 1994).

1.1.1.1.2.1. Poly(α-hydroxy acids)

Polyesters of naturally occuring α-hydroxy acids, including poly(glycolic acid) (PGA), poly(lactic acid) (PLA), and poly(lactic-co-glycolic acid) (PLGA), are widely used as biomaterials and in tissue engineering. These polymers have gained FDA approval for human use for a variety of applications, including sutures. Because these polymers are thermoplastics, they can be easily formed into desired shapes by various techniques including molding, extrusion or by solvent casting. PGA, which has the simplest structure among linear aliphatic polyesters, is highly crystalline and thus has a high melting point and low solubility in organic solvents. PLA is more hydrophobic than PGA due to the presence of an extra methyl group in the structure of lactic acid and dissolves more readily in organic solvents (Pachence and Kohn, 1997).

The degradation rate of the copolymers can be tailored from several weeks to several years by alteration of their crystallinity, molecular weight, and the ratio of lactic to glycolic acid. However, it should be noted that there is no linear relationship between the ratio of glycolic acid to lactic acid and the physicochemical properties of their copolymers. Although PGA is crystalline, this feature is lost in PGA-PLA copolymers and degradation takes place more rapidly than either PGA or PLA. The ester bonds in these polymers are hydrolytically labile, and these polymers degrade by nonenzymatic hydrolysis. PGA hydrolyses in water to glycolic acid, which can be converted enzymatically to glycine to be used in protein synthesis or pyruvate that will enter the tricarboxylic acid cycle and eventully eliminated from the body in the form of carbon dioxide and water. PLA also undergoes hydrolytic deesterification

into lactic acid, which becomes icorporated into the tricarboxylic acid cycle to be converted to CO_2 and H_2O.

Lactic acid is a chiral molecule and exists in two stereoisomeric forms that give rise to four morphologically distinct polymers. D-PLA and L-PLA are the two stereoregular polymers, D,L-PLA is the racemic polymer consisting of a mixture of D- and L-lactic acid, and meso-PLA can be obtained from D,L-lactide. The polymers derived from the optically active D and L monomers are semicrystalline, while the optically inactive D,L-PLA is always amorphous. Generally, use of L-PLA is preferred to D-PLA, since the hydrolysis of L-PLA yields L(+)-lactic acid, which is the naturally occuring stereoisomer of lactic acid (Pachence and Kohn, 1997). Since D,L-PLA is an amorphous polymer, it is usually considered for applications such as drug delivery, where it is important to have a homogeneous dispersion of the active species within a monophasic matrix. On the other hand, the semicrystalline L-PLA is preferred in applications where high mechanical strength and toughness are required- (for example, sutures and orthopedic devices).

Although these polymers have been widely used in a variety of biomedical applications, their acidic degradation products, that cause delayed inflammatory reaction, and lack of functional groups available for covalent modification limit their usefulness. However, to overcome their lack of biological recognition, there are approaches towards incorporation of cell-recognition domains into these materials: synthesis of copolymers with amino acids (Barrera et al., 1995), coupling PLA with RGD peptides using poly (L-lysine) (Yang et al., 2001).

1.1.1.2. The Living Component : Cells

Whatever the intended mode of action of tissue engineered grafts, the function is provided by the cellular component. Therefore determining where these cells will come from plays a pivotal role (Young et al., 1997).

The source of the cells used in a tissue engineered construct will depend upon many factors including the functional requirement of the final product as well as technical feasibility and economic considerations. The ability to source, cultivate, and manipulate some cell types often limits what can be accomplished in tissue engineereing. Depending on their source, cells can be grouped as a) autologous, when the source is the patient himself, b) allogeneic, when they are obtained from another donor individual, or c) xenogeneic, when the source is another species.

The simplest source of cells is autologous tissue. Cells are harvested from a patient via biopsy, grown in culture to the desired number, and then reimplanted into the patient. There are no legal problems with their use and no risk of immune reaction or rejection, which is the major problem with other cell sources. For autologous cells to be useful, cultivation of the cell type must permit expansion of the population to a number sufficient to meet the functional need of the implant within a time frame that suits the needs of the patient. The time required to harvest tissue from the patient, expand the cells in culture, and construct the implant can be a critical limitation of autologous material. In addition, healthy tissue may be sparse or unavailable, and donor site morbidity is always a problem.

The use of allogeneic cells allows one to grow and preserve cells in sufficient quantity to have them readily available for immediate use. Allogeneic material

permits the development of a reproducible and cost-effective product of more consistent quality. However, there is a high possibility of immune rejection of these cells, unless immunosuppression is employed and there is the possibility of transmission of infectious diseases from the donor.

For some cell types, the tissue demand cannot be met through the use of autologous or allogeneic sources. This has led to strategies which employ xenogeneic tissues. Technologies employing cell encapsulation, immune protection, and genetic manipulation are being developed to enable the use of xenogeneic tissues and organs. The use of xenogeneic cells presents a special safety consideration, the possibility of introducing viruses which are not known or understood and might be pathogenic in humans. Therefore, animal tissues must also be thorougly screened and should come from tightly controlled, closed herds.

Destruction of implanted tissues by the patient's immune system is the greatest challenge when nonautologous cells are used. Strategies to avoid this destruction therefore become major design considerations.

Cells have different potencies, depending on the developmental stage they are in. During development, in the progress from zygote to adult, cells gradually lose their ability to differentiate into many types of cells and to proliferate while they become specialized in their ultimate function (Fig. 1.2.).

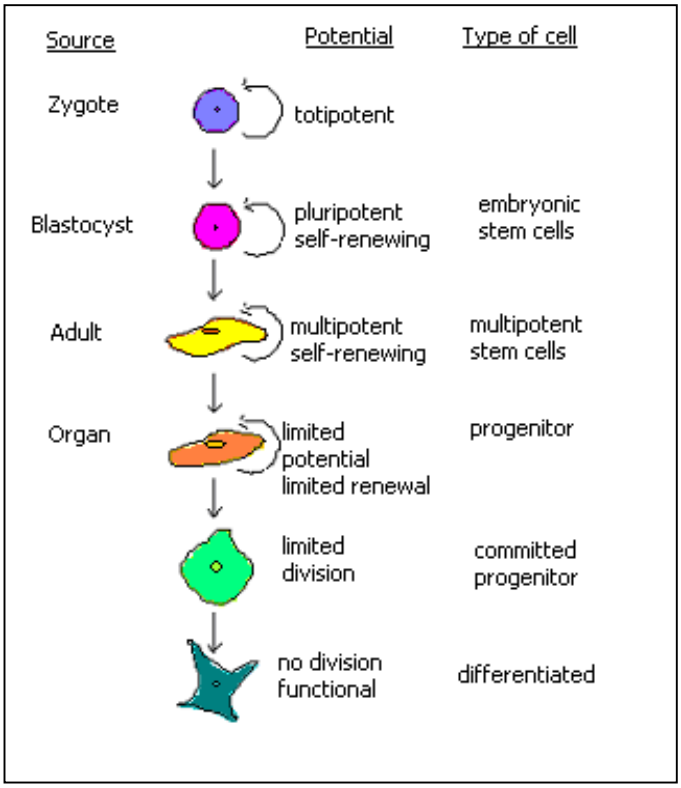

Figure 1.2. Potency of cells at different developmental stages
(Adapted from http://www.thebiotechclub.org/industry/emerging/stem_cells.php)

The zygote itself is totipotent, meaning that it can give rise to a whole organism. Embryonic stem cells, on the other hand, are pluripotent, that is they are undifferentiated cells taken from the inner cell mass of the blastocyst stage embryo that have the potential to become a wide variety of specialized cell types *in vitro* and to all cell lineages *in vivo*. In the adult there are still multipotent cells, adult stem cells. These are undifferentiated cells found in a differentiated tissue that can renew themselves and with certain limitations differentiate to yield all the specialized cell types of the tissue from which they originated. Adult stem cells self-renew *in vivo*. Their progeny includes both new stem cells and committed progenitors with a more

restricted differentiation potential. These progenitors, in turn, give rise to differentiated cell types.

In most cases, differentiated cells released from adult tissues exhibit a very limited proliferation capacity. This poses serious limitations to their expansion in culture and their use for in vitro reconstruction of engineered tissues to be transplanted in patients. In addition, the availability of autologous differentiated cells is restricted and their functional state does not favor regeneration. These cells may undergo dedifferentiation when cultured in vitro, due to lack of crucial influence of physiological cell-cell and cell-ECM interactions. Therefore, the use of undifferentiated (stem or progenitor) cells that have a higher proliferative and regenerative capacity is more promising. The use of embryonic stem cells poses potential immunologic and major ethical problems, while the use of adult stem cells is generally well accepted by the society. Recent evidence indicates that even differentiated tissues contain populations of undifferentiated multipotent cells that have the capacity to regenerate tissue after trauma, disease or aging (Bruder et al., 1998). Currently, wide attention has been focused on adult mesenchymal stem cells from the bone marrow, in which they reside as supportive cells for haematopoiesis and possibly as a reservoir and regeneration pool for various mesenchymal tissues. The mesenchymal stem cells are characterized by their ability to proliferate in culture and by their properties to differentiate into multiple mesenchymal lineages (e.g., bone, cartilage, muscle, marrow stroma, tendon and fat) under defined culture conditions (Fig. 1.3).

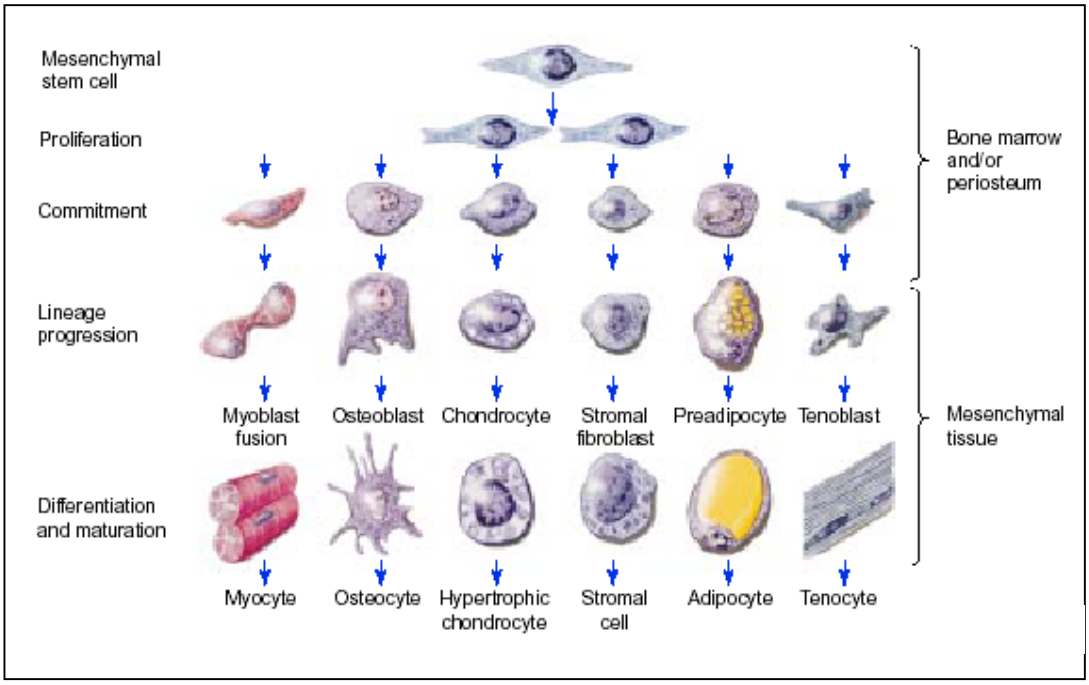

Figure 1.3. Scheme presenting differentiation of mesenchymal tissue cells from a common mesenchymal stem cell (Risbud et al., 2002)

Although it was previously thought that tissue-specific stem cells could only differentiate into cells of the tissue of origin, recent studies (Orlic et al. 2001, Lagasse et al. 2000, Sanchez-Ramos et al. 2000) suggested that they can differentiate into lineages other than the tissue of origin. After transplantation of bone marrow or enriched haematopoietic stem cells, skeletal myoblasts, cardiac myoblasts, endothelium, hepatic and biliary duct epithelium, lung, gut and skin epithelia, and neuroectodermal cells of donor origin have been detected. Jiang et al. (2002) identified a rare multipotent adult progenitor cell co-purifying with mesenchymal stem cells that differentiate *in vitro*, at the single cell level, not only into mesenchymal cells, but also into cells with visceral mesoderm, neuroectoderm and endoderm characteristics. They showed that cells capable of differentiating *in vitro* to cells of the three germ layers can be selected from rodent bone marrow.

An important issue for work with stem cells or progenitor cells is understanding how to induce and control permanent differentiation into the desired cell type. In fact, for any cell used in tissue engineering, it is critical to comprehend the mechanism of induction and control of differentiation and proliferation in order to obtain normal and functional cells.

1.2. Bone Tissue Engineering

Bone lesions or defects occur in a wide variety of clinical situations, and their reconstruction to provide mechanical and functional integrity is a necessary step in the patient's rehabilitation. Because of the potential of bone to spontaneously regenerate, most bone lesions, such as fractures, heal well with conventional conservative therapy or surgery. Nevertheless, a bone graft or a bone substitute is often required in orthopedic and maxillofacial surgery to assist healing of large traumatic or post surgical defects and of osseous congenital deformities. Prostheses lack mechanisms of biological repair and their use may cause long term problems like malignant tumor formation or graft calcification. Conventional approaches in bone repair have involved biological grafts such as autogenous bone, allogenic bone and xenografts, and also vascularized grafts of the fibula and iliac crest. Since bone grafts are avascular and dependent on diffusion, the size of the defect and the viability of the host bed can limit their application. In large defects, the grafts can be resorbed by the body before osteogenesis is complete. Currently, autograft is the preferred biological graft most often used in the clinical setting, having success rates as high as 80–90% and no risk of immune rejection or disease transfer. However, the

limited availability of autografts and risks of donor site morbidity associated with infection, pain, and hematoma have fueled great interest in the development of alternative approaches to bone repair. Allografting introduces the risk of disease and/or infection and immune rejection; it may cause a lessening or complete loss of the bone inductive factors. Vascularized grafts require a major microsurgical operative procedure with a sophisticated infrastructure. Tissue engineering has emerged as a possible alternative strategy to regenerate bone. One potentially successful repair solution seeks to mimic the success of autografts by removing cells from the patient by biopsy and growing sufficient quantities of mineralized tissue *in vitro* on implantable, three-dimensional (3D) carriers for use as a functionally equivalent autogenous bone tissue. In this way, an ideal bony repair environment is created by reproducing the intrinsic properties of autogenous bone material, which include the following: 1. a porous, 3D architecture allowing osteoblast, osteoprogenitor cell migration and graft revascularization, 2. the ability to be incorporated into the surrounding host bone and to continue the normal bone remodeling processes, and 3. the delivery of bone-forming cells and osteogenic growth factors to accelerate healing and differentiation of local osteoprogenitor cells. Thus, an appropriately designed cell carrier can mimic the structural environment necessary to promote bone regeneration and define the ultimate shape of the new bone via its architecture. Bone structure and bone repair and formation processes serve as models for design of functional engineered constructs.

1.2.1. Structure and Function of Bone

Bone is a complex, highly organized, constantly changing tissue. It gives the skeleton the necessary rigidity to function as attachment and lever for muscles and supports the body against gravity. The bones of the adult skeleton consist of cortical (compact) bone (80%) and cancellous (trabecular) bone (20%) (Buckwalter et al., 1995). The proportions of cortical and trabecular bone differ at various locations in the skeleton. Compact bone is almost solid (10% porosity), with spaces only for osteocytes, canaliculi and blood vessels. In contrast, cancellous bone is 50-90% porous, making its modulus of elasticity and ultimate compressive strength as much as 10 times less than that of cortical bone. Cancellous bone has a sponge-like morphology, with branching bars, plates and rods of various sizes called trabeculae. If a cancellous area is converted to cortical bone, the new bone is wrapped around the existing "struts" of the cancellous meshwork (Buckwalter et al., 1995).

On the basis of general shape, bones can be classified into three groups: short, flat, and long. Short bones measure approximately the same in all directions while flat and long bones have one dimension that is much shorter or longer than the other two. Long bones are divided into three physiologic sections. The epiphysis lies between the physis (growth plate) and the bone and is covered with cartilage. The metaphysis is the transition from the wide part of the bone to the tubular section, called the diaphysis. Cancellous bone is found mainly in the metaphysis, while cortical bone comprises the diaphysis. However, cortical bone often forms a layer over cancellous bone to improve mechanical properties. Matrix of both cortical and cancellous bone is deposited in form of lamellae, but lamellae in cancellous bone do not form Haversian systems.

An outer bone sheath, the periosteum, covers both cortical and cancellous bone. The periosteum is continuous except near joints and is composed of two layers. The outer layer is more fibrous and is used to connect bones at the joint. The inner layer is more vascularized and contains cells that are capable of becoming osteoblasts. As well as playing an important role in endochondral bone formation, the periosteum provides a large portion of the bone's blood supply. A thin layer of cell-rich connective tissue, the endosteum, lines the surface of the bone facing the marrow cavity. Both the periosteum and endosteum possess osteogenic potency. Following injury, cells in these layers may differentiate into osteoblasts (bone forming cells) which become involved in the repair of the damage.

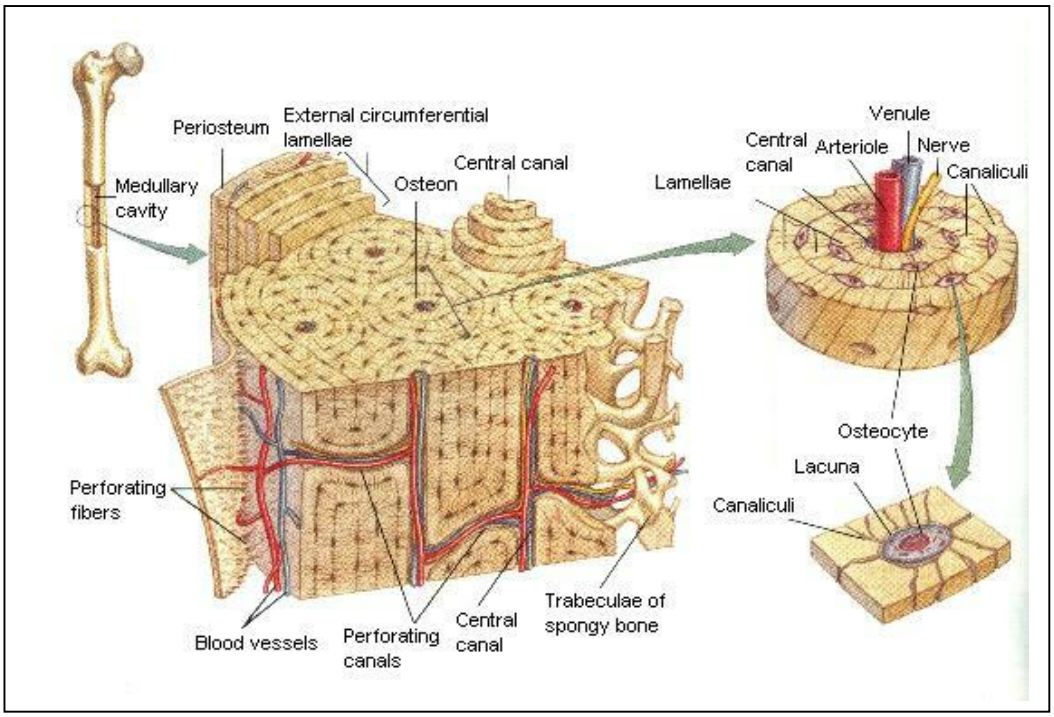

Figure 1.4. Bone structure and organization (Van de Graaff, 1998)

The matrix of the bone makes up 90% of the volume of the tissue, with the remainder being mostly cells, cell processes, and blood vessels. Bone matrix is a composite material consisting of an organic and an inorganic component. The organic component gives bone its form and contributes to its ability to resist tension, while the inorganic material primarily resists compression. Collagens, predominantly type I along with small amounts of types V and XII, make up approximately 90% of the organic matrix; the other 10% consists of non-collagenous proteins (osteocalcin, osteonectin, bone sialoprotein etc.) that may influence the organization of the matrix, bone mineralization, and behavior of bone cells, and bone-specific proteoglycans. Bone matrix also contains growth factors that can influence the function of bone cells including TGF-β, insulin-like growth factors, bone morphogenetic proteins, platelet-derived growth factors,interleukin-1 and –6, and colony-stimulating factors. The inorganic matrix, or mineral phase, of bone serves as an ion reservoir and gives bone most of its stiffness and strength. Approximately 99% of the body calcium, 85% of the phosphorus, and 40-60% of the total body sodium and magnesium are associated with the bone mineral crystals, the major source of these ions to and from the extracellular fluid. Bone mineral crystals are not pure hydroxyapatite ($Ca_{10}(PO_4)_6(OH)_2$). Instead, they contain both carbonate ions and acid phosphate groups. Unlike pure hydroxyapatite, bone crystals do not contain OH groups and therefore should be classified as apatite rather than hydroxyapatite.

To carry out diverse functions like bone formation, bone resorption, mineral homeostasis, and bone repair, bone cells assume specialized forms. They originate from two cell lines: mesenchymal stem-cell line and hematopoietic stem-cell line. The mesenchymal stem-cell line consists of undifferentiated cells of preosteoblasts,

osteoblasts, bone-lining cells, and osteocytes. The hematopoietic stem-cell line consists of circulating or marrow monocytes, preosteoclasts, and osteoclasts. Undifferentiated mesenchymal cells that have the potential to become osteoblasts reside in the bone canals, endosteum, periosteum, and marrow. They remain in their undifferentiated state until they are stimulated (after a fracture for example) to proliferate and differentiate into osteoblasts. The most apparent function of osteoblasts is the synthesis and secretion of the organic matrix of bone, but they may also have a role in controlling electrolyte fluxes between the extracellular fluid and osseous fluid and may influence the mineralization of bone matrix through the synthesis of organic matrix components and the production of matrix vesicles. Systemic hormones like parathyroid hormone and local cytokines may stimulate osteoblasts to release mediators that activate osteoclasts. Active osteoblasts may remain on the bone surface, decrease their synthetic activity and assume the flatter form of bone-lining cells; they may surround themselves with matrix and become osteocytes; or they may disappear from the site of bone formation, possibly due to apoptosis. Bone-lining cells may have a role in attracting osteoclasts to specific sites and stimulating them to resorb bone, when exposed to parathyroid hormone. Osteocytes send out long branches that connect them to other osteocytes through the canaliculi. The interconnections between osteocytes, osteoblasts, and bone-lining cells may allow this cell network to sense deformation of bone and streaming potentials occurring and to coordinate the formation and resorption of bone and the flow of mineral ions between the bone matrix and the extravascular fluid spaces of the bone.

The osteoclasts, unlike other bone cells, are derived from a precursor that can also form cells of the monocyte family. When stimulated, the mononuclear osteoclast precursors proliferate and then fuse to form multinucleated osteoclasts, which are rarely found in normal bone. These cells have large numbers of mitochondria, which supply the great amount of energy necessary to resorb bone, and lysosomes. On the face that is in contact with the bone, the cell membrane has characteristic folds known as a ruffled border.

Bone Formation

Bone formation (osteogenesis) begins during prenatal development and persists throughout adulthood. There are three ways in which osteogenesis occurs: endochondral, intramembranous and appositional ossification.

The process of endochondral bone formation, as occurs in embryogenesis, begins when mesenchymal stem cells (MSCs), progenitor cells that can differentiate into bone or cartilage-forming cells, start to differentiate into chondrocytes and secrete a cartilaginous matrix (Sikavitsas et al., 2001). During this time, the cells continue to divide. As they pass through various lineage states, they secrete different molecules and eventually lose the capability to proliferate. Also at this time, a periosteal layer appears around the middle of the long bone (the periosteum is comprised of MSCs that are enticed to form bone rather than cartilage). Shortly after the appearance of the first bone, the chondrocytes surrounded by the periosteum enter the final stage of development and become hypertrophic chondrocytes, which produce proteins that are important in calcification of the matrix. At this time,

phagocytic cells degrade some of the bony periosteum and resorb some of the interior matrix. Until this point, the tissue is completely avascular, but followingmatrix resorption, the first capillaries begin to appear. Both vascularization and phagocyte migration is mediated by chemical signals from within the hypertrophic cartilage matrix. The cells that migrate into the hypertrophic cartilage work to create a highly vascularized marrow cavity. At this point, a new set of MSCs begin to differentiate into osteoblasts (bone-forming cells) that proliferate and form a bone matrix on the calcified cartilage, eventually even remodeling the periosteal layer. It has been shown that there are two major regulation points for osteoblast development (Caplan et al., 1994). Near the end of osteoblast proliferation, there is an increase in gene transcription for proteins associated with the bone matrix. Calcification of the new matrix signals a movement through the second restriction point, which produces proteins seen in mature bone, such as osteocalcin. The bone produced by this process is immature woven bone. This type of bone is rich in osteocytes (mature bone cells) and has small collagen fibrils, which are oriented randomly. The spaces around blood vessels in woven bone are extensive. This bone will be remodeled to form lamellar bone, which is more organized and has superior mechanical properties.

Endochondral bone formation produces both long and short bones in the body. Flat bones usually develop via intramembranous ossification, which differs from the previous process in that no cartilaginous model is formed. Instead, MSCs aggregate into layers and then begin to produce a matrix that includes blood vessels and more MSCs. These MSCs differentiate into osteoblasts and begin to secrete organic bone matrix, the osteoid. The collagen fibres of osteoid form a woven bone, which

calcifies to form primitive trabecular bone. Diaphysis increases in width throughout postnatal growth by intramembraneous ossification.

A third type of bone development, called appositional formation, occurs during enlargement of bones and during remodeling. In this case, osteoblasts attach to existing bone and secrete matrix, often in layers. All three types of formation occur constantly and a particular bone can be formed through any combination of these developmental schemes (Buckwalter et al., 1995).

Calcification

As bone formation occurs, the predominant collagen matrix secreted by the osteoblasts undergoes calcification. Mineralization of woven bone occurs 24-74 h after creation of the matrix. There are two steps to matrix mineralization: nucleation of calcium phosphate crystals, and crystal growth (Robey, 1989).

Nucleation can occur either heterogeneously or homogeneously. Homogeneous nucleation is the formation of crystals due to supersaturation of the local environment with the appropriate ions. It is thought that this could occur in the lumen of matrix vesicles. These are small, membrane-bound vessels of cellular origin. Crystals are found first on the inner face of the membrane, which may be because, phosphatidylserine (PS), a phospholipid, is a major component of the vesicle membrane, and is known to have a high affnity for calcium (Robey, 1989).

After nucleation, amorphous calcium phosphate may be the first precipitate, which is then converted to octacalcium phosphate and finally to hydroxyapatite. The crystals in the matrix vesicles disrupt the membrane; the newly released crystals fuse

and collagen-mediated precipitation predominates from this point on. After the first small crystals form, they quickly grow from the whole regions in the collagen molecules to the overlap regions, where they are aligned along the fiber axis.

As woven bone is formed and calcified, it is remodeled to form mature lamellar bone. On a larger scale, both woven and lamellar bone can be found in either trabecular or cortical bone. Lamellar bone is generated more slowly than woven bone and is less mineralized. Collagen fibers are thicker and have a preferential orientation, which alternates between layers or lamellae. These lamellae can be stacked if deposited on a flat surface or concentric if laid centered around a blood vessel. Collagen fibrils extend between lamellae, thus increasing the bone's strength. In a system with concentric lamellae, the blood vessel is contained in a central canal, called the Haversian canal. Canaliculi extend outward from the central canal so that the canal can nourish the osteocytes, residing in lacunae. A central canal and its associated osteocytes are termed an osteon. The central canals branch and eventually join the Volkmann canals which run perpendicular to the central canals, and connect them to the periosteal surface (Buckwalter et al., 1995).

Remodeling

Lamellar bone is formed via the process of remodeling, a tightly regulated combination of bone formation and resorption. Bone remodeling continues throughout life to mend damage to bone and counteract the wearing of bone. The primary cells involved are the osteoblasts that form bone, and the osteoclasts that digest bone.

Bone remodeling has five distinct phases (Parfitt, 1984):

1. *Resting state*: The surface of the bone is lined with inactive cells. Former osteoblasts are trapped as osteocytes within the mineralized matrix.

2. *Activation*: Hormonal or physical stimuli signal mononuclear monocytes and macrophages to migrate to the remodeling site and differentiate into osteoclasts. Sites with microfractures or microdamage may exhibit a certain tendency for remodeling.

3. *Resorption*: Osteoclasts begin to remove the organic and mineral components of bone and form a cavity of characteristic shape and dimensions called a Howship's lacuna in trabecular bone and a cutting cone in cortical bone.

4. *Reversal*: Osteoclasts disappear and mononuclear macrophage-like cells smooth the resorbed surface by depositing a cement-like substance that will bind new bone to old. Pre-osteoblasts begin to appear. This phase is characterized by factors that stimulate osteoblast precursors to proliferate, including IGF-2 and TGF-β.

5. *Formation*: Differentiated osteoblasts fill in the resorption cavity and begin forming new osteon in a two stage process. First, they deposit osteoid (mostly collagen type I). With the onset of mineral apposition, the rate of mineralization exceeds the rate of matrix apposition and continues, with a substantially lower rate, even after the termination of matrix synthesis, until the bone surface returns to its original resting state.

Fracture healing

Bone fracture repair is similar in many ways to embryonic bone formation and involves three stages: inflammation, repair and remodeling. Fractures usually first result in blood clot formation. The fibrin clot releases chemoattractants for phagocytic cells that remove cellular debris from the wound site. This is the inflammatory phase, and it is the shortest of the three. The repair process begins when proliferating osteoblasts from the periosteum around the fracture begin to cover the blood clot. MSCs migrate to the fracture area and, if the fracture is mechanically stable, differentiate into osteoblasts to aid in regeneration of the tissue. If the fracture is unstable, the MSCs differentiate into chondrocytes that secrete collagen to act as a temporary bridge (Sikavitsas et al., 2001). This cartilaginous tissue is called the fracture callus. The cartilage is then replaced by woven bone via endochondral bone formation. In the remodeling phase, the woven bone is gradually resorbed and replaced with lamellar bone (Yaszemski et al., 1996).

1.2.2. Approaches to Engineering the Bone

The key to successful repair/regeneration of bone is to provide the repair site with sufficient osteogenic progenitor cells in a suitable vehicle to ensure osteoblastic differentiation and optimal secretory activities. The materials commonly used in bone tissue engineering include ceramics, polymers and composites. Among the critical aspects to consider during the design of the 3D scaffolds are average pore size (200-400 μm optimum for osteoblast growth), and porosity, increase of which

usually decreases mechanical strength. Other considerations common with all materials used to correct physical and mechanical properties are maximal bone growth promotion through osteoinduction and/or osteoconduction, adaptability of shape to wound site, and absorption in predictable manner in concert with bone growth (Burg et al., 2000). There has been a persistent orthopedic interest in demineralized bone matrix, obtained by decalcifying the bone matrix via acid extraction, because of its therapeutic potential in the treatment of bone defects and nonunions due to its inherent osteoinductive and osteoconductive properties, and its application in joint fusion procedures. Another natural polymer, collagen, has been applied as a cellular scaffold system, although it does not possess suitable mechanical properties. Engineering modifications are necessary to provide a stiffer structure. Yaylaoglu et al. (1999) demonstrated that porous collagen foams could be treated with calcium and phosphate solutions to allow the deposition of calcium phosphate and improvement of mechanical integrity, with great potential for bone applications. Poly(3HB-co-3HV), a natural microbial polyester, was used by Köse (2002) to form 3D porous matrices for bone tissue engineering. These PHBV matrices were found to be very suitable for osteoblast growth leading to mineral formation, especially when treated with O_2 rf-plasma for surface chemistry and hydrophilicity modification. In addition, PHBV served as a better support matrix for osteoblasts when compared to the calcium-phosphate loaded collagen sponges. Synthetic matrices have also been assessed as cellular and acellular bone tissue-engineering materials. In one of their study with PLLA, Meinig et al. (1997) used the Yucatan pig model to create a critical defect, 25% of the length of the radius. The defects were covered with a PLLA or a poly(L-co-D,L-lactide) (P(L/DL)LA)

membrane or with PLLA or P(L/DL)LA membrane that had been manufactured with calcium carbonate in order to decrease the relative polymer content of the membrane. They demonstrated that the membrane facilitated the rapid formation of new bone growth without adverse reactions; addition of calcium carbonate up to 50% did not change the dynamics of the membranes. PLGA sponges or combinations of PGA and PLA in 3D structures are also employed as cellular carriers. A specific bone application has been accomplished by coating a PGA-based tube with PLA (Puelacher et al., 1996). They applied PGA mesh seeded with osteoprogenitor cells to the hollow portion of the PGA tubes stabilized with PLA, and these constructs showed promise as long bone defect replacements in a rat femoral defect model.

Polymer composites with ceramic fillers have also been investigated. Peter et al. (2000) demonstrated that the osteoconductivity of poly(propylene fumarate)/β-tricalcium phosphate composites, with mechanical properties similar to trabecular bone, was similar to or better than that of control tissue culture polystyrene *in vitro*. Injectable polymers reinforced with hydroxyapatite or tricalcium phosphate can be used to fill irregular osseous defects (Bennett et al. 1996, Peter et al. 1999).

The most widely studied calcium phosphate ceramics include tricalcium phosphate and hydroxyapatite (HA). The appeal of the calcium phosphates rests largely in their biocompatibility. Since they are protein free, minimal immunological reactions, foreign body reactions, or systemic toxicity have been reported with their use (Hammerle et al., 1997). Although the inorganic ceramics have not shown osteoinductive ability, they certainly possess osteoconductivity along with a remarkable ability to bind directly to bone. HA-based constructs with different porosity and pore size are available commercially, such as Hyaff 11 constructs with

100-400 μm pore size and porosity of 80%, and ACP constructs with 10-300 μm pore size and porosity of 85% (both of Fidia Advanced Biopolymers; Abano Terme, Italy) are examples of these. Difficulties with malleability can be encountered with high porosity ceramics, while a good cell distribution is an advantage. Correct pore size selection with appropriate degradation properties is again critical.

1.3. Guidance in Tissue Engineering

The microenvironment of an engineered tissue must be properly regulated during the process of tissue development to induce the appropriate pattern of gene expression in cells forming the new tissue. The expression of genes by cells in engineered tissues may be regulated by multiple interactions with the microenvironment, including interactions with the adhesion surface, with other cells and with soluble growth factors, and mechanical stimuli imposed on the cells (Kim et al., 1998). Synthetic ECM should provide the appropriate combination of these signals.

The ECM to which cells adhere can regulate the cell phenotype. Cell adhesion to ECM is mediated by cell-surface receptors. The integrin transmembrane receptors found on the cell surface bind to relatively short amino acid sequences, Arg-Gly-Asp (RGD), of extracellular matrix (ECM) molecules. The cytoplasmic domain of integrins interacts with the cytoskeleton suggesting that ECM signaling through integrins is transduced via the cytoskeletal elements and can induce cell shape changes, which in turn may lead to growth and/or differentiation through influence of gene expression. For many years, ECM was thought to serve only as a structural

support for tissues. Bissel and his colleagues (1982) proposed the model of "dynamic reciprocity" between the ECM on one hand and the cytoskeleton and nuclear matrix on the other. In this model, ECM interacts with the receptors on the cell surface, which transmit signals across the cell membrane to molecules in the cytoplasm. These signals initiate a cascade of events through the cytoskeleton into the nucleus, resulting in the expression of specific genes, whose products in turn affect the ECM in various ways.

It is the continuous interaction between the cells and surrounding matrix environment that leads to formation of patterns, the development of form and acquisition and maintenance of differentiated phenotype during embryogenesis. Similarly, during wound healing these interactions contribute to the process of clot formation, inflammation, granulation, tissue development and remodeling. ECM molecules interact with their receptors and transmit signals directly or indirectly to second messengers that in turn unravel a cascade of events leading to the coordinated expression of a variety of genes involved in cell adhesion, migration, proliferation, differentiation and death (Fig. 1.5). Three potential categories of cell-ECM interactions can lead to these cellular events (Green, 1997):

Type I) These interactions involve primarily integrins and proteoglycan receptors and they are involved in cell adhesion or desorption processes during migration.

Type II) These cell-ECM interactions involve processes affecting proliferation, differentiation and/or maintenance of the differentiated phenotype. In this case, the ECM interacts with its receptors and cooperates with growth factors or cytokine receptors. Anchorage of cells is required to enter DNA synthesis (S) phase. Even in the presence of growth factors, cells will not enter the S phase without being

anchored to a substrate. Type III) These cell-ECM interactions involve mostly processes leading to cell death and epithelial-mesenchymal transitions. Enzymatic degradation of the ECM contribute to release of soluble factors and fragments of ECM that contain specific sequences that affect cell behavior.

The challenge of tissue engineering for the future is to develop tissue substitutes that restore the normal physiological functions of living tissues, in addition to structural features. It has become clear that both chemical and mechanical determinants play important roles in tissue formation in which biochemical signals mediate the process and mechanical forces play a regulatory role. In other words, chemical regulators mediate tissue morphogenesis while the signals that are actually responsible for dictating tissue pattern are often mechanical in nature. For production of functional structural tissues (e.g., bone), the correct mechanical stimuli may be provided by an appropriate synthetic ECM during the process of tissue engineering.

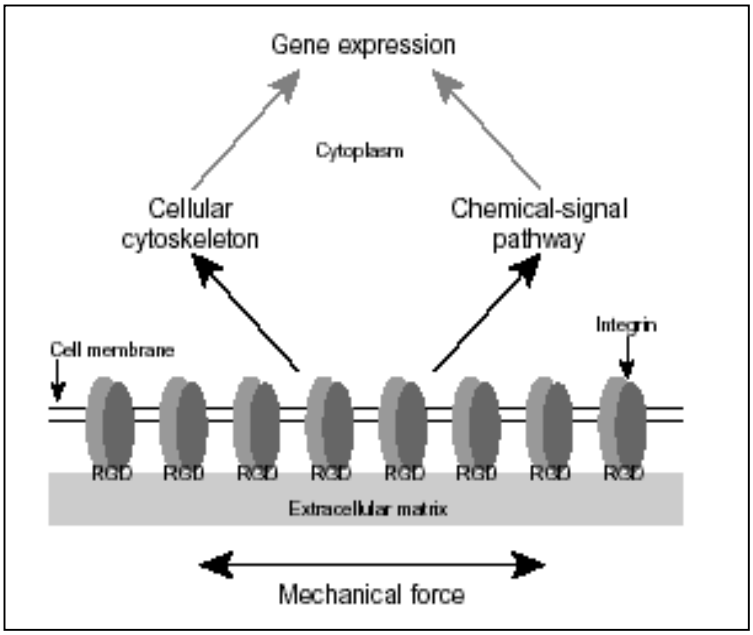

Figure 1.5. Scheme of cell adhesion on ECM containing RGD groups via integrin receptors and subsequent activation of gene expression (Kim et al., 1998)

Biological cells in a tissue are arranged in distinct patterns; the orientation and alignment of the cells depending on the purpose of the tissue (Curtis et al., 2001). If the tissue is to be repaired, the new cells must be aligned and positioned correctly. The reconstruction of organs is even more demanding; here cells of different types have to be aligned correctly with respect to each other, and the whole complex of tissue cells, blood vessel cells and nerve cells has to work correctly together. During development, cues are provided to the proliferating cells to dictate their final position and orientation. These cues can be chemical in nature as in presence of adhesion promoting proteins or purely physical, as the response of cells to the topography of their surroundings. An understanding and use of cues that influence cell positioning and alignment is crucial in tissue engineering. Cellular and subcellular function can be significantly improved through the incorporation of micro and nanoscale features. A tissue engineered construct that has a well-controlled microstructure is expected to better maintain cell morphology, differentiation and functionality over long periods of time (Desai, 2000). General approach to organizing cells on exogeneous matrix is to use physical (topographical), chemical or biological cues.

1.3.1. Methods for Preparation of Patterned Carriers

Microfabrication techniques enable the researcher to design, with micrometer-level control, the chemical composition and topology of the substrate and the type of cells in the vicinity of each cell (Folch and Toner, 2000). Microfabrication technology offers the potential to control cell-surface and cell-cell interactions on a micrometer scale. Desired substrate microtopography can be produced by electron

beam etching, laser lithography, photolithography or 3D printing, while bioactive molecules and/or cells can be patterned directly on the substrate surface via soft lithography.

1.3.1.1. Photolithography

Modern microfabrication technology is based on photolithography, the patterning of a layer of photosensitive polymer (photoresist) by means of light (Folch and Toner, 2000). Ultraviolet (UV) light is shone through a "mask" containing the desired pattern in the form of opaque features (made of chrome) on a transparent background (glass or plastic). The photoresist is spun on a flat surface (usually silicon wafer) from solution to a thin film and dried before exposure through the mask. The exposure chemically alters the photoresist by modifying its solubility in a certain "developer" solution. Depending on the nature of the photoresist (positive or negative), the UV exposed parts of the photoresist are either rendered insoluble in the developer (negative photoresist) or are readily dissolved away (positive photoresist) (Fig. 1.6). Development and rinse of the photoresist creates the desired pattern on the substrate. This pattern or geometry can be made deeper by subsequent dry or wet etching into the underlying substrate (Desai, 2000). If wet chemical etching in hydrofluoric acid is used, the action of the etch is isotropic and sloping walls result (Curtis and Wilkinson, 1997). Etching with the assitance of reactive ions directed by an electric field vertically onto a horizontal substratum gives, under the correct conditions, vertical sided structures. Photolithography must be carried out in clean-room facilities, which are costly to build and maintain.

Patterned surfaces obtained by photolithography can be used as templates to generate patterned polymer surfaces by solvent casting or embossing methods. To cast a replica, a solution of desired polymer is allowed to dry on top of the template and then the polymeric film is peeled off and used. In embossing, the template is pressed into the heated polymer in a press (Wilkinson et al., 2002).

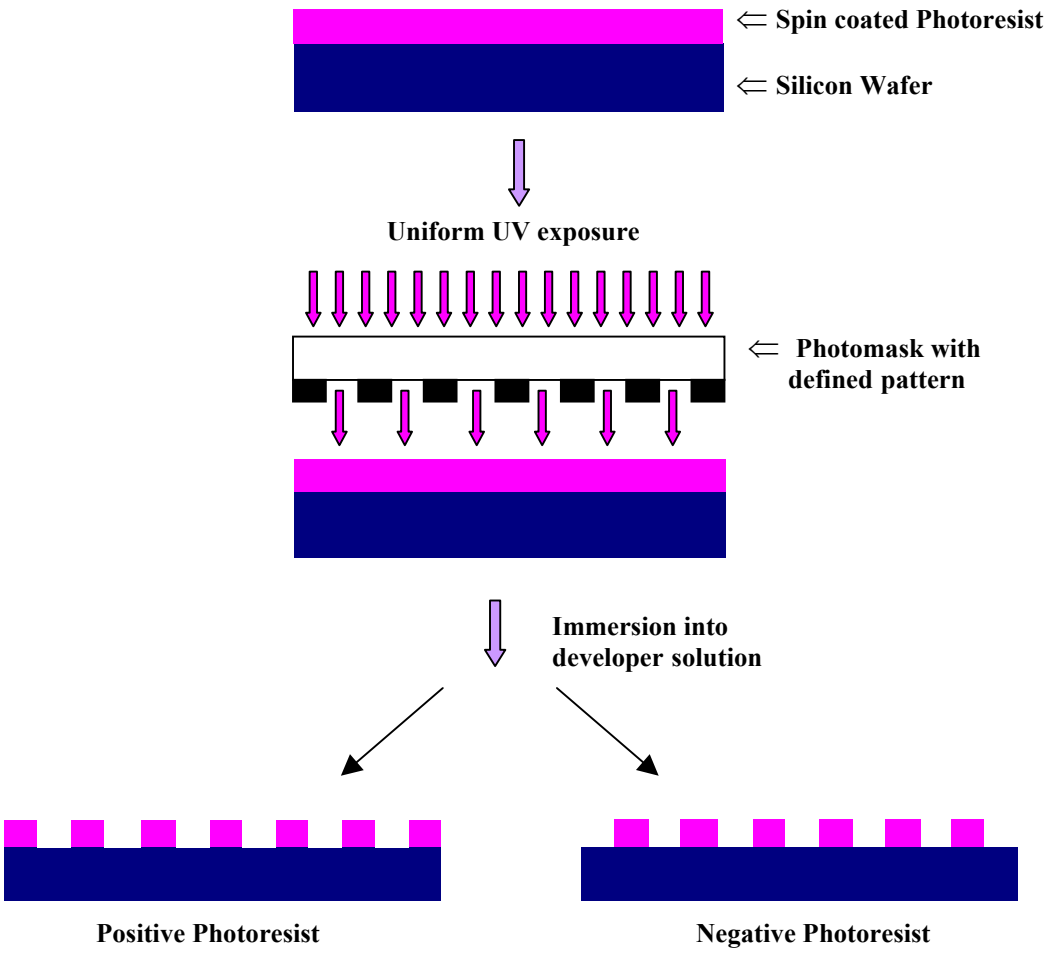

Figure 1.6. A representative scheme of photolithography process.

1.3.1.2. Soft Lithography

Soft lithography includes several techniques which have in common the utilization of a microstructured surface made of poly(dimethylsiloxane) (PDMS, a transparent, elastomeric rubber) as a stamp or channel to transfer microscale patterns of chemicals, biomolecules or cells onto a substrate. The microstructured PDMS surface is prepared by casting its liquid prepolymer against a master template taht has a patterned structure (Kane et al., 1999). Photolithography is used only for the fabrication of the master templates. This method is inexpensive because the PDMS surface can be replicated nondestructively from a microfabricated master wafer, thus reducing clean-room processing expenses, and biopatterning does not damage the PDMS surface. The PDMS surface can be reused many times, and can be applied even on non-planar surfaces. Microcontact printing, microfluidic patterning and stencil patterning are the major soft lithography techniques (Folch and Toner, 2000).

1.3.1.2.1. Microcontact Printing

Microcontact printing is based on the contact-transfer of the material of interest from a PDMS stamp onto a surface only on the areas contacted by the stamp. Because of its additive nature, microcontact printing can be applied to nonpolar surfaces. Multiprotein patterns can be generated with this method. Self assembled monolayers (SAMs) of alkanethiol, later to be used for protein adsorption, or proteins can be patterned on a surface (Kane et al., 1999). The PDMS stamp is inked by immersion in solution of protein, peptide or alkanethiol and on pressing the stamp onto a

substarte the protein, peptide or alkanethiol is transferred onto the substrate with the pattern of the stamp. The ability to pattern SAMs with different terminal groups by microcontact printing, and the resulting control over the adsorption of adhesive proteins, enables the patterning of cells on substrates (Lopez et al., 1993). Alkanethiol molecules form upon solvent evaporation a nonvolatile, oily thin film on the stamp, with a high molecular mobility, which ensures efficient transfer (Folch and Toner, 2000). Proteins, however, tend to form crystalline aggregates when dried. Still efficient transfer of proteins to the surface is possible, because the surfaces in air are covered by molecularly thin aqueous layer and water can act as the intermediary solvent.

1.3.1.2.2. Microfluidic patterning

Patterning can also be carried out by restricting fluid flow to desired regions of a substrate. The microstructured PDMS surface forms a network of microchannels on the areas where it does not contact the surface. The microchannels can be used to deliver fluids to selected areas of the substrate. In microfluidic patterning, as opposed to microcontact printing, the material is added at sites where the PDMS does not come into contact with the surface. The fluids are blocked from wetting the substrate in the areas where the PDMS stamp contacts the surface, due to the reversible self-seal of the stamp against the other smooth, dry surface (Folch and Toner, 2000). Hydrophobicity of the PDMS surface impedes wetting of liquids at the substrate-PDMS interface. With this method, proteins can be chemically immobilized or adsorbed only on the areas exposed to the protein solution, and cells can be selectively delivered to desired areas of a substrate.

1.3.1.2.3. Stencil patterning

Micropatterning by means of a thin piece of material containing holes (a stencil) constitutes a straightforward strategy: The substrate is physically prevented from coming into contact with the material to be patterned. Stencils made of thin metal foil have been used for patterning cell suspensions. PDMS has been micromolded into a self-sealing stencil that can be applied to a substrate to protect the areas that are contacted by PDMS and leave the substrate exposed through the holes for adding or removing inorganic material or living cells (Folch and Toner, 2000). The stencil can be peeled off after cell attachment without harming the cells, and reused after a simple ethanol wash.

1.3.2. Guidance Studies in Literature

There have been many studies showing topographical and chemical control of cells and tissues and the techniques of microfabrication have been extended to create more complex controlled biomaterial surfaces. The arrangement of cells in controlled two- and three-dimensional patterned surfaces have been shown to have beneficial effects on cell differentiation, maintenance, and functional longevity. One of the first studies using microfabricated substrates to study cellular behavior was performed by Brunette et al. (1983). This group demonstrated the use of a silicon mask etching technique to prepare grooved surfaces to control the direction of outgrowth of human gingival explants. They found better osteointegration and induction of mineralized tissue using surface microtexture. In their studies, titanium coated epoxy replicas of different micromachined grooved or pitted (30-120 μm deep) surfaces, as well as

smooth control surfaces were implanted percutaneously and fixed to the parietal bone of rats (Chehroudi et al., 1997). Mineralization was found to be more frequent with increase in depth of pit and decrease in depth of grooves, while was rare on smooth surfaces, indicating the importance of surface topography. Many researchers have shown that surface topography can influence cell migration and orientation. Eisenbarth et al. (2002) demonstrated that osteoblasts and fibroblast-like cells in contact with ground cp-titanium aligned and spread in the direction of the surface structure and had higher density of focal contacts, better cytoskeleton organization and stronger actin filaments that resist detaching forces more effectively. It has been demonstrated by Deutsch et al. (2000) that 3D surface topography of membranes significantly affects in vitro cardiac myocyte orientation and attachment. By creating culture surfaces with topographic features corresponding to cellular dimensions (10-50 μm), cells seem to exhibit a more *in vivo*-like cellular morphology (Desai et al., 2000). The microtopography provides directional growth for cells and thus, can recreate tissue architecture at the cellular and subcellular level in a reproducible manner, facilitating the culture and maintenance of differentiated state. Petersen et al. (2002) cultured chondrocytes on polysaccharide (agarose) gel with microstructures on its surface (15-65 μm wide; 40 μm deep), and this method proved to be effective in maintaining key aspects of the chondrogenic phenotype: rounded cell morphology and significant production of type II collagen. Differentiation in chondrocytes is maintained through restriction of cell spreading. Invaginations found in the native basal lamina of the skin were mimicked by micropatterning collagen and gelatin membranes, which influenced the differentiation of keratinocytes seeded on them through enhanced stratification (Pins et al., 2000).

Microtechnology also enable us to apply defined chemistries, found in the extracellular environment, to the microenvironment of the cells. Chemical patterning of adhesive and nonadhesive regions onto a substrate in order to control special organization of cells on 2D constructs is possible by this way. Adhesion and orientation of the bovine aortic endothelial cells and PC12 nerve cells to the 70 and 50 μm wide lines of anchored RGD and IKVAV peptides, respectively, on the PLA-PEG surfaces was achieved with the use of microfluidic patterning to generate the adhesive strips on nonadhesive PLA-PEG surfaces (Patel et al., 1998). Directionally controlled neurite outgrowth was stimulated by the IKVAV micropattern, with neurites extending between groups of cells often hundreds of microns apart. Another group investigated the effect of initial attachment and spreading of bone derived cells on the rate of matrix mineralization (Healy et al., 1996). Cell adhesive *N*-(2-aminoethyl)-3-aminopropyl-trimethoxysilane (EDS) strips (50 μm) were generated in alteration with nonadhesive dimethyldichlorosilane (DMS) strips (100 μm). Cells were organized on the EDS regions within 30 min., but after 15 days in culture, cells had grown over both EDS and DMS regions, while mineralization occurred only on the EDS strips, emphasizing the role of initial shape in determining differentiated function. Spatial control of cell-cell interactions in co-cultures is also posible with 2D micropatterning. When hepatocytes were co-cultured with fibroblasts by Bhatia et al. (1999), an increase in hepatocyte/fibroblast interaction was achieved through micropatterning, and improvement of cell function over randomly oriented cell cultures was found. Variation of initial heterotypic cell-cell interactions was found to modulate long-term bulk tissue function.

Combinations of 2D and 3D micropatterning, that is both chemical and physical cues, are used for more effective guidance of cellular organization. Miller et al. (2001) investigated the effect of substrate-mediated chemical and physical guidance on the growth and alignment of Schwann cells in vitro. Laminin was selectively adsorbed onto the grooves of micropatterned biodegradable films (PLA), and was found to improve adhesion of the cells on the substrates. Microgrooves were found to cause alignment of Schwann cells along their direction, where groove width was the effective parameter. Groove widths closer to the cellular dimensions were found to be optimal for alignment of the Schwann cells. In another study, rat osteoblasts were cultured on hydroxyapatite or titanium coated smooth and micromachined grooved substrates (Perizzolo et al., 2001). Osteoblasts aligned on both micropatterned substrates and produced significantly more bone-like nodules than on smooth surfaces. There was a statistically significant interaction, that is synergism, between topography and chemistry in the formation of mineralized nodules. The results of this study indicated that surface topography and chemistry can interact and affect osteogenesis.

The studies related with 3D and 2D bone cell micropatterning are summarized in Tables 1.1. and 1.2., respectively.

Table 1.1. Osteoblast cell culture studies on three dimensional, micropatterned surfaces

Cell Type	Material	Method	Groove width (μm)	Groove depth (μm)	Results	Reference
MC3T3-E1 osteoblast	Microgrooved deformable silicone dishes	Molding silicone against microgrooved wafer (produced by photolithography and reactive ion etching)	1-6	1.6	With or without 4% stretching in direction of microgrooves, cells aligned in microgrooves of all sizes, evidenced by alignment of actin cytoskeleton and nuclei. After 4% cyclic stretching for 3,4 and 7 days, cell numbers in the microgrooves were not significantly different from those on the smooth surface.	Wang et al., 2000
Rat osteoblast	Hydroxyapatite or titanium coated smooth and microgrooved substrates	Anisotropic etching	42	3, 10 and 30	Osteoblasts elongated, aligned, and moved in the direction of the grooves on both Ti and HA grooved surfaces. HA surfaces produced significantly more bonelike nodules than Ti surfaces. There was a significant interaction between topography and chemistry in the formation of mineralized nodules. The increase in the number of nodules brought about by HA was largest on the 30 μm-deep grooved surface. A strong correlation between ALP at 2 weeks and nodule counts at 6 weeks was observed.	Perizzolo et al., 2001

Table 1.1. Osteoblast cell culture studies on three dimensional, micropatterned surfaces (Cont'd)

Cell Type	Material	Method	Groove width (μm)	Groove depth (μm)	Results	Reference
MC3T3-E1 osteoblast	Titanium	Grinding with SiC papers of different grain sizes		Surface roughness (peak-to-valey height): 1.4, 1.0, 0.35, 0.12, and 0.08	Osteoblasts in contact with ground titanium surface spread in the direction of the surface structures, while those on polished surface showed less organized actin skeleton. The osteoblasts produced more actin stress fibers on ground discs than on those untextured and polished. With the stronger actin cytoskeleton in cells adhering to ground surfaces, the cells were stiffer and resisted detaching shear forces acting on them more efficiently.	Eisenbarth et al., 2002
Rat bone marrow derived bone cells	Poly(L-lactic acid) and polystyrene	Solvent casting on microgrooved wafer	1,2,5 or 10	0.5, 1.0 or 1.5	Alignment of the cells and matrix to the surface grooves was observed. More mineralized ECM was formed on the PLA than on the PS. PLA surfaces with a groove depth of 1 μm and groove width of 1 and 2 μm induced most mineralized ECM. ALP activity was higher on most microgrooved PLA surfaces, compared to other surfaces.	Matsuzaka et al., 1999

Table 1.2. Osteoblast cell culture studies on two dimensional, micropatterned surfaces

Cell Type	Material	Method	Pattern dimensions	Results	Reference
Osteoblast and fibroblasts	Borosilicate glass	Microcontact printing to pattern circles of DETA surrounded by OTS borders on borosilicate glass. Immobilization of either the cell-adhesive peptides RGDS and KRSR, or the non-adhesive peptides RDGS and KSSR on DETA circles	Circular domains 10, 50,100 and 200 μm in diameter	In the absence of serum, adhesion of either osteoblast or fibroblasts on surfaces patterned with the non-adhesive peptides RDGS and KSSR was random and low. Both cell types adhered and formed clusters onto circles modified with RGDS, whereas only osteoblast adhered and formed clusters onto the circles modified with KRSR, a peptide that selectively promotes adhesion of osteoblast.	Hasenbein et al., 2002
Primary human osteoblast	Chemically patterned, metal oxide based surfaces (combin's of titanium, aluminium, vanadium, and niobium)	Surface pattern (circles or parallel strips) produced by photolithographic techniques.	Array of dots or stripes of 50, 100, and 150 μm width/ diameter. Topographical step of 20 nm between foreground and background	No effect of 20 nm step on cell orientation. Regarding the cell number and activity there was no significant difference between any of the single metal surfaces. However, the morphology of cells on vanadium became spindle-like. Cells exhibited a pronounced reaction on bimetallic surfaces that contained Al. They tended to stay away from Al, the least favored metal in all two-metal combinations. Cell alignment relative to the pattern geometry was detected. The organization of f-actin and microtubules were more pronounced on non-Al regions. It was hypothesized that the differences in cell response could be associated with differences in the adsorption of serum proteins onto the various metal oxides	Scotchford et al., 2003

1.4. Scope of This Study

In this study it was intended to guide the organization of osteoblasts derived from rat bone marrow on biodegradable polymeric films with defined surface microtopography and chemistry and to assess the effect of cell alignment on osteoblast phenotype expression.

Poly(3-hydroxybutyrate-co-3-hydroxyvalerate) (PHBV), a polymer of natural origin, and poly(L-co- D,L-lactic acic) (P(L/DL)LA), a synthetic polymer, were blended to form the carrier for osteoblasts. A marked difference between these polymers is their degradation rate and pattern: PHBV matrices lose mass very slowly when compared to the bulk degradation of P(L/DL)LA. Thus a scaffold formed from the blend of these polymers is expected to degrade more uniformly while maintaining its integrity for a longer time assisting the gradual bone regeneration. Photolithography was used to form a micropattern with alternating parallel grooves on a silicon template. Both PHBV and P(L/DL)LA have mechanical strengths suitable for bone tissue engineering and are capable of precisely replicating the sharp features of a micropatterned silicon template when solvent cast. Fibrinogen, which carries RGD amino acid sequences in its alpha chain, was adsorbed or immobilized on the micropatterned films to promote cell adhesion on hydrophobic carrier surface and/or serve as a chemical cue for cell guidance.

Cell guidance was evaluated with various microscopical techniques, and osteoblast proliferation and phenotype expression were studied with biochemical and microscopical methods.

CHAPTER 2

MATERIALS AND METHODS

2.1. MATERIALS

Poly(3-hydroxybutyrate-co-3-hydroxyvalerate) (PHBV8, with 8% molar hydroxyvalerate) was purchased from Aldrich Chem.Co. (Milwaukee, WI, USA). Poly(L-lactide-co-D,L-lactide) (P(L/DL)LA, 70:30) was obtained from Boehringer Ingelheim Pharma KG (Germany). Dichloromethane was of analytical grade and potassium dihydrogen phosphate was extra pure, both of which were purchased from E. Merck AG (Germany). Trizma® Base, Trypsin-EDTA (0.25%) , glutaraldehyde, cacodylic acid (sodium salt), L-ascorbic acid, β-glycerophosphate, dexamethasone, Coomassie Brillant Blue G, and BCECF-AM (2′,7′-bis-(2-carboxyethyl)-5-(6)-carboxyfluorescein, tetrakis-(acetoxymethyl)ester) were all purchased from Sigma Chemical Company (USA). Coomassie Brillant Blue R-250 and Acridine Orange were obtained from BDH Chemicals Ltd (England). Dulbecco's Modified Eagle Medium (DMEM, high glucose, 4.5 g/L, and low glucose, 1 g/L) and foetal calf serum were purchased from PAA Laboratories GmbH (Austria). Alkaline phosphatase kit (ALP 50) was purchased from ABX Diagnostics (France). MTS kit was obtained from Promega Corporation (USA). Tetracycline was a gift of

Dr. I. Yılmaz of FAKO İlac San. (İstanbul, Turkey). Alexa Fluor 546 Phalloidin and Sytox Orange were obtained from Molecular Probes Company, and Triton X-100 was purchased from Applichem.

2.2. METHODS

2.2.1. Production of Macro- and Micropatterned Templates

Macropatterned Teflon templates with a repeating, parallel groove-ridge pattern (ridge width: 250 μm, groove width: 100 μm and groove depth of 250 μm) were lathe cut.

Micropatterned Silicon templates in the dimensions of ridge width 27 μm, groove width 2 and 12 μm alternating and groove depth 20 μm were produced by photolithography. The original design was in the dimensions of 30 μm, 0 and 10 μm, and 20 μm, but experimentally could not be exactly matched. First, silicon nitride was deposited by plasma enhanced chemical vapor deposition on a clean silicon wafer, until a silicon nitride film with thickness of 200 nm was obtained. Then, a light sensitive (positive) photoresist was spun on the silicon nitride film and the composite was dried at 120 ^{o}C. The photoresist was exposed to UV light through a mask which carried the desired pattern and was placed tightly over it. After exposure, the photoresist film was chemically etched (developed) in a solution of developer and deionized water (1:4). Exposed areas of silicon nitride on the sample were then etched with a solution of HF in water (1:30). After that step, the remaining photoresist on the sample was removed with acetone. Then, KOH solution, which

can etch the exposed silicon but not the silicon nitride, was used to etch the desired pattern on the silicon wafer. A KOH solution containing KOH, water, and isopropanol in the volume ratio of 1:3:1 was used as the etchant. The sample was left in the KOH solution until the desired etch depth was reached, at a rate of 60 nm/min. Once the silicon etching was completed, the sample was rinsed in deionized water and the remaining silicon nitride film was removed with the same HF solution used before. Thus, after all these steps the pattern on the mask was transferred onto the silicon wafer with the desired etch properties (Fig. 2.1).

2.2.2. Preparation of PHBV- P(L/DL)LA Films

All PHBV-P(L/DL)LA films were prepared by a solvent casting method. A dichloromethane solution of 4% w/v PHBV-P(L/DL)LA (1:1 w/w) was used in film formation. Equal weights of PHBV and P(L/DL)LA were dissolved in dichloromethane separately, and then mixed to form a polymer blend.

In order to obtain the patterned films, PHBV-P(L/DL)LA solution was poured on the macropatterned (Teflon) and micropatterned (Si) templates, and air dried. Unpatterned films, on the other hand, were obtained by casting the same solution on a glass Petri plate surface. After solvent evaporation, the films were peeled off the templates and plate surface.

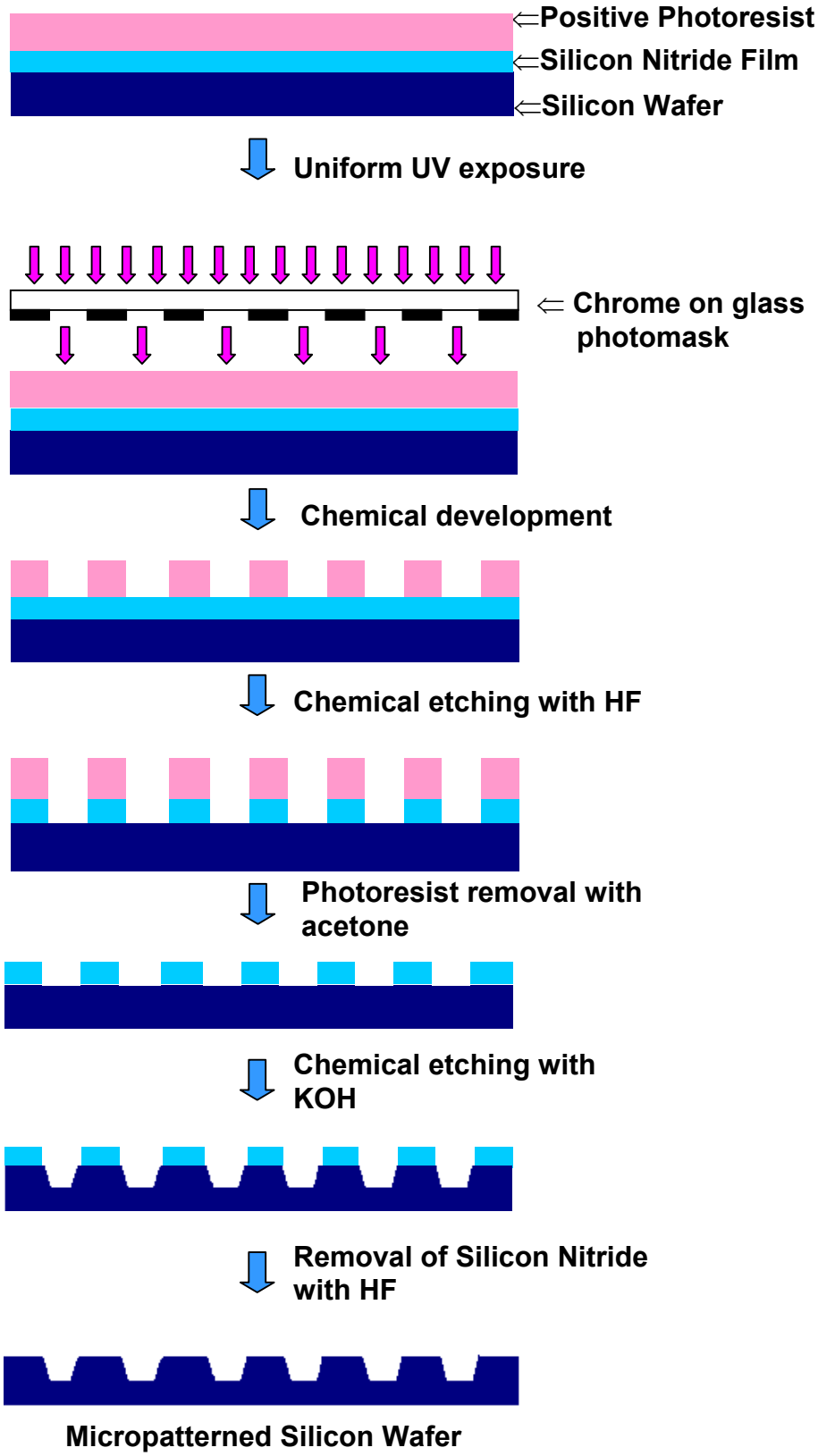

Figure 2.1. Representative scheme for production process of the micropatterned template

2.2.3. Chemical Modification of Films with Fibrinogen

2.2.3.1. Via Adsorption

Unpatterned, macro- and micropatterned films were sterilized in EtOH (70%) for 2 hours, then washed in PBS (pH 7.2, 10 mM), and air dried. Fibrinogen solution (1 mg/mL) was prepared by dissolving fibrinogen in PBS, and applied on the dry films. After 10 min, the excess fibrinogen solution was removed from the film surface, and the films were left to dry. All these steps were carried out under sterile conditions.

2.2.3.2. Via Covalent Bonding

Fibrinogen was immobilized covalently on the micropatterned films via epichlorohydrin spacer, following UV treatment of film surface (Fig. 2.2).

Micropatterned films were exposed to UV (λ= 313 nm, 75 watts) for 2 h. Following this step, surface was activated by incubating the films in epichlorohydrin solution (2%, 4.3 mL, 2 M NaOH : 1 mL dH_2O : 0.1 mL epichlorohydrin) for 15 minutes and subsequently washing in PBS (0.1 M, pH 7) for 1 h to remove the unbound epichlorohydrin, in a shaking water bath at 37^{o}C. The films were sterilized in 70% EtOH for 2 h, washed in 50% EtOH for 30 min, and left in 2 mg/mL fibrinogen solution (in borate buffer, 0.2 M, pH 9) overnight (17 h) for protein immobilization. Lastly, films were washed in PBS and left for drying in a class II laminar flow cabinet.

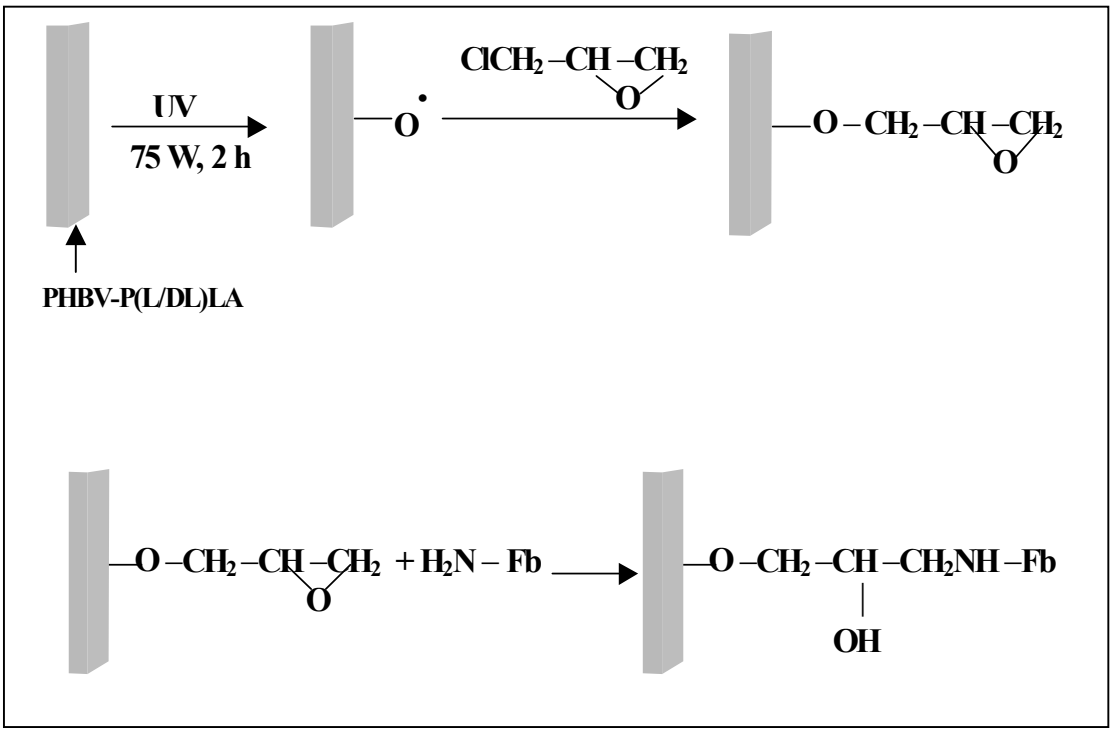

Figure 2.2. Activation of the PHBV-P(L/DL)LA film with UV and epichlorohydrin attachment, and coupling of the fibrinogen (Fb) with the activated surface.

* **O**$^{\bullet}$ represents all the possible reactive groups formed during UV irradiation

2.2.4. Surface Characterization of Templates and Films

2.2.4.1. Microscopic Examination

2.2.4.1.1. Light Microscopy

Micropatterned Si template was examined for surface pattern using a microcamera (Optic Ivymen System, model R-350-350X). Unpatterned, macropatterned and micropatterned film surfaces were examined via inverted phase contrast microscope (Olympus IX 70, Japan).

2.2.4.1.2. Scanning Electron Microscopy

The film samples were coated with gold and examined with scanning electron microscope (JEOL (Japan), Model JSM 6400).

2.2.4.2. Water Contact Angle Measurement

The hydrophilicity of the films was determined via water contact angle measurements. Distilled water (15 μL) was placed on the film surface at five different locations and the horizontal image of the droplet-surface contact site was obtained using a digital camera (Fuji-Fine Pix 6900 zoom camera) immediately after droplet-surface contact. Average contact angles were calculated from the images using a software.

2.2.4.3. Determination of Fibrinogen Content

2.2.4.3.a. In Solution

In order to quantitatively assess the amount of fibrinogen immobilized on the micropatterned films, Bradford assay (Bradford, 1976) was used. Fibrinogen amount was determined using the Fibrinogen standard curve plotted by determination of absorbance of fibrinogen solutions with different concentrations at 595 nm with the Bradford assay. The concentration difference between the fibrinogen solution prior to immobilization and the remaining fibrinogen solution after immobilization and the

wash solution was used as the amount of protein immobilized on the film surface. The results were expressed as μg protein immobilized / cm^2 of film surface .

The relation used in the calculations:

W_{Fb} per unit area (g/cm^2)=[$(W_{Fb})_{\text{before immob}}$–(($(W_{Fb})_{\text{after immob}}$+$(W_{Fb})_{\text{wash soln}}$)]/ A ($cm^2$)

where W_{Fb} is the amount of fibrinogen (g) and A is film surface area (cm^2).

2.2.4.3.b. On the Films

For qualitative assessment of fibrinogen immobilization, the micropatterned films were stained with Coomassie Brilliant Blue R-250. The fibrinogen immobilized films were rinsed with absolute methanol for 30 s and then stained with 0.1% Coomassie blue R-250 in 1% acetic acid/ 40% methanol for 5 min. After that, the films were washed with 50% methanol and observed under inverted phase contrast microscope. The same staining procedure was applied to epichlorohydrin attached films, which served as negative controls.

2.2.5. In Vitro Studies

2.2.5.1. Isolation of Mesenchymal Osteoprogenitor Cells

Mesenchymal osteoprogenitor cells were obtained from the bone marrow of young adult Sprague-Dawley rats. The rats were euthanized by diethyl ether inhalation and their femurs and tibia were excised and washed within Dulbecco's Modified Eagle Medium (DMEM) with 1000 units/mL penicillin and 1000 μg/mL

streptomycin under aseptic conditions. The bones were cleaned of the surrounding soft tissue, their metaphyseal ends were cut off and the marrow residing in the midshaft was flushed out with primary media (DMEM containing 20% fetal calf serum (FCS) and 100 units/mL penicillin and 100 μg/mL streptomycin) using a syringe and collected in a 15 mL sterile centrifuge tube. Then, the cells were centrifuged at 500 g for 5 min and the resulting cell pellets were resuspended in 12 mL of primary media and plated in T-75 flasks (cells from one femur per flask) (Köse, 2002). These primary cultures were incubated in a 5% CO_2 incubator (SANYO MCO-17 AIC, Sanyo Electric Co. Ltd., Japan) at 37 ^{o}C for 2 days.

2.2.5.2. Osteoblast Culture

After 2 days of incubation, hematopoietic and other unattached cells were removed from the flasks by repeated washes with PBS (10 mM, pH7.2) and the primary medium of the flasks was renewed every other day until reaching confluency. Then, following the first passage complete media consisting of DMEM supplemented with 20% FCS , 100 units/mL penicillin, 100 μg/mL streptomycin, 10 mM β-glycerophosphate, 50 μg/mL L-ascorbic acid and 10 nM dexamethasone was used to promote osteoblastic differentiation (phenotype expression) of the marrow mesenchymal cells (Köse, 2002). L-ascorbic acid influences the differentiation of preosteoblasts and plays an important role in the production of the collagenous bone ECM by increasing expression of collagen in a dose-dependent manner (Stein et al., 1993). β-glycerophosphate serves as a source of phosphate ions and is strictly required for the formation of a mineralized ECM by the osteoblasts (Coelho and Fernandes, 2000). Dexamethasone accelerates upregulation of postproliferative

osteoblast genes resulting in induction of ALP activity and increase in number of bone nodules (Stein et al. 1993, Coelho and Fernandes, 2000).The complete medium of the cell cultures was renewed every other day.

2.2.5.3. Osteoblast Characterization

2.2.5.3.1. Microscopic Evaluation

Mesenchymal osteoprogenitor cells and osteoblasts cultured in tissue culture grade polystyrene (TCP) flasks were visualized under inverted phase contrast microscope during the primary culture and after the first and second passages. The B (blue) filter mounted on the microscope was used to obtain the images. In order to investigate the osteoblast morphology, the second passage cells were seeded on the glass coverslips, in very dilute concentrations, fixed with glutaraldehyde at the end of the third day and stained with Phalloidin and Sytox Orange. These cells were examined using a confocal microscope (Zeiss LSM Pascal (Germany), Carl Zeiss).

2.2.5.3.2. Viable Cell Number Determination via Cell Titer 96 ™ Non-Radioactive Cell Proliferation Assay (MTS Assay)

When the second passage osteoblasts reached confluency, they were detached from the TCP flask surface by trypsinization and counted using a haemocytometer. Different amounts of cells ($0.5x10^4$, $1x10^4$, $1.5x10^4$, $2x10^4$, $3x10^4$, $4x10^4$, $5x10^4$, $7.5x10^4$) in the same concentration were seeded on 24-well tissue culture plates and incubated for 3 h at 37 ^oC in the CO_2 incubator for cell attachment to the well

surface. At the end of the incubation period, the medium of the cells was removed and 1 mL from 10% solution of MTS/PMS reagent was added to each well of the 24-well plate which was then incubated for 2 h at 37 ^{o}C in the CO_2 incubator. Absorbance of the medium from each well was determined at 490 nm using an Elisa Plate Reader (Molecular Devices (USA), Model Maxline) and a calibration curve using the absorbances obtained for different numbers of osteoblasts was constructed. This calibration curve was then used to determine the cell number on the polymeric films and TCP.

2.2.5.4. Osteoblasts on the Films

Upon obtaining confluent monolayers (in 12 days), second passage osteoblasts were lifted from the flask surface enzymatically using a 500 μg/mL solution of trypsin. The cells were obtained as a pellet by centrifugation at 500 g for 5 min and resuspended in 4-5 mL complete media. The cells were counted by using haemacytometer and concentrated to 8.5-10 x 10^5 cells/mL in complete media. Aliquots of 20-25 μL of cell suspension were seeded on the sterile and dry unpatterned, macropatterned and micropatterned films (Fig. 2.3) with and without adsorbed fibrinogen and on the fibrinogen immobilized micropatterned films (0.5x0.65 cm^2) placed in the wells of 24-well plate. Cell seeded films were left undisturbed for 3 h at 37 ^{o}C in the CO_2 incubator to allow cell attachment to the film surface. Same amount of cells was also seeded directly on the TCP well surface to serve as a positive control. Lastly, 1 mL of complete medium was added to each well. The plates were incubated at 37 ^{o}C in the CO_2 incubator for 1 or 3 weeks and the medium in the wells was renewed every other day.

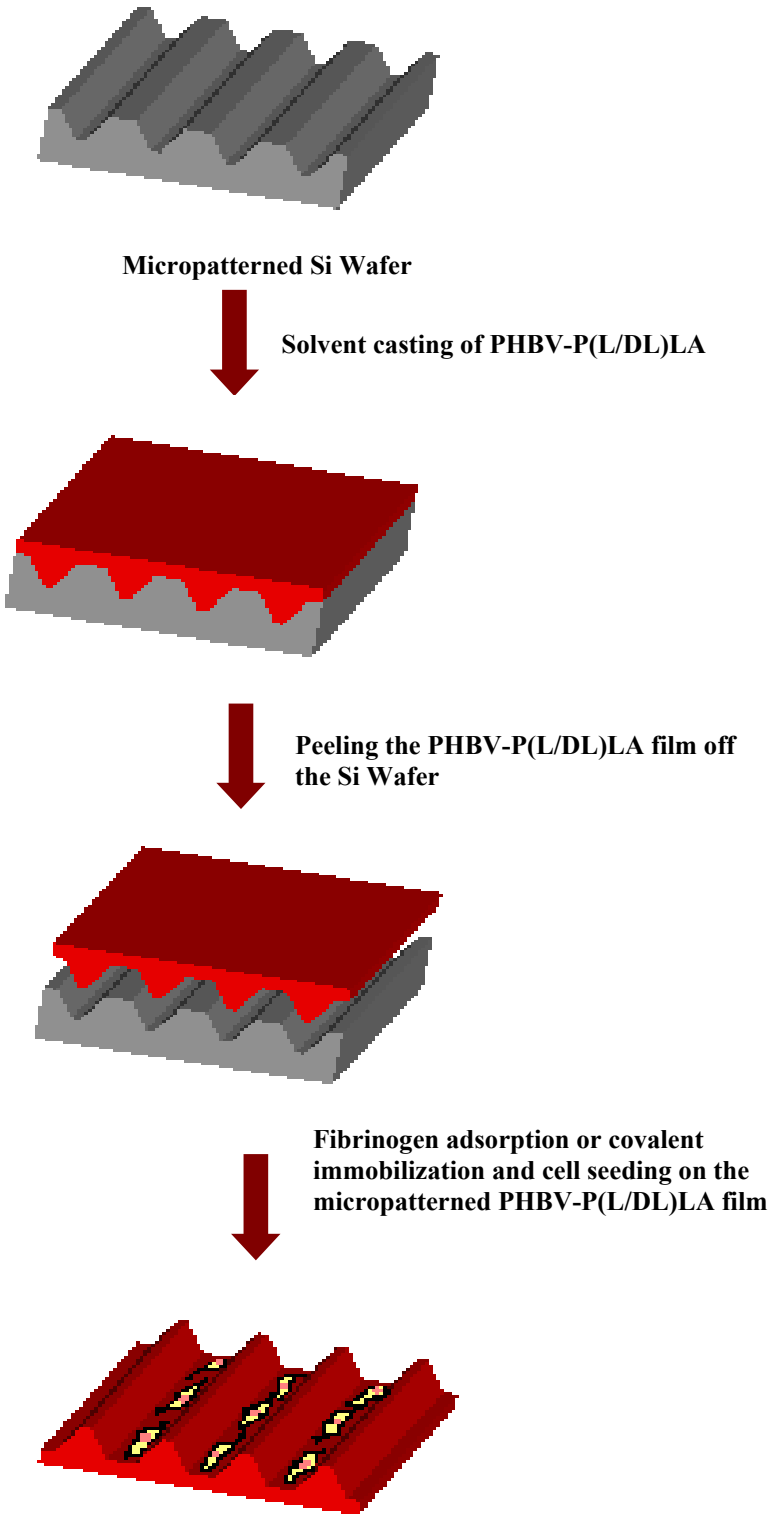

Figure 2.3. Schematic presentation of the method used for cell guidance on micropatterned polymer surfaces

2.2.5.4.1. MTS Assay for Determination of Cell Proliferation

MTS assay was carried out immediately after seeding the cells on the films by using the cells seeded on TCP wells to determine the initial cell amount seeded on each sample, and one and three weeks post seeding to determine the cell proliferation on each sample.

Following a 3-h incubation period of cells on the films and TCP for cell attachment immediately after cell seeding, MTS assay was applied to the cells on TCP. MTS/PMS reagent (1 mL, 10%) was added to two wells and the plate was then incubated for 2 h at 37 ^{o}C in the CO_2 incubator. Absorbance of the medium from each well was determined at 490 nm using the Elisa Plate Reader. Cell amount was determined from the MTS calibration curve.

At the end of 1 and 3 week incubation periods, the films were transferred into clean wells and 1 mL from 10% solution of MTS/PMS reagent was added onto each sample and to the cell containing TCP wells and the plate was then incubated for 2 h at 37 ^{o}C in the CO_2 incubator. Absorbance of the medium of each well was determined at 490 nm using the Elisa Plate Reader. Cell amount was determined from the MTS calibration curve.

2.2.5.4.2. ALP Assay for the Assessment of Osteoblast Phenotype

In order to determine the effect of cell-material surface interaction on the osteoblast phenotype expression, amount of alkaline phosphatase produced by the cells was determined. The cells were seeded on the TCP and films as described in

section 2.5.4 and cultured for 1 and 3 weeks at 37 ^{o}C in the CO_2 incubator. The cells on the TCP and the films were then washed three times with PBS (10 mM, pH 7.2). The films were transferred into 0.5 mL Tris buffer (10 mM, pH 7.5, 0.1% Triton®X-100), and the cells on TCP were lifted from the surface with the same amount of that buffer. Then, the samples were frozen and thawed three times and sonicated for 5 min at 25 Watts on ice . The samples were centrifuged at 2000 rpm for 10 min and an aliquote of 100 μL of each sample was added to 200 μL of p-nitrophenyl phosphate solution (6.2 mg/mL) at room temperature in the well of a 96-well plate and incubated for 60 min at 37 ^{o}C in the CO_2 incubator. p-Nitrophenol was produced in the presence of alkaline phosphatase and its absorbance was measured at 405 nm at the end of 15, 30, 45 and 60 min during incubation by the Elisa Plate Reader. The slope of the absorbance vs time plot was used to calculate the alkaline phosphatase activity per minute. Calibration curve of p-nitrophenol at 37 ^{o}C was used to determine the enzyme activity in units of μmole substrate converted to product / min.

2.2.5.4.3. Determination of Mineralization

Mineralization produced by osteoblasts was detected on the films and TCP via labelling with tetracycline, which is autofluorescent. The cells were seeded on the TCP and films as described in section 2.5.4 and cultured for 1 and 3 weeks at 37 ^{o}C in the CO_2 incubator. On the third day of culture the previously used antibiotics, 100 units/mL penicillin and 100 μg/mL streptomycin, in the complete medium were replaced with tetracycline (10 μg/mL). At the end of 1 and 3 week culture periods,

the cells on the films and TCP were washed twice with PBS (10 mM, pH 7.2), twice with 70% ethanol and fixed in 96% ethanol at 4 ^{o}C for six h (Matsuzaka et al., 1999). The ethanol was discarded and the films were left to dry in a dark place. Mineralization was observed at 480 nm using the fluorescence microscope (Olympus IX 70, Japan, with inverted reflected light fluorescence observation attachment).

2.2.5.4.4. Evaluation of Cell Alignment

Effect of surface topography and chemistry on the cell morphology and cytoskeleton organization was determined by microscopy. The cells were seeded on the polymeric films with defined topography and chemistry and TCP as described previously in section 2.5.4. At the end of 1 and 3 week culture periods, the samples were prepared for microscopy.

2.2.5.4.4.1. Fluorescence Microscopy

2.2.5.4.4.1.1. Acridine Orange Staining

As a preliminary study, cells seeded on the macropatterned films and on the films containing both unpatterned and micropatterned regions were stained 3 weeks postseeding with Acridine Orange for determination of cell spreading direction preference, and influence of surface topography. The cells on the films were washed with PBS (10 mM, pH 7.2) and fixed at room temperature in 2.5% glutaraldehyde prepared in sodium cacodylate buffer (0.1 M, pH 7.4) for 2 h. They were washed

then with cacodylate buffer (0.1 M, pH 7.4) and stored at 4 ^{o}C. Prior to staining, the cells were permeabilized to the dye by a treatment with 0.1 M HCl for 1 min. The cells were then stained with acridine orange (6 μg/mL) for 15 min and washed with distilled water before the microscopic examination at 480 nm.

2.2.5.4.4.1.2. Phalloidin Staining

The cells seeded on the films and TCP were stained with Phalloidin at the end of 24 h, 1 week and 3 week for visualization of actin filament organization of the cell cytoskeleton. The cell-polymer constructs were washed with PBS (10 mM, pH 7.2) and fixed at room temperature in 2.5% glutaraldehyde in sodium cacodylate buffer (0.1 M, pH 7.4) for 2 h. They were washed first with cacodylate buffer (0.1 M, pH 7.4) and then with 0.1 M PBS. The cells were permeabilized with 0.1% Triton X-100 (in 0.1 M PBS) for 5 min and then the film surface was blocked with 1% BSA solution for 30 min. Lastly, the cells were stained with 5 U/mL Alexa fluor 546 Phalloidin in 1% BSA solution for 30 min at 37 ^{o}C and washed with 0.1 M PBS before examination with a fluorescence microscope at 510-550 nm.

Some of the samples were stained with the nuclear stain Sytox Orange, following the Phalloidin staining. The cell-polymer constructs and cells on the TCP were incubated in 5 μM Sytox Orange for 15 min at 37 ^{o}C and washed with 10 mM PBS prior to microscopic examination at 510-550 nm.

2.2.5.4.4.1.3. BCECF (2′,7′-bis-(2-carboxyethyl)-5-(and-6)-carboxyfluorescein) Staining

The cells seeded on films and TCP were stained with BCECF-AM at the end of 1 week and 3 weeks. The conversion of nonfluorescent BCECF-AM to fluorescent BCECF via the action of intracellular esterases can be achieved only by alive cells, and thus this staining serves as a tool for proving cell viability while visualizing them. The cells were washed with serum-free DMEM (4.5 g/L glucose content) and incubated at 37 ^{o}C for 1 h in 1 μM BCECF-AM prepared in the serum-free DMEM. At the end of incubation period, the cells were washed with the serum-free DMEM and observed at 480 nm with the fluorescence microscope.

2.2.5.4.4.2. Scanning Electron Microscopy

The cell-polymer constructs mentioned in section 2.5.4.4. were washed with PBS (10 mM, pH 7.2) and fixed at room temperature in 2.5% glutaraldehyde in sodium cacodylate buffer (0.1 M, pH 7.4) for 2 h. They were then washed with cacodylate buffer (0.1 M, pH 7.4) and frozen overnight at -20 ^{o}C prior to freeze-drying. Following the 8 h freeze drying, the samples were stored at 4 ^{o}C and before the microscopic observation, the samples were coated with gold. Scanning electron microscopy was carried out in a JEOL (Japan), Model JSM 6400.

CHAPTER 3

RESULTS AND DISCUSSION

3.1. Surface Characterization of Templates and Films

3.1.1. Microscopic Examination of Surface Topography

3.1.1.1. Light Microscopy

Surface pattern of the micropatterned Si template was examined using a microcamera (Fig. 3.1.a). There are two regions on the template: a smooth (unpatterned) region and a micropatterned region. The ridges of the micropatterned region are the continuum of the smooth region while the grooves are invaginations made in the Si wafer as a result of the chemical etching. Ridge width was the same all over the micropatterned region, but there were two different alternating groove widths (2 μm, 12 μm), as designed at the beginning. The micropatterned PHBV-P(L/DL)LA film, obtained by solvent casting method, was a precise match of the negative replica of the micropatterned template (Fig. 3.1.b).

Light micrographs of the macropatterned film, showing the whole surface pattern, could not be obtained clearly due to its features being too large to focus all at once.

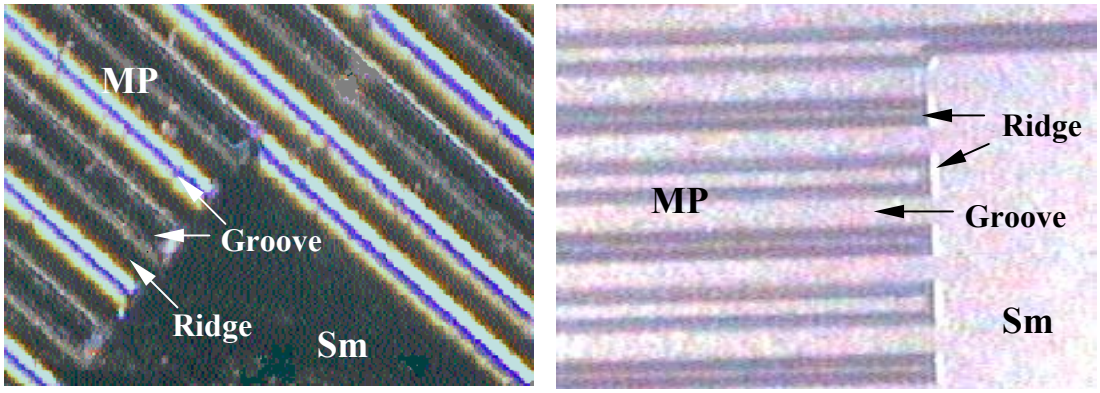

(a) **(b)**

Figure 3.1. Light micrographs of a) micropatterned Si template (x350) and b) micropatterned PHBV-P(L/DL)LA film (x100). **Sm**: smooth (unpatterned) region, **MP**: micropatterned region

3.1.1.2. Scanning Electron Microscopy

The polymeric films with different surface pattern and treatment were examined with scanning electron microscope (SEM) to gain information about the surface microstructure. Since the cells seeded on the films will interact with the microstructure of the polymeric surface, there is a strong need to define the surface texture. According to the micrographs obtained, the unpatterned and micropatterned film surfaces had a very smooth texture while the macropatterned one had a rough texture, in addition to the intended pattern (Fig. 3.2. a-c).

The rough texture of the macropatterned film surface can be attributed to the surface characteristics of the teflon template; it is not possible to control the pattern borders formed during machining and the surfaces obtained, by lathe cut. Moreover, the gas bubbles generated during film preparation, caused by the thickness of the polymer solution, prevented the intact ridge formation on the macropatterned films (Fig. 3.2.b).

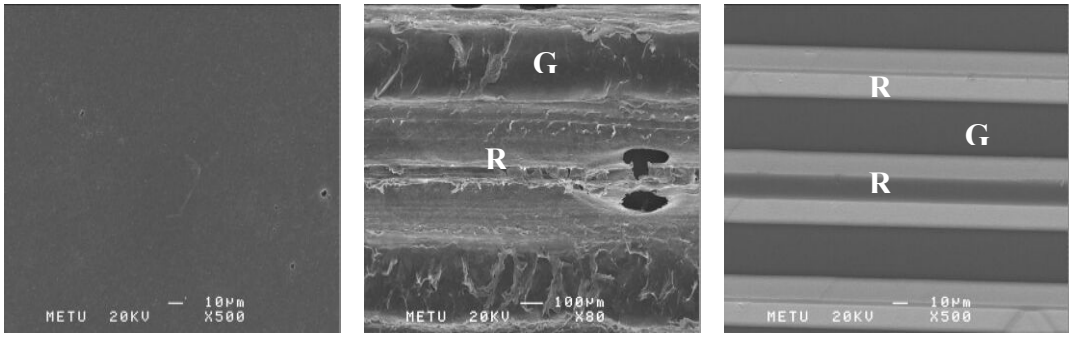

(a) **(b)** **(c)**

Figure 3.2. Scanning electron micrographs of a) unpatterned film (x500), b) macro-patterned film (x80) and c) micropatterned film (x500). **R**: ridge, **G**: groove

In the case of micropatterned film, the inverse of the micropattern on the Si template was perfectly replicated, the corners were very sharp and the whole surface had a smooth texture. The micropattern dimensions were determined to be as follows: ridge widths: 2 and 12 μm alternating, groove width: 27 μm, and groove depth: 20 μm.

In order to determine the effect of different surface treatments on the surface microstructure during the Fb covalent immobilization procedure, the scanning electron micrographs of the films were obtained following each step (Fig. 3.3). UV exposure had no effect on the surface microstructure, but with epichlorohydrin treatment, following the UV exposure, the surface acquired a granular appearance (Fig. 3.3. a and b), which may indicate that one of the polymers in the blend was partially dissolved by the epichlorohydrin solution around the phase boundaries.

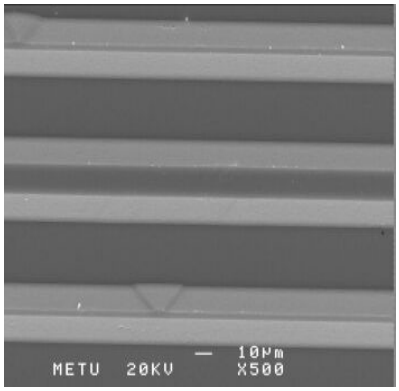

(a) MP+UV

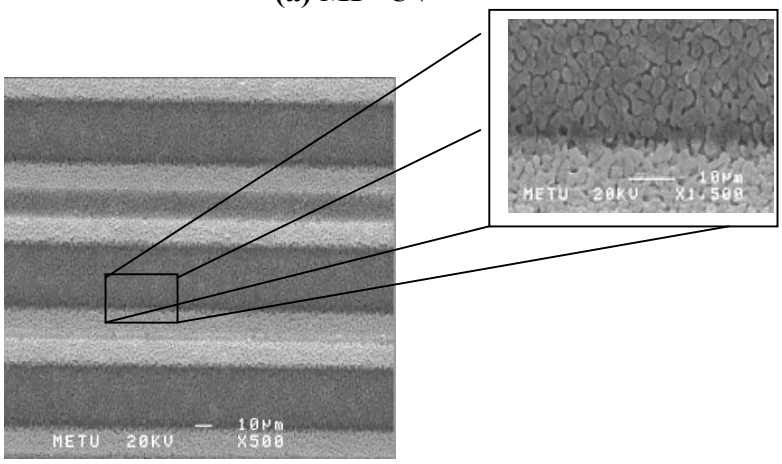

(b) MP+UV+EPI

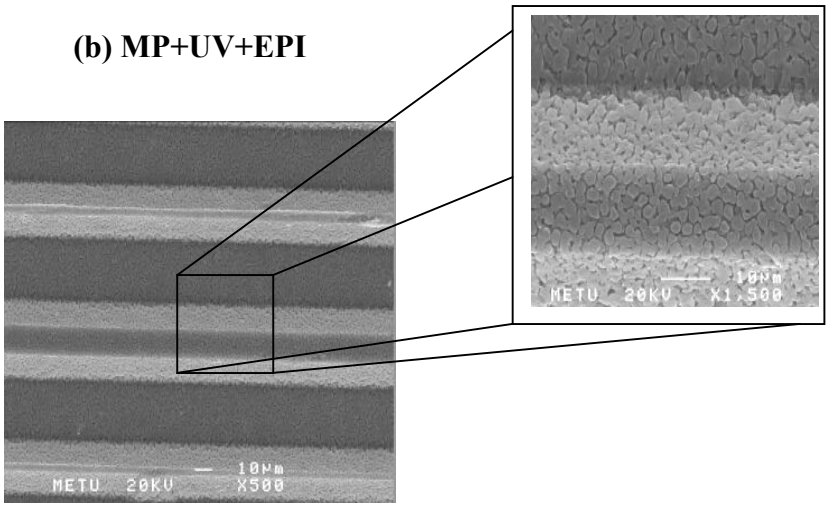

(c) MP+UV+EPI+Fb_i

Figure 3.3. Scanning electron micrographs of micropatterned films with a) UV exposure, b) UV exposure and epichlorohydrin treatment, and c) UV exposure, epichlorohydrin treatment and immobilized fibrinogen

However, the granular structure formation did not have an adverse effect on the micropattern of the surface, which remained intact, and the cracks (openings) formed were not large enough for cell penetration within the polymeric film. Fibrinogen immobilization on the film surface following the epichlorohydrin treatment did not cause any further changes in the surface microstructure.

3.1.2. Water Contact Angle Measurements

The hydrophilicity of the films with different surface treatments was determined via water contact angle measurements. Since surface topography and roughness affected the result, unpatterned films were used for that purpose.

Surface hydrophilicity changes in accordance with the chemical groups present on the surface and is important for the initial phase of cell-material interaction. It is reported that cells generally prefer to attach on surfaces with intermediate hydrophilicity (contact angle 40^{o}-90^{o}) (Saltzman, 1997). Table 3.1 shows the water contact angles of unpatterned films with different treatments. Upon exposure of the film surface to UV, the hydrophilicity of the surface increased slightly probably due to radical or ion formation or introduction of other reactive groups on the film surface. Activation of the surface with epichlorohydrin for fibrinogen binding after UV exposure led to a drastic decrease in the contact angle, probably due to the epoxy group of epichlorohydrin. Binding of Fb to the surface via this epichlorohydrin spacer, however, caused a sharp increase in the contact angle. Since covalent bonding of the protein to the epichlorohydrin is achived through its NH_2 groups, one Fb molecule would be bound by a number of epichlorohydrin molecules which would prevent the protein's free motion and exposure of its

hydrophilic regions upon facing the water. Contrary to the Fb immobilized surface (Fb_i), Fb adsorbed films (UNP+Fb_a) showed a significant decrease in the contact angle (from 61 to 51.5) indicating an increase in hydrophilicity when compared to the untreated polymer surface. This can be explained by the fact that during the adsorption process weak forces such as van der Waals interactions are in effect. Since the polymers, and therefore the surface, are hydrophobic in nature, it is likely that hydrophobic regions of the Fb interact with the polymer surface while the hydrophilic regions face the water phase.

Table 3.1. Water contact angles of unpatterned films with different surface treatments

Sample Type	**Contact Angle (Degree)**
UNP*	61.0 ± 0.7
UNP+UV	59.2 ± 0.4
UNP+UV+EPI	37.4 ± 0.4
UNP+UV+EPI+Fb_i	68.3 ± 1.4
UNP+Fb_a	51.5 ± 0.6

* Unpatterned film, EPI: epichlorohydrin, Fb_i: immobilized fibrinogen, Fb_a: adsorbed fibrinogen

3.1.3. Determination of Immobilized Fibrinogen Content of Micropatterned Films

3.1.3.a. Quantitative Evaluation

Bradford assay was used for quantitative assessment of the amount of Fb covalently immobilized on the micropatterned film surface. Protein concentration of

the solutions used during and after immobilization was determined using the Fb standard curve shown in Appendix A.

The following relation was used in the calculations:

W_{Fb} per unit area (g/cm^2)=[$(W_{Fb})_{\text{before immob}}$–($(W_{Fb})_{\text{after immob}}$+$(W_{Fb})_{\text{wash soln}}$)]/ A

where W_{Fb} is the amount of fibrinogen (g) and A is film surface area (cm^2).

The average amount of Fb covalently immobilized per sample was calculated as 99.5 ± 27.6 μg/sample considering that both sides of the film are used for Fb binding, and thus 49.8 ± 13.8 μg/ sample side. The surface area of the film used in the Fb immobilization process was determined as 0.65 cm^2, and therefore, the Fb amount covalently immobilized on the film surface was calculated as 153.1 ± 42.4 $\mu g/cm^2$, or 2.7 x 10^{14} Fb molecules/ cm^2 using 340 kDa/mol molecular weight for fibrinogen [Sigma Catalog, 2002-2003].

3.1.3.b. Qualitative Detection

The presence of covalently immobilized protein on the micropatterned films was proved qualitatively with Coomassie Brilliant Blue R-250 staining. The same staining procedure was applied to both Fb immobilized and epichlorohydrin activated film, which served as a negative control (Fig. 3.4 and Fig. 3.5).

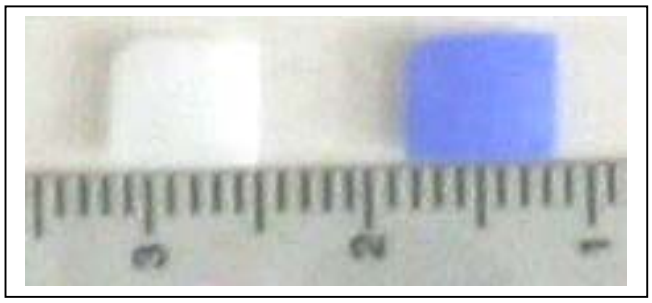

Figure 3.4. Photograph of the Coomassie Brilliant Blue R-250 stained micropatterned films: epichlorohydrin activated film (left), and Fb immobilized film (right)

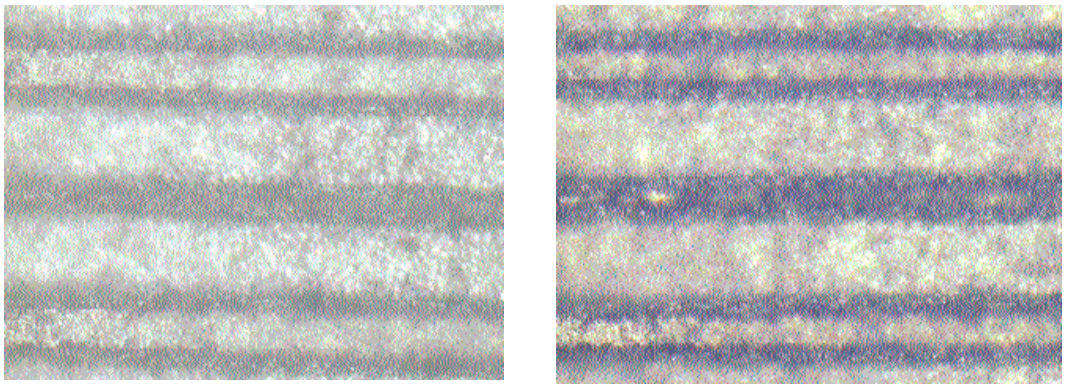

(a) **(b)**

Figure 3.5. Light micrographs of Coomassie Brilliant Blue R-250 stained micropatterned films: a) epichlorohydrin activated film (x200), and b) Fb immobilized film (x200)

The distinct blue color of the stain remained on the Fb immobilized films while it was removed from the epichlorohydrin activated films after the wash with 50% methanol. A homogeneous Fb immobilization was achieved through out the film surface, although the blue coloration appears to be concentrated on the side walls of the ridges, which can be explained by the angle of observation.

3.2. In Vitro Studies

3.2.1. Osteoblast Characterization

3.2.1.1. Microscopic Evaluation

Bone marrow cells and osteoblast cultures at different passages were observed under inverted phase contrast microscope (Fig. 3.6). Smoother and more homogeneous confluent monolayers with better cell-to-cell interactions were formed as the cells went through the primary culture to the second passage. However, it was not possible to differentiate the individual cell morphology with light microscopy due to increased cell-to-cell interactions.

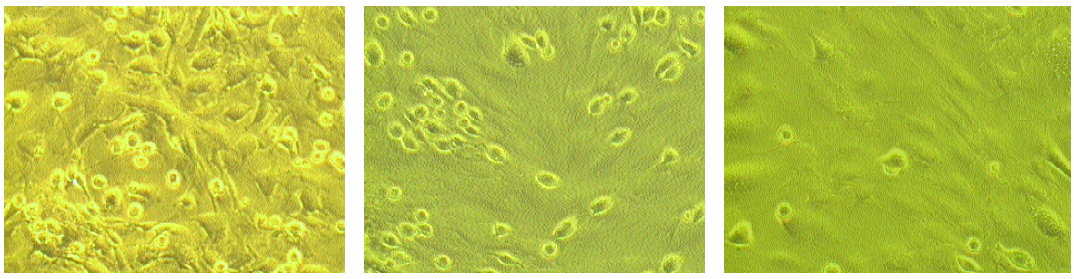

(a) **(b)** **(c)**

Figure 3.6. Light micrographs of confluent cell monolayers at different passages under blue filter, a) primary culture of bone marrow cells (x100), b) first passage osteoblast cell culture (x100), and c) second passage osteoblast cell culture (x100)

In order to investigate the osteoblast morphology, very dilute second passage cells were seeded on glass coverslips, fixed with glutaraldehyde at the end of the third day and stained with Phalloidin and Sytox Orange. The typical polygonal

morphology of osteoblasts (Attawia et al.,1999) was revealed with confocal microscopy (Fig. 3.7.b). In addition, the actin cytoskeleton was successfully stained with Phalloidin (Fig. 3.7.c) and this stain was used in subsequent studies for investigation of cell orientation.

Osteoblasts, derived from mesenchymal stem cells in bone marrow, are responsible for the formation and organization of the extracellular matrix of bone and its subsequent mineralization. They may influence mineralization of the bone matrix through the synthesis of organic matrix components (collagen Type I, alkaline phosphatase, osteocalcin, etc.) of bone and the production of matrix vesicles (Buckwalter et al., 1995). In addition systemic hormones may stimulate osteoblasts to release mediators that activate osteoclasts. Osteoblasts are active in bone-remodeling and fracture-healing sites in adults.

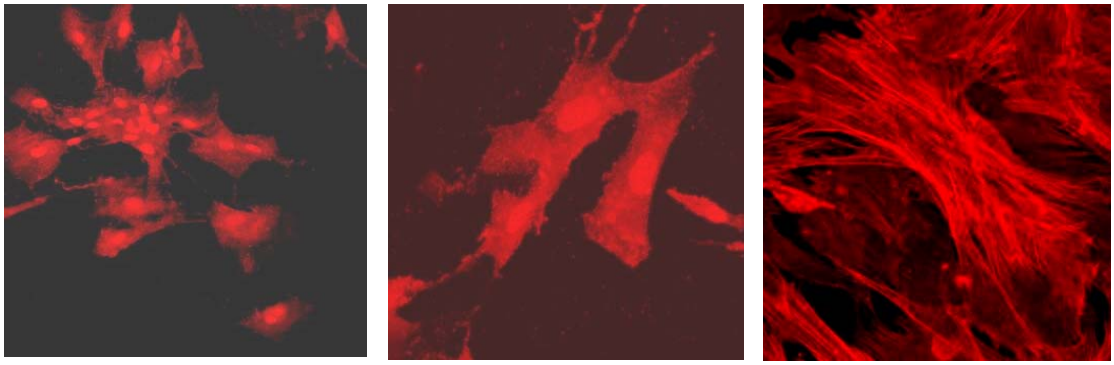

Figure 3.7. Confocal micrographs of second passage osteoblasts on a glass coverslip. a) aggregate formation by osteoblast cells (Phalloidin and Sytox Orange, x100), b) typical osteoblast polygonal morphology (Phalloidin and Sytox Orange, x200), and c) osteoblast actin cytoskeleton organization, (Phalloidin, x200)

Various staining procedures (Giemsa, Sytox Orange, BCECF, Acridine Orange) revealed the presence of another cell type within the osteoblast culture. These non-osteoblastic cells had a four times larger cell diameter with a circular morphology when compared to osteoblasts, and most of them had one or two nuclei while few of them were multinucleated (Fig. 3.8). Their morphology suggested that these are osteoclast precursors and some are osteoclasts. Osteoclasts share a hematopoietic stem cell precursor with cells of the monocyte family, unlike osteoblasts which originate from mesenchymal stem cells (Buckwalter et al., 1995). The hematopoietic stem cells can develop into mononuclear osteoclast precursors, found in the bone marrow, which in turn proliferate and fuse to form the large multinucleated osteoclasts when stimulated (Buckwalter et al., 1995). These findings suggest that the osteoblast isolation procedure used in this study is not completely exclusive to cells other than osteoblastic origin. Sequential enzymatic digestions are used to eliminate fibroblasts during isolation of osteoblasts from calvaria (Attawia, 1999), and special medium combinations are used to favor Schwann cell proliferation while reducing fibroblasts during Schwann cell isolation from sciatic nerve (Miller, 2001). Therefore, a mixed cell culture is usually the problem faced during isolation of cells from any organ or tissue of a multicellular organism, and there is a need to adopt more effective isolation procedures to obtain a pure cell culture.

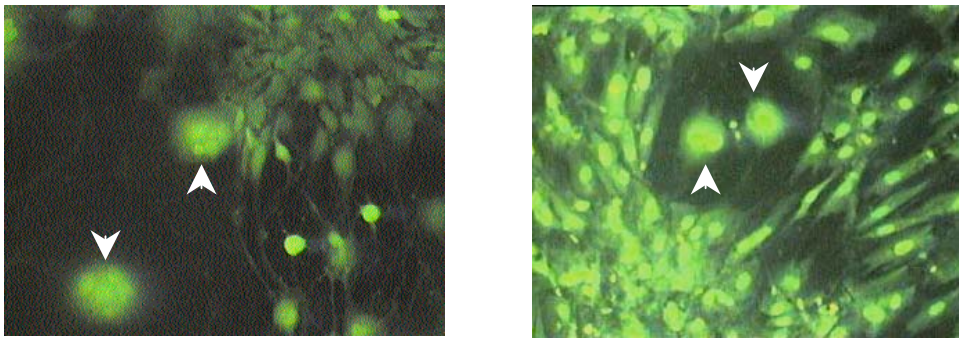

Figure 3.8. Non-osteoblastic cells (arrow heads) detected within the osteblast cell culture (x100) with Acridine Orange (right), and BCECF (left) staining

3.2.1.2. Viable Cell Number Determination via Cell Titer 96 ™ Non-Radioactive Cell Proliferation Assay (MTS Assay)

Different amounts (but same concentration) of osteoblasts ($0.5x10^4$, $1x10^4$, $1.5x10^4$, $2x10^4$, $3x10^4$, $4x10^4$, $5x10^4$, $7.5x10^4$) were seeded on 24-well tissue culture plates and viable cell number was determined with the MTS assay to construct a calibration curve (Fig. 3.9). This curve was used to determine the cell number on the films and TCP control at different time periods of incubation in the studies presented in section 3.2.2.1.

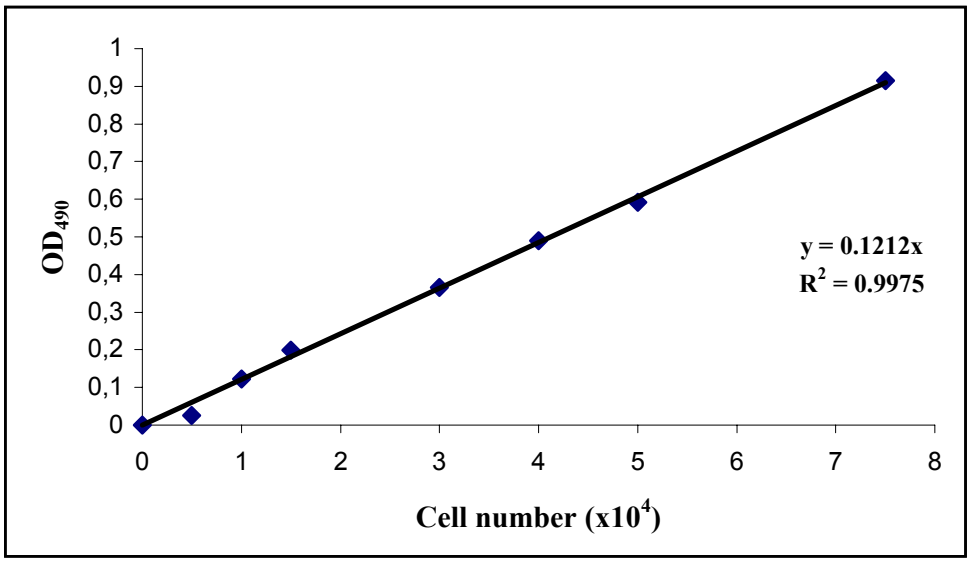

Figure 3.9. MTS calibration curve for viable osteoblast number determination

The perfect linearity of the curve and the absence of an intercept in the calibration curve equation indicates that this is a reliable method for detecting cells while they are viable. Mean OD values corresponding to each cell amount can be found in Appendix B.

3.2.2. Biochemical and Morphological Characteristics of Osteoblasts on the Films

3.2.2.1. Cell Proliferation

TCP, unpatterned and micropatterned films with and without adsorbed fibrinogen and with covalently immobilized fibrinogen (0.325 cm^2) were seeded with osteobasts and then incubated for 1 and 3 weeks at 37 ^oC in the CO_2 incubator (5%

CO_2), to study the effect of pattern presence and chemical modification on cell proliferation.

MTS assay was carried out immediately after cell seeding by using the cells seeded on TCP wells, to determine the initial cell amount seeded on each sample, and one and three weeks after seeding to determine the cell proliferation on each sample. Initial cell amount seeded on the samples was determined as 20,000 cells/sample.

One week MTS results revealed that there was no significant difference between unpatterned (UNP) and Fb adsorbed unpatterned (UNP Fb_a) films in terms of cell proliferation on their surface (Fig. 3.10). Osteoblasts are anchorage dependent cells, that is, they need to attach to a surface in order to be able to start proliferation. Cells attach to a surface via their integrin receptors, which can bind to the RGD (arginine-glycine-aspartic acid) amino acid sequence of proteins adsorbed on the surface. These proteins can already be present when the cells are seeded or can be adsorbed during the cell seeding procedure, carried in the FCS delivered to the surface together with the cells. Fibrinogen, which was adsorbed on the film surface prior to cell seeding, itself bears RGD sequences in its alpha chain (Suehiro et al., 2000). On the other hand, the cell seeding medium contained a high amount of FCS (20%), which means that concentration of cell binding proteins that could adsorb on the surface was high. Therefore presence of adsorbed Fb on the unpatterned surface prior to cell seeding made no difference in terms of cell attachment.

In contrast to these results, Fb adsorption on the micropatterned films (MP Fb_a) caused a significant difference in cell proliferation when compared to the cell

proliferation on the micropatterned films without fibrinogen (MP). Probably the serum protein adsorption to MP surface was not sufficient to make cells attach within the grooves of hydrophobic polymer and they preferred to form cell aggregates (as revealed by microscopy, section 3.2.2.4.1.3) with high probability of leaving the film surface. The highest cell proliferation rate and the lowest standard deviation was obtained on the MP Fb_a films, when compared to other film surfaces.

Cell proliferation on the Fb immobilized micropatterned films (MP Fb_i) was similar to that on the MP films and significantly lower than that of the MP Fb_a ($11.3x10^3$ to $23.5x10^3$, the first week). The two possible reasons for that unexpected result may be: a) increased hydrophobicity (as shown by contact angle) of the surface when compared to the original polymer surface or b) improper or inaccessible configuration of the RGD sequence due to covalent immobilization. Both of these could lead to a decrease in cell attachment efficiency when compared to the MP Fb_a film. Interestingly, MP Fb_i films showed the highest standard deviation among all the samples.

The highest cell proliferation, at the end of the first week, was observed on the TCP, which was significantly higher than the cell proliferation on all films. The cell numbers on the surfaces of the films, except MP Fb_a, were less than the initial cell amount seeded on each sample, suggesting that not all the cells seeded adhere to the surface.

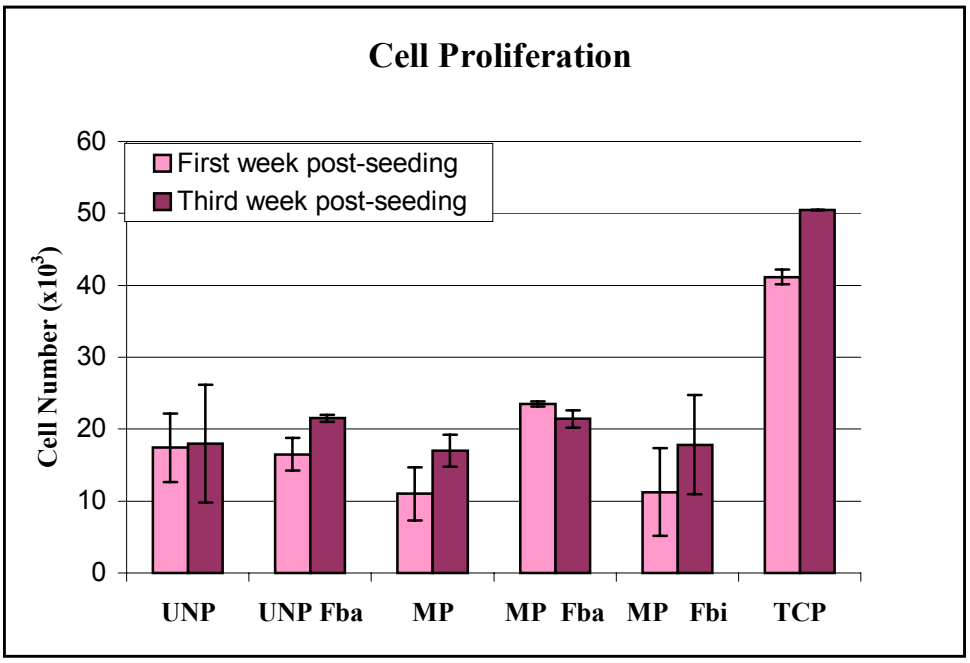

Figure 3.10. Cell proliferation on the polymeric films with different microtopography and surface chemistry, and on TCP control.

Although it was found that cell proliferation was higher on the MP Fb_a films when compared to the UNP Fb_a samples one week post-seeding, at the end of three weeks the cell numbers on these two samples with very different microtopography were almost equal. The same result was obtained regarding the cell proliferation on the MP and UNP films, at the end of three weeks. These results suggest that the presence of a micropattern has no effect on cell proliferation on the long run. In a recent study, Wang et al. (2000) showed that proliferation of MC3T3-E1 osteoblasts in three different patterns on silicone (12/12, 18/18 and 24/24 μm in groove/ridge widths, and 2 μm in groove depth) was not different from that on the smooth (unpatterned) silicone surfaces, indicating that surface micropattern does not affect the cell proliferation.

A slightly higher proliferation rate between the first and third week was observed on the MP and MP Fb_i samples, although the cell amount was still lower than the Fb_a samples. On the third week, there was no difference in cell number on the UNP films when compared to the first week results and a small increase (from $16.5x10^3$ to $21.5x10^3$) was found on the UNP Fb_a. Considering the whole picture at the end of three weeks, presence of adsorbed Fb on both unpatterned or micropatterned films was better for the promotion of cell proliferation. This may be explained by the more stable and intense integrin-RGD sequence interaction, which could lead to induction of cell proliferation via signal transduction. However, this difference in cell proliferation was found to be insignificant.

The lowest standard deviation was observed on the MP Fb_a and TCP. Numerical values of the cell proliferation on different samples can be found in Appendix B.

3.2.2.2. Alkaline Phosphatase Activity of Osteoblasts

TCP, unpatterned and micropatterned films with and without adsorbed fibrinogen and with covalently immobilized fibrinogen (0.325 cm^2) were seeded with osteoblasts and incubated for 1 and 3 weeks at 37 ^oC in the CO_2 incubator, to study the effect of micropattern and chemical modification on the osteoblast phenotype expression. Alkaline phosphatase (ALP) enzyme activity of cell lysates, obtained from each sample, was determined by spectroscopical detection of the enzyme product within one hour following the start of the reaction at 37 ^oC. The results were expressed as μmol of substrate coverted to product/min/sample, and

μmol of substrate coverted to product/min/cell, which was also named as ALP specific activity.

Alkaline phosphatase is an extracellular enzyme secreted by osteoblasts during the early stages of mineralization. Although the precise mode of action for ALP is still unclear, it has the ability to hydrolyze phosphate from various compounds and thus could help supply the inorganic phosphate necessary for the nucleation of hydroxyapatite crystals during mineralization. ALP is present on the surface of matrix vesicles released by osteoblasts and entrapped in the extracellular matrix. The matrix vesicles have been recognized as the earliest sites of mineral deposition in woven bone (Wuthier et al., 1982). With the down regulation of proliferation, during the osteoblast developmental sequence, proteins associated with the bone cell phenotype are detected (Stein et al.,1993). ALP mRNA and enzyme activity can be increased by more than 10-fold. As the cultures progress into the mineralization, all cells become ALP positive histochemically (Stein et al.,1993). Level of this enzyme has been routinely used in *in vitro* studies as a relative marker of osteoblastic differentiation.

ALP activity of osteoblast cells in this study was low in general in the first week, but increased significantly (approximately 5 fold) at the end of third week for all samples (Fig. 3.11). Similar increase in ALP activity was reported by Peter et al. (2000). According to their results, ALP activity of bone marrow derived rat osteoblasts was low at 7 and 14 days time points but increased significantly at 21 days, both on the TCP and on poly(propylene fumarate)/β-tricalcium phosphate biodegradable composites.

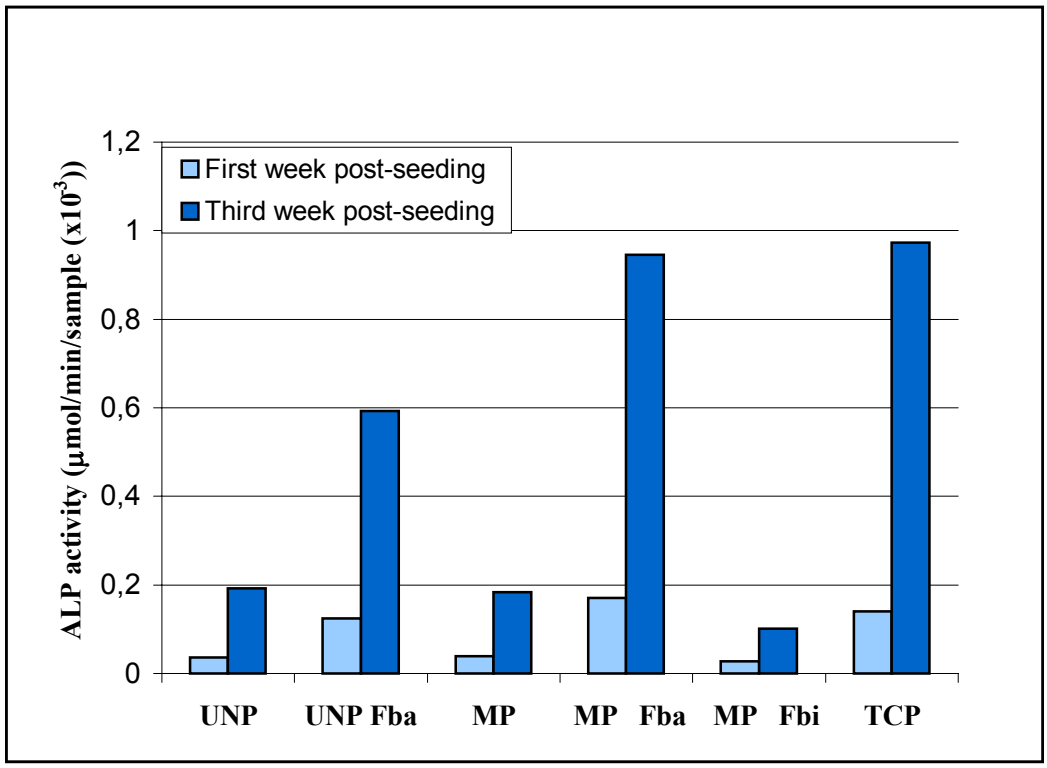

Figure 3.11. ALP activity of osteoblasts cultured on polymeric films with different microtopography and surface chemistry, and TCP control.

In addition, human bone marrow derived osteoblasts grown in DMEM with differentiation factors favoring the osteoblastic phenotype, showed an increase in ALP activity between the first and third week (Coelho et al., 2000).

Considering the ALP activities per sample, there was no difference between the enzyme activity on UNP and MP films (0.1925 and 0.1835 µmol/min/sample ($x10^{-3}$), respectively at the end of third week), however the presence of adsorbed Fb on the films led to a significant increase in enzyme amount (from 0.1248 on the first week to 0.5926 µmol/min/sample ($x10^{-3}$) on the third week for UNP Fb_a). The highest ALP activity per sample was obtained on the MP Fb_a films, indicating the synergistic effect of the micropattern and the chemical cue used for cell alignment.

The ALP activity per sample on the MP Fb_a films (0.9450 μmol/min/sample ($x10^{-3}$)) was comparable to that obtained on the TCP (0.9725 μmol/min/sample ($x10^{-3}$)) at the end of third week. The lowest activity was obtained on the MP Fb_i samples. In order to eliminate the effect of cell number and to determine the ALP amount produced by a single cell, it is preferred to calculate the ALP specific activity (Fig. 3.12). On the first week, the highest ALP specific activity was observed on the UNP Fb_a and MP Fb_a samples, with no significant difference (7.56 and 7.26 μmol/min/cell ($x10^{-9}$), respectively). This was even higher than that on TCP (3.41 μmol/min/cell ($x10^{-9}$)). ALP specific activity on the MP film (3.59 μmol/min/cell ($x10^{-9}$)) was comparable to that on TCP, and higher than the specific activity on the UNP film (2.10 μmol/min/cell ($x10^{-9}$)).

At the end of the third week the ALP specific activities on the MP and UNP films were very similar with no significant difference (10.79 and 10.69 μmol/min/cell ($x10^{-9}$), respectively), suggesting that the micropattern had no effect on osteoblast phenotype expression in long run. However, this is expected since the cells on this surface could not align.

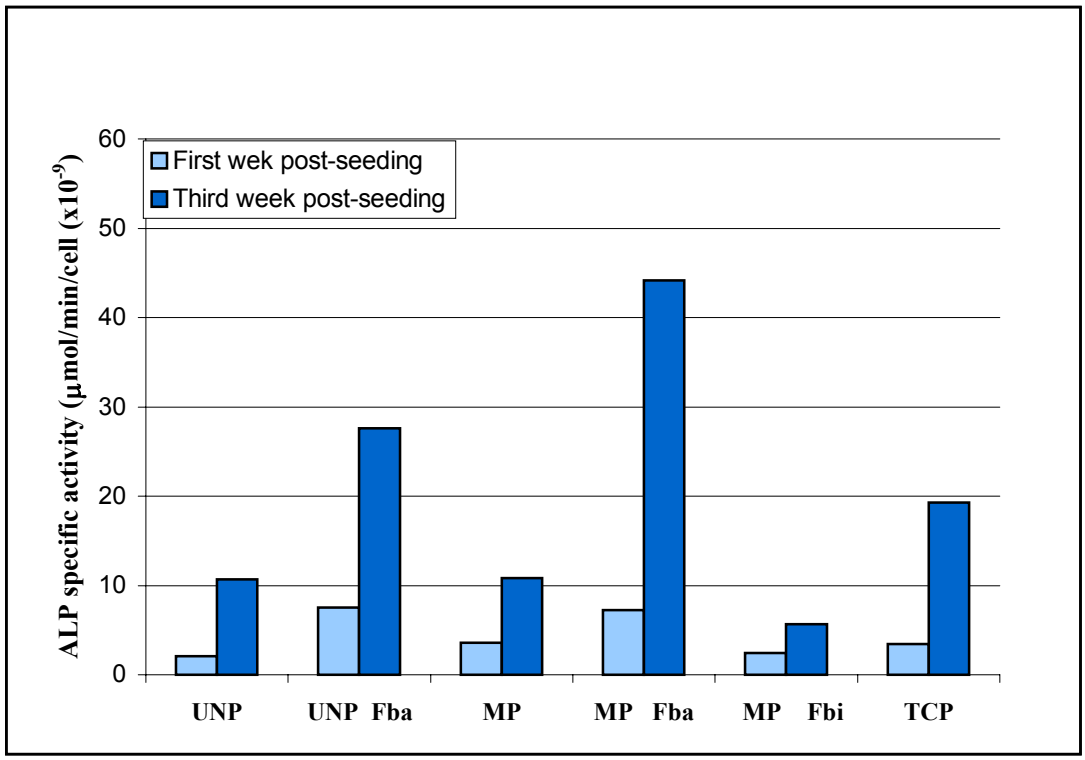

Figure 3.12. ALP specific activity of osteoblasts cultured on polymeric films with different microtopography and surface chemistry, and TCP control.

The highest ALP specific activity was obtained on the MP Fb_a samples (44.13 µmol/min/cell ($x10^{-9}$)), followed by the specific activity on the UNP Fb_a (27.6 µmol/min/cell ($x10^{-9}$)), both of which were higher than that on TCP (19.25 µmol/min/cell ($x10^{-9}$)) at the end of the third week. This result is an evidence for the significant effect of patterning combined with a chemical cue on osteoblast differentiation. In the study carried out by Matsuzaka et al. (1999), rat bone marrow derived osteoblasts were aligned parallel to the surface grooves of micropatterned PLA (0.5, 1.0 or 1.5 µm deep with 1, 2, 5, or 10 µm groove and ridge widths), and showed significantly higher ALP specific activity when compared to the cells on the smooth surfaces, which proliferated in a random fashion with no discernible

orientation. In aggrement with this study, Perizzolo et al. (2001) showed that ALP activity of rat calvarial osteoblasts was higher on micropatterned silicon wafers (ridge width: 5 μm, groove width: 42 μm, groove depth: 3 or 10 μm) coated with hydroxyapatite or titanium than the ALP activity on smooth surfaces of the same composition, both at 2 and 3 weeks.

The lowest ALP specific activity was obtained on the MP Fb_i films, which had the highest hydrophobicity and could not be much effective in cell alignment (see section 3.2.2.4.1.3) due to homogeneous covalent immobilization of Fb throughout the surface.

In general, a negative correlation was observed between the cell number increase rate between weeks 1 and 3 (Fig. 3.10) and the ALP specific activity change in the same period (Fig. 3.12).

The comparison of the ALP specific activity of this study obtained on TCP to those obtained by Peter et al. (2000) on the TCP by using the same type of cells revealed that our results at the end of 21 days (19.25×10^{-9} μmol/min/cell) were significantly lower (ca 100-fold) than theirs (12×10^{-7} μmol/min/cell). This could be explained by the fact that ALP activity of osteoblasts decreases as the number of passages increases (Köse et al., 2002); cells in this study were at the third passage while Peter and coworkers used first passage cells. The differences in cell culture medium composition could also lead to such significantly different results. Numerical values of the ALP activities on different samples can be found in Appendix B.

3.2.2.3. Mineralization of Extracellular Matrix

Mineralization of the extracellular matrix by the osteoblasts could be observed via labelling with tetracycline on the TCP, unpatterned and micropatterned films with and without adsorbed fibrinogen and with covalently immobilized fibrinogen. Tetracycline is an autofluorescent compound, which chelates free calcium in the medium and is deposited within the calcium phosphate mineral by the osteoblasts during the mineralization process. It was added into cell medium during the one and three week incubation periods.During the mineralization of bone, granules of calcium phosphate appear in osteoblast mitochondria and matrix vesicles, extracellular membrane-bound structures formed from the osteoblast plasma membrane (Buckwalter et al., 1995). Calcification should be visualized in two phases. During phase 1 the intravesicular calcium concentration is increased due to its affinity for lipids of the vesicle and vesicle membrane and also, perhaps, due to an inwardly directed calcium pump at the vesicle membrane (Anderson, 1976). Phosphatase at the vesicle membrane hydrolyzes ester phosphate of the matrix fluid to produce a local increase in orthophosphate. The intravesicular ionic product, Ca^{2+} and PO_4^{3-}, is thereby raised, which results in the initial deposition of calcium phosphate as hydroxyapatite (and probably also as amorphous calcium phosphate). With accumulation and growth of intravesicular crystals the vesicle membrane ruptures. Phase 2 begins with the exposure of preformed apatite crystals to the extravesicular environment and further crystal proliferation into the nonvesicular matrix occurs.

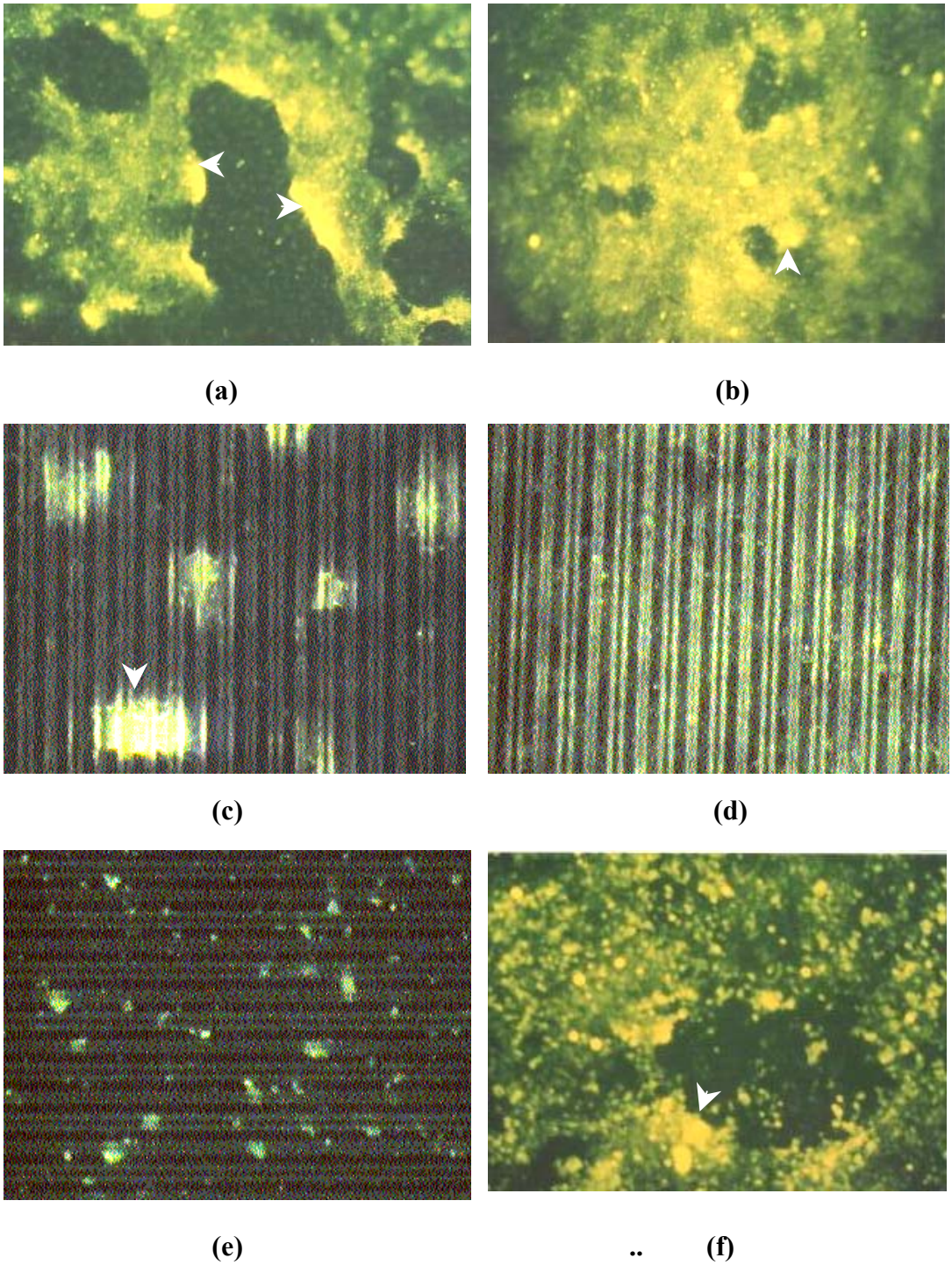

Figure 3.13. Mineralization, labelled with tetracycline, on the films with different microtopography and surface chemistry and TCP control at the end of one week. a) UNP (x40), b) UNP Fb_a (x40), c) MP (x40), d) MP Fb_a (x40), e) MP Fb_i (40), and f) TCP (x100). Arrow heads indicate the bone nodules

In this study, mineralization was observed on all the samples in the form of matrix vesicles (see Appendix C, Fig C-1), at the end of first week. The mineralization on the UNP films was in the form of interconnected patches in appearance and was more intense in the bone nodules (Fig. 3.13.a). On the other hand, mineralization on the MP (Fig 3.13.c) and MP Fb_i (Fig. 3.13.e) films was not interconnected; it was confined in the bone nodules (or cell aggregates) on the MP samples and was in very small point structures on the MP Fb_i samples. In contrast, the mineralization on UNP Fb_a and MP Fb_a was very homogeneous in appearance, found more intensely at the center of UNP Fb_a samples and within the grooves and their side walls on the MP Fb_a films. Small, unmineralized patches were present within this homogeneous mineralization, probably formed due to cell movement to form a multilayered structure or bone nodules.

At the end of three-week period, the mineral on the films became more crystalline, and more concentrated in the bone nodules (see Appendix C, Fig C-2). Staining of the same samples with Acridine Orange, which binds to nucleic acids and thus can stain both nuclei and partially the cytoplasm of cells (Fig. 3.14 b, d, f), revealed that the mineral was more intense in the inner part of the nodules. In the study carried out by Perizzolo et al. (2001), nodule formation, which was labelled with tetracycline more intensely at its center, was observed at the end of three weeks on hydroxyapatite coated smooth surfaces. The mineralization on the UNP film was again as interconnected patches, but there was a large, empty space at the center of the UNP Fb_a film (probably caused by cell movement to form the bone nodules) surrounded by very intensely labeled region.

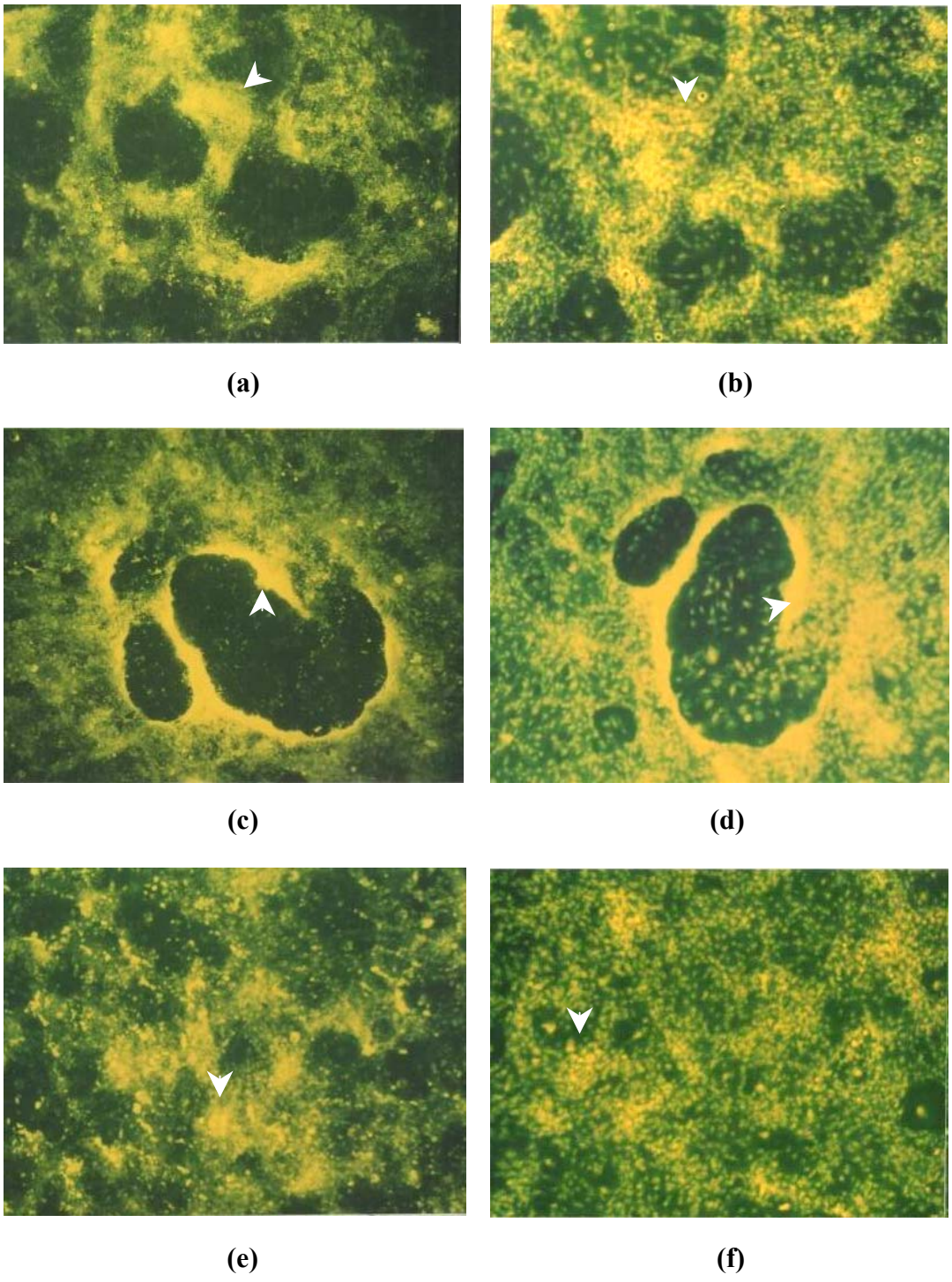

Figure 3.14. Single and double staining to reveal mineralization and cell organization at week three. Mineralization shown by tetracycline (a,c,e), and cell organization, stained with Acridine Orange in addition to tetracycline (b,d,f).
a and b) UNP (x40), c and d) UNP Fb_a (x40), and e and f) TCP (x40). Arrow heads indicate the bone nodules

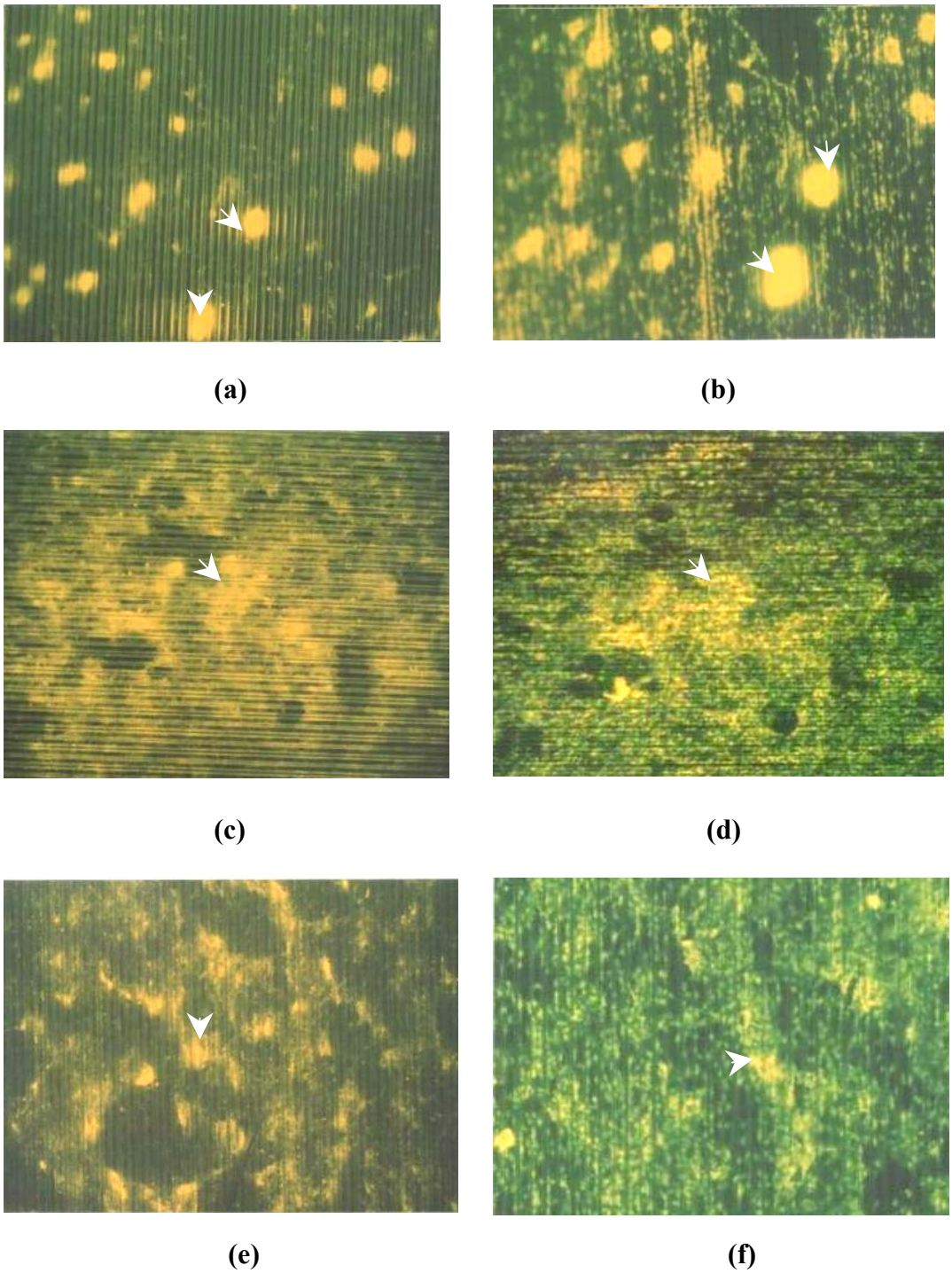

Figure 3.15. Single and double staining to reveal mineralization and cell organization at week three. Mineralization shown by tetracycline (a,c,e), and cell organization, stained with Acridine Orange in addition to tetracycline (b,d,f).
a and b) MP (x40), c and d) MP Fb_a (x40), and e and f) MP Fb_i (x40). Arrow heads indicate the bone nodules

A much more homogeneous mineralization was observed on the MP Fb_a samples, with few small empty spaces (gaps) throughout the film. Compared to other parts of the film, a more intense mineralization was observed in the bone nodules of MP Fb_a, some of which were formed across the ridges, and there was a general increase in mineral amount in all the surface, when compared to results of first week. There was an increase in the bone nodule size, and thus mineral patch size, on the MP Fb_i samples and they seemed to be interconnected when compared to the ones observed at the end of first week. In general, it seems that bone nodule formation is retarded on MP Fb_i samples in comparison to MP Fb_a. This may occur due to slow migration of cells on the surface to form a multilayered structure, due to the presence of covalently immobilized fibrinogen on the surface, which may have increased the strength of cell adhesion, or due to lower cell number with homogeneous non-confluent distribution lacking cell-cell interactions. In the study by Matsuzaka et al.(1999) it was shown that more tetracycline label, expressed as percent mineralized area, was found on grooved subtrates than on the smooth controls, for both PLA and TCP. The same comment can be made about the UNP Fb_a and MP Fb_a samples in this study, if we consider the whole film surface, at the end of three weeks (Fig. 3.14.c and Fig. 3.15. c, respectively).

Therefore, the most homogeneous mineralization was obtained on the MP Fb_a films, indicating that cell organization and mineralization is better controlled with cell alignment within the grooves of the micropattern especially when supported by chemical cues.

3.2.2.4. Cell Alignment Evaluation

3.2.2.4.1. Fluorescence Microscopy

Effect of the surface topography and chemistry on the cell morphology and actin cytoskeleton organization was determined by microscopy. Cells were seeded on the polymeric films and TCP, and were prepared for microscopy at the end of 24 h, 1 week and 3 week incubation periods.

3.2.2.4.1.1. Acridine Orange Staining

As a preliminary study, cells seeded on the macropatterned films and on the films with both unpatterned and micropatterned regions were fixed and stained with Acridine Orange at the end of three week incubation period to determine the effect of the surface topography and chemistry on the spreading direction of the cells.

No orientation was observed towards a specific direction on the macropatterned films with or without adsorbed Fb probably because the pattern dimensions were much larger than dimensions of a single cell (Fig. 3.16.a and b). On the other hand cells on the macropatterned film with adsorbed Fb (MacP Fb_a) were higher in amount and spread homogeneously when compared to the cells on the macropatterned film without Fb (MacP), which formed small cell clumps (located centrally in Fig. 3.16.a).

Cells on the micropatterned films (MP) did not show a proper orientation either, and formed cell-to-cell contacts (even with the cells on the unpatterned

region) some being perpendicular to the axis of the micropattern (Fig. 3.16.c). In contrast, cells on the micropatterned film with adsorbed Fb (MP Fb_a) showed a perfect orientation in the direction of the micropattern axis (Fig. 3.16.d and e). The cells on the micropatterned region were confined within the grooves, few cells were observed on the ridges, and this indicated that the Fb had been adsorbed successfully within the grooves and cells followed this chemical cue. The cells on the unpatterned region of the film spread randomly without any orientation. Cells on the MP films (Fig. 3.16. c) were lower in amount than those on the MP Fb_a films (Fig. 3.16. d), which indicated that Fb had a significant effect on cell attachment to and thus proliferation on the film surface.

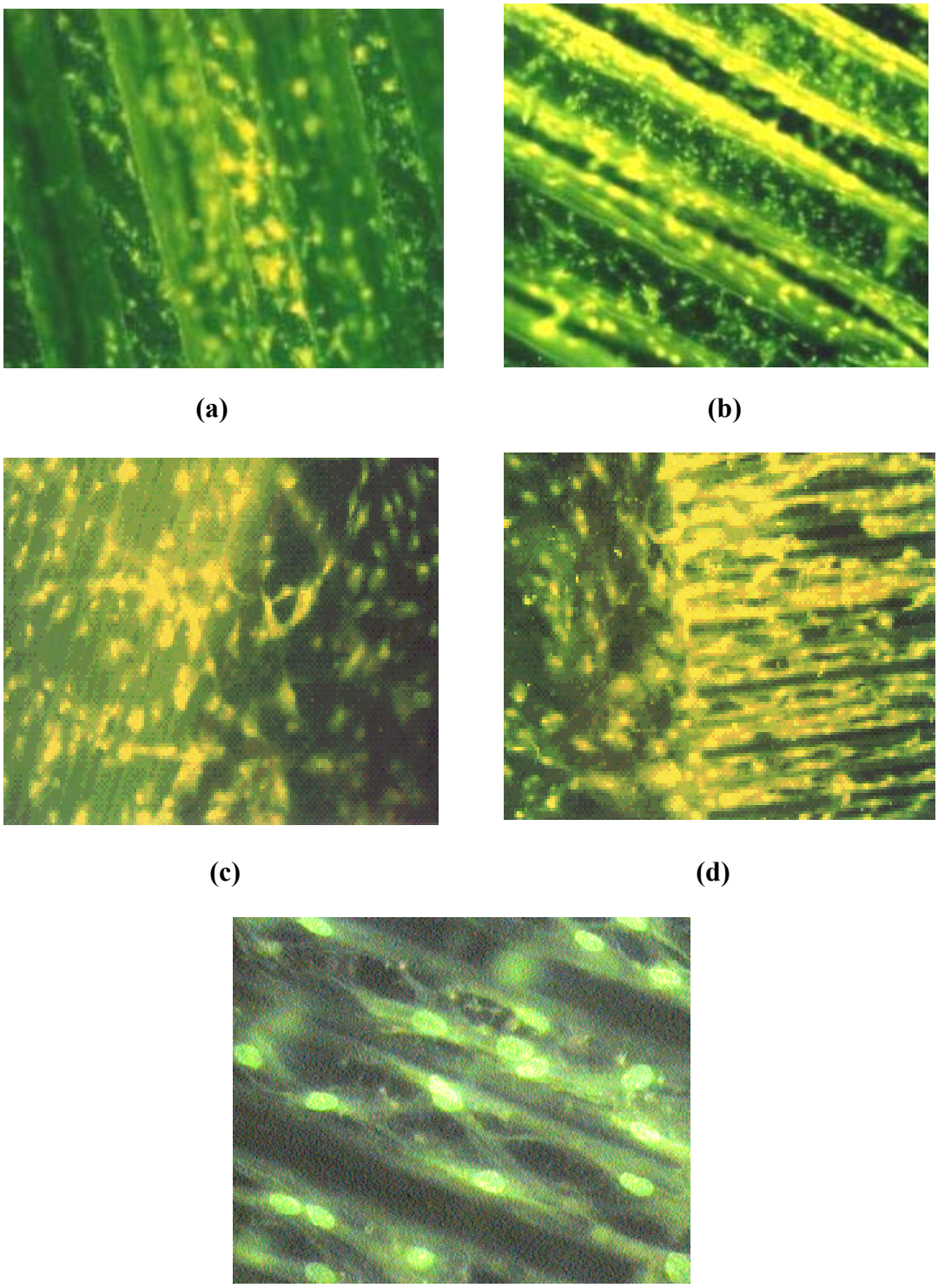

Figure 3.16. Cell distribution on the films with different surface topography and chemistry, stained with Acridine Orange a) macropatterned film (x40), b) macropatterned film with adsorbed Fb (x40), c) micropatterned film (x40), d and e) micropatterned film with adsorbed Fb (x40, x200)

3.2.2.4.1.2. Phalloidin Staining

In order to visualize actin filament orgnization of the cell cytoskeleton the cells seeded on the TCP, unpatterned and micropatterned films with and without adsorbed fibrinogen and with covalenrly immobilized fibrinogen were stained with Phalloidin at the end of 24 h, 1 week and 3 weeks. Some samples were also stained with the nuclear stain Sytox Orange following the Phalloidin staining, to be able to comment on nuclear alignment.

Twenty four hours after cell seeding, cells, a large number of which remained in circular form, were attached on all surfaces. Actin filament organization could, therefore, not be observed in a large number of them. It was, however, possible to deduce the initial cell-surface interaction. Most of the cells on the UNP Fb_a samples were in spread form, while those on the UNP films were still circular (Fig. 3.17. a and b). Similar results were obtained by Yang et al. (2001), who found negligible osteoblast adhesion and spreading on PLA while more spreading was recorded on the fibronectin adsorbed or RGD peptide coupled PLA surfaces, 5 h post-seeding. In addition, Nebe et al. (2001) showed that both osteosarcoma and epithelial cells exhibit rounded cell shape due to reduced spreading on PHB discs at the end of 24 h. The cells on the MP film surface formed large cell aggregates with no evidence of cell spreading (Fig. 3.17. c), which can be attributed to the hydrophobic nature of the polymer. On the other hand cells on the MP Fb_a were distributed homogeneously in much smaller cell groups, most of which were on the side walls of the grooves (Fig. 3.17. d). Osteoblasts on the MP Fb_i samples were grouped as small cell aggregates also with few cells in spread form (Fig. 3.17. e). All these results show the contribution of Fb to cell attachment and spreading.

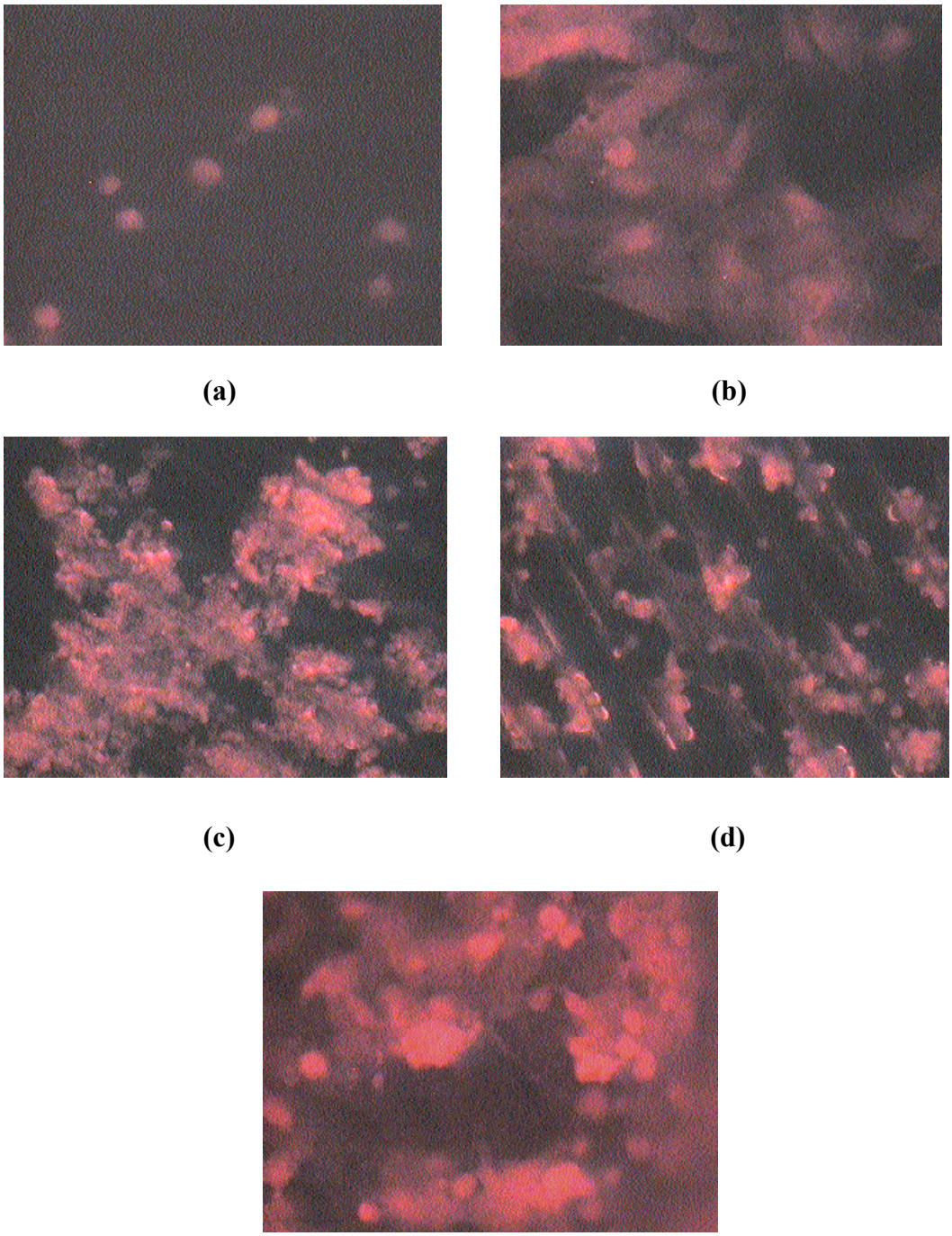

Figure 3.17. Osteoblast distribution on the micropatterned and unpatterned films with different surface chemistry 24 h post-seeding. a) UNP (x200), b) UNP Fb_a (x200), c) MP (x100), d) MP Fb_a (x100), e) MP Fb_i (x200) stained with Phalloidin

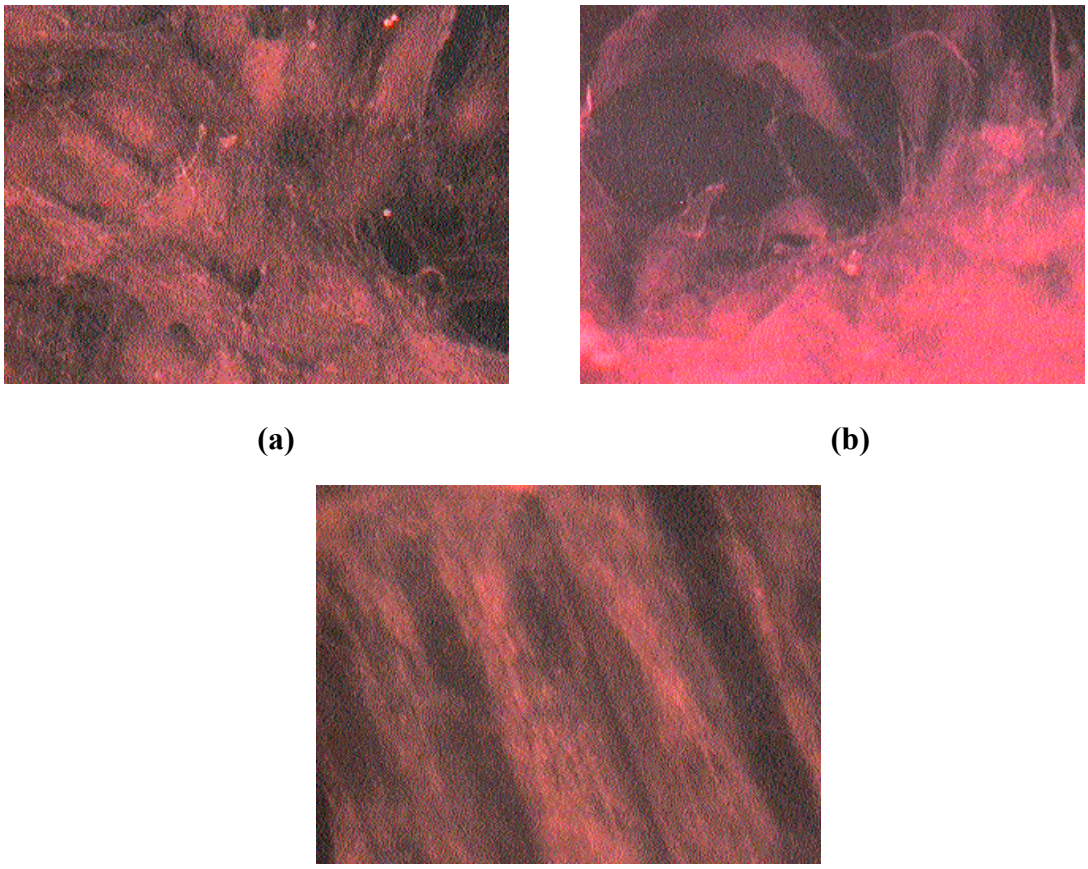

(a) **(b)**

(c)

Figure 3.18. Actin filament organization of cells three weeks post-seeding**.** a) TCP (x200), b) UNP Fb_a (x200), and c) MP Fb_a (x200), stained with Phalloidin

There was no significant difference between week one and week three in terms of actin filament organization, except the 3D interconnections across the ridges on MP Fb_a and MP Fb_i films on the third week. In general cells on the unpatterned surfaces, UNP and TCP, showed curved actin bundles due to random cell orientation (Fig. 3.18. a and b). Actin filaments of the cells within the grooves of MP Fb_a, however, were oriented parallel to the groove direction (Fig. 3.18. c). Similar actin filament orientations were observed by Wang et al. (2000), who cultured MC3T3-E1 osteoblasts on micropatterned (5 μm groove width, 2 μm ridge width and 2 μm

groove depth) and smooth silicone surfaces. The single cells, which were spread at the edges of the grooves of MP films, showed the same behavior. With MP Fb_i samples, actin filament organization could not be visualized at the end of first week due to the opaque nature of the film, but cells were confined mostly within the grooves in patches. Actin filament organization of the 3D cell structures, that is a) globular cell aggregates on MP films, b) interconnections of thick cell layers across the ridges of MP Fb_a and MP Fb_i films, and c) bone nodules of MP Fb_a, UNP and UNP Fb_a films, could not be visualized due to the high stain intensity.

When Sytox Orange was used along with Phalloidin, nuclei were also distinctly visible. Nuclei of the cells on the unpatterned surfaces had no apparent specific orientation and made a mean angle of 63.2 degrees with the horizontal line (Fig. 3.19. a,b,e and f). Nuclei on the MP Fb_a films, however, were mostly oriented parallel to the groove direction with a mean deviation angle of 13.1 degrees (Fig. 3.19. d). Even this deviation could have been avoided if the dimensions of the grooves were not larger than the dimensions of individual cells. In the present case three cells could stay side by side and thus, not all cells within the groove could align properly. The nuclei of the cells residing at the edges of the grooves were perfectly aligned along with the cells, but the nuclei of the cells extending from one wall of the groove to the other were not aligned properly (Fig. 3.19. c and d). Although the exact mechanism is not clear, the cell alignment, and thus nuclear alignment, may be due to physical restriction on the formation of certain linear bundles of microfilaments involved in cell locomotion (Dunn and Heath, 1976). Therefore, the reason of deviation from the perfect alignment can be attributed to the groove width of our micropattern being large and thus unable to restrict physically each cell from both sides.

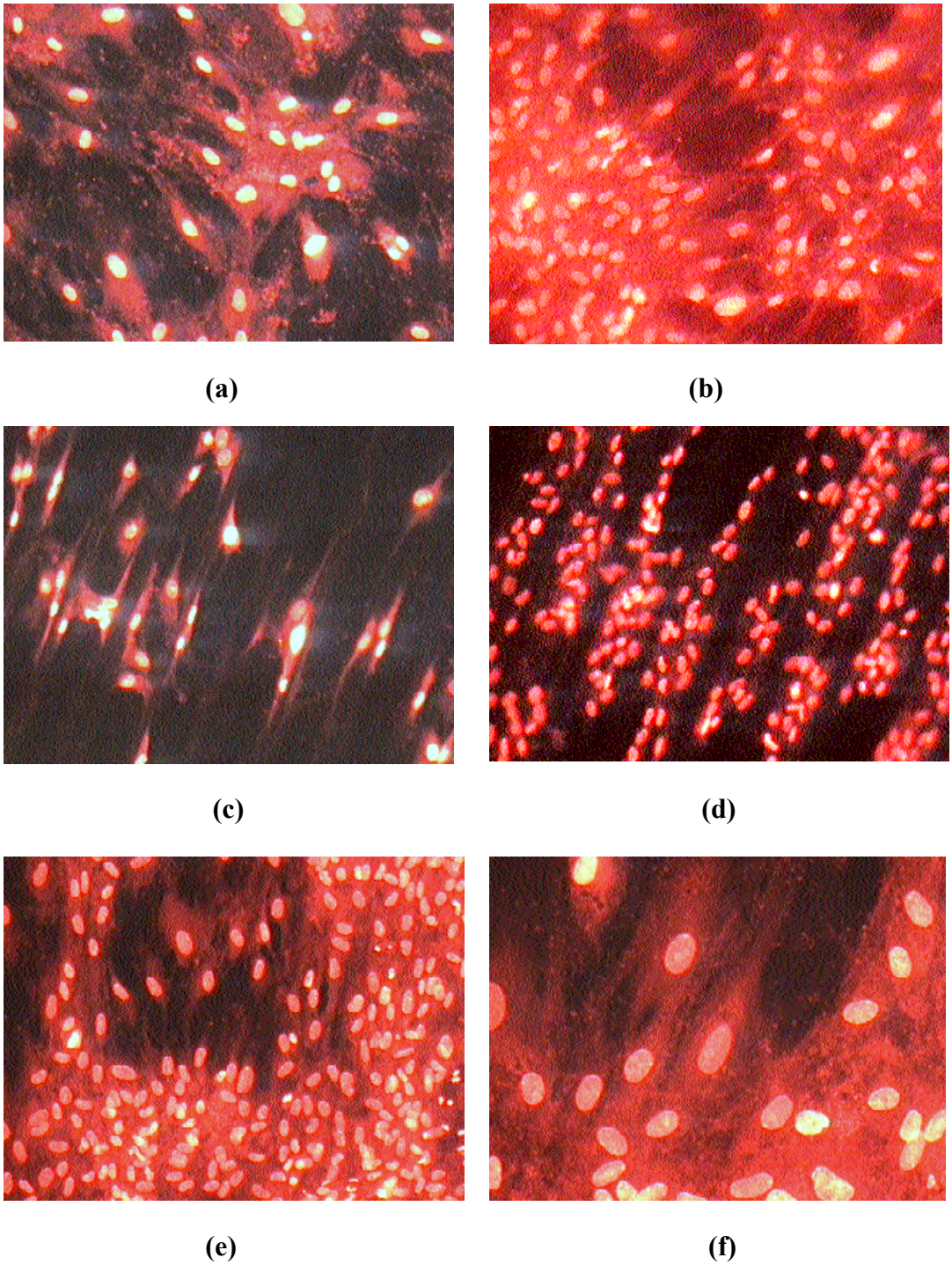

Figure 3.19. Cell and nuclei distribution, visualized by Phalloidin and Sytox Orange staining. a) UNP (x100) and c) MP surface, when seeded in dilute concentrations; b) UNP Fb_a (x100), e,f) TCP (x100 and x200), three weeks posseeding **;** d) MP Fb_a (x100), one week post seeding

This was supported by Wang. (2000), who found that nuclei of all osteoblasts on the micropatterned surface with 5 and 2 μm in groove and ridge width, respectively, and 2 μm in groove depth were aligned parallel to the groove direction. Grooves with 5 μm width could restrict physically the osteoblasts on both sides, while our substrate grooves with 27 μm width could not achieve this in an effective manner, unless the cells adhered to the edges of the grooves.

Another support comes from the study of Miller et al. (2001), who seeded Schwann cells on microgrooved PDLA films and found that the groove width was the key parameter for the alignment of these cells. The width of the Schwann cells varied between 5 and 10 μm and pattern widths or spacings of 10-20 μm were found to be optimal for alignment.

3.2.2.4.1.3. BCECF Staining

The importance of BCECF stain is that the cells are stained while viable, without fixing, and this results in a more true-to-life microscopic examination. BCECF staining was done at the end of one and three week incubation periods while eliminating possible cell losses or pattern deformations during the wash steps of the fixation procedures.

One week post-seeding, a very homogeneous cell distribution was obtained on the TCP, UNP Fb_a and MP Fb_a films (Fig. 3.20. b,d, and f). While the cells on the unpatterned surfaces were oriented randomly with no apparent preference (Fig. 3.20. b and f), the ones on the MP Fb_a samples (Fig. 3.20. d) were confined within the

grooves and aligned parallel to the axis of the grooves. Alignment of osteoblasts parallel to the groove direction on micropatterned surfaces with groove widths ranging from 1 to 42 μm was shown by several resarchers (Matsuzaka et al. (1999), Perizzolo et al. (2001), Wang et al. (2000)). The cell distribution on the UNP films was patchy in appearance (Fig. 3.20. a), some patches interconnected while the others not, and some being organized like bone nodule structures. Completely different from these patterns, cells on the MP film (Fig. 3.20. c) formed large globular cell aggregates (starting in the third day of incubation) which were not interconnected. Single cells were observed at the edges of the grooves, aligned parallel to groove direction. These results revealed the invaluable effect of the Fb in homogeneous cell attachment and distribution on the films, and showed that the untreated polymer surface is not suitable for cell accomodation, in agreement with the studies of Yang et al. (2001) and Nebe et al. (2001) carried out with PLA and PHB, respectively.

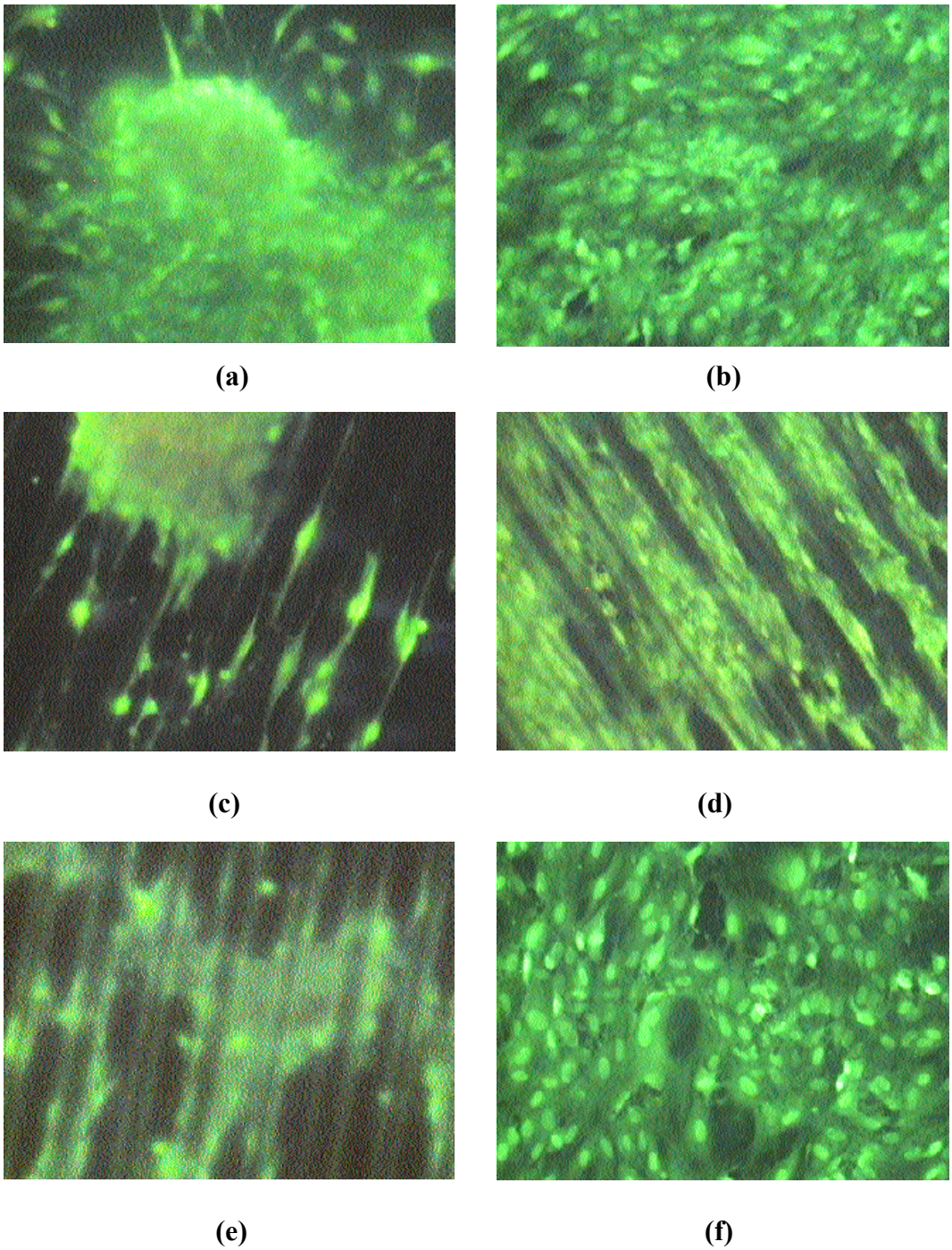

Figure 3.20. Cell organization on the surfaces with different microtopography and chemistry, one week post-seeding (x100). a) UNP, b) UNP Fb_a, c) MP, d) MP Fb_a, e) MP Fb_i, and f) TCP stained with BCECF

A multilayer of cells was observed on all surfaces except the MP Fb_i film. This could be caused by covalently immobilized Fb retarding cell migration, or could be due to low cell number with homogeneous non-confluent distribution. Multilayered osteblast structures and globular aggregates (possibly bone nodules) were observed on the Ti and hydroxyapatite coated surfaces within two weeks in the study of Perizzolo et al. (2001). The cells on the MP Fb_i film were found both in the grooves and on the ridges, with the ones within the grooves being interconnected with the cells on the ridges. The cell distribution was very irregular with large unoccupied regions on the film, but single cells found at the ridges of the grooves were aligned parallel to the groove axis.

No apparent change was observed in the cell distribution pattern on the MP and UNP films at the end of 3 weeks (Fig. 3.21. a and c). However, bone nodule formation took place on the TCP, UNP Fb_a, MP Fb_a and MP Fb_i films. Bone nodule formation involved relocation of cells, leaving gaps behind. These gaps were almost homogeneously distributed on the TCP, while those on the UNP Fb_a and MP Fb_a were scattered in several places; usually larger central one was formed on the UNP Fb_a samples. Nodules on the UNP Fb_a and MP Fb_a were integrated into homogeneous cell layers. The nodules on the MP Fb_i were at the edges of cell layer pathches, and the ones on TCP were interconnected by the cells. Cell alignment on the MP Fb_a samples was undisturbed, except in places where bone nodule formation took place across the ridges.

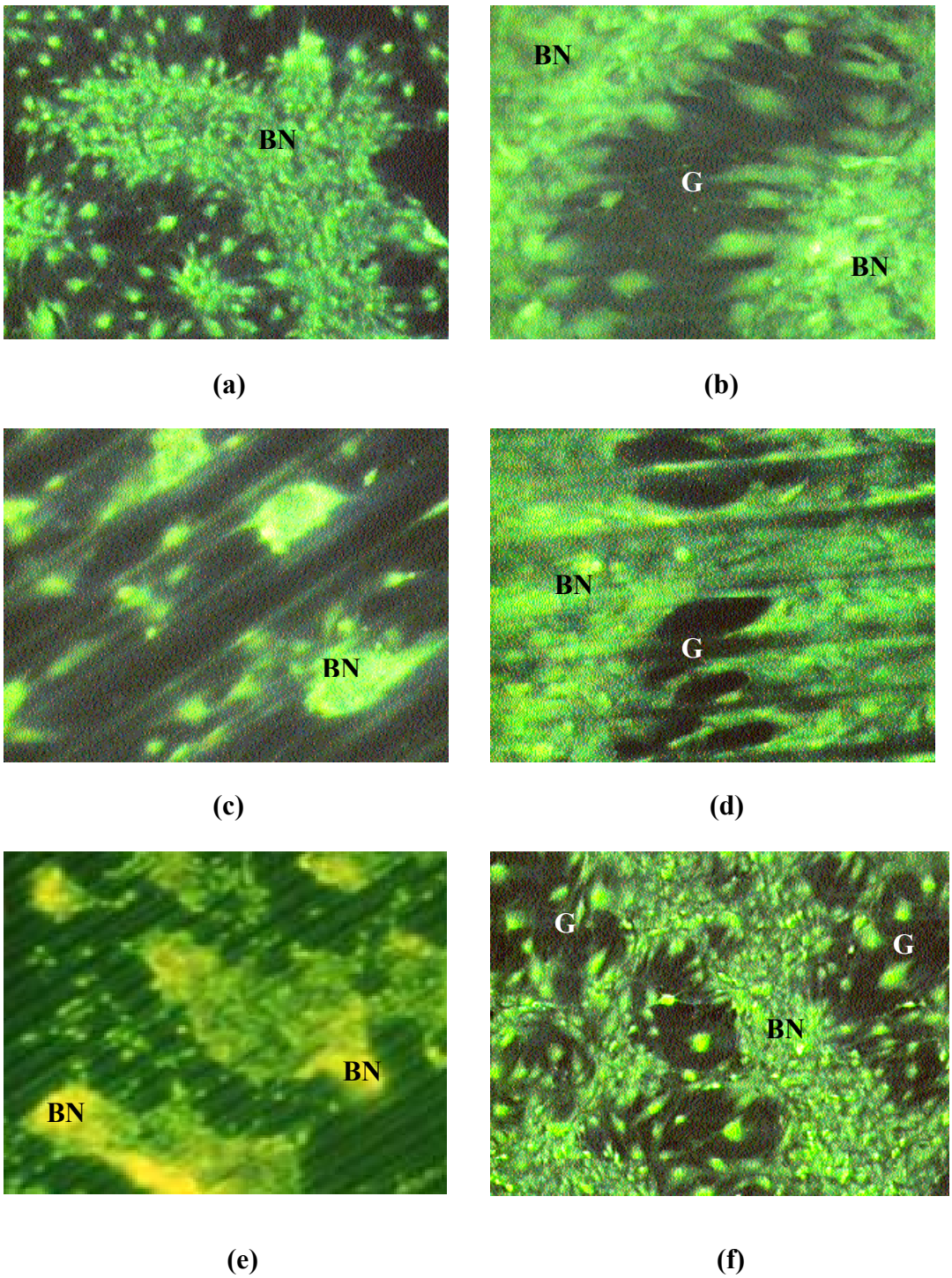

Figure 3.21. Cell organization on the surfaces with different microtopography and chemistry, three weeks post-seeding. a) UNP (x40), b) UNP Fb_a (x100), c) MP (x100), d) MP Fb_a (x100), e) MP Fb_i (x40), and f) TCP (x40), stained with BCECF. **BN**: bone nodule, **G**: gap left behind due to cell movements

3.2.2.4.2. Scanning Electron Microscopy

Scanning electron micrographs of cells on unpatterned, macropatterned and micropatterned films were obtained at the end of one and three week incubation periods.

At the end of first week, in agreement with the BCECF staining results, cell clump formation was observed on the UNP films while an even cell distribution was present on the UNP Fb_a films (Fig. 3.22.a and b).

The ridges of macropatterned films (MacP) were not intact due to gas bubble formation during the solvent evaporation step of film formation. Cells on the MacP film were observed to reside at the bottom of the grooves, and formed globular clumps, some of which were interconnected (Fig. 3.22.c). However, cells on the MacP Fb_a were found both on the ridges and in the grooves, and formed a sheet-like 3D cell layer at the bottom of a groove, which was connected to the cell layers on the ridges (Fig. 3.22.d). As expected, no cell orientation could be detected on the macropatterned films. Fig. 3.22.e shows the cell clump formed accross the ridges on the MP film, and Fig. 3.22.f shows the sheet of aligned cells within the grooves of MP Fb_a sample, previously mentioned in section 3.2.2.4.1.3.

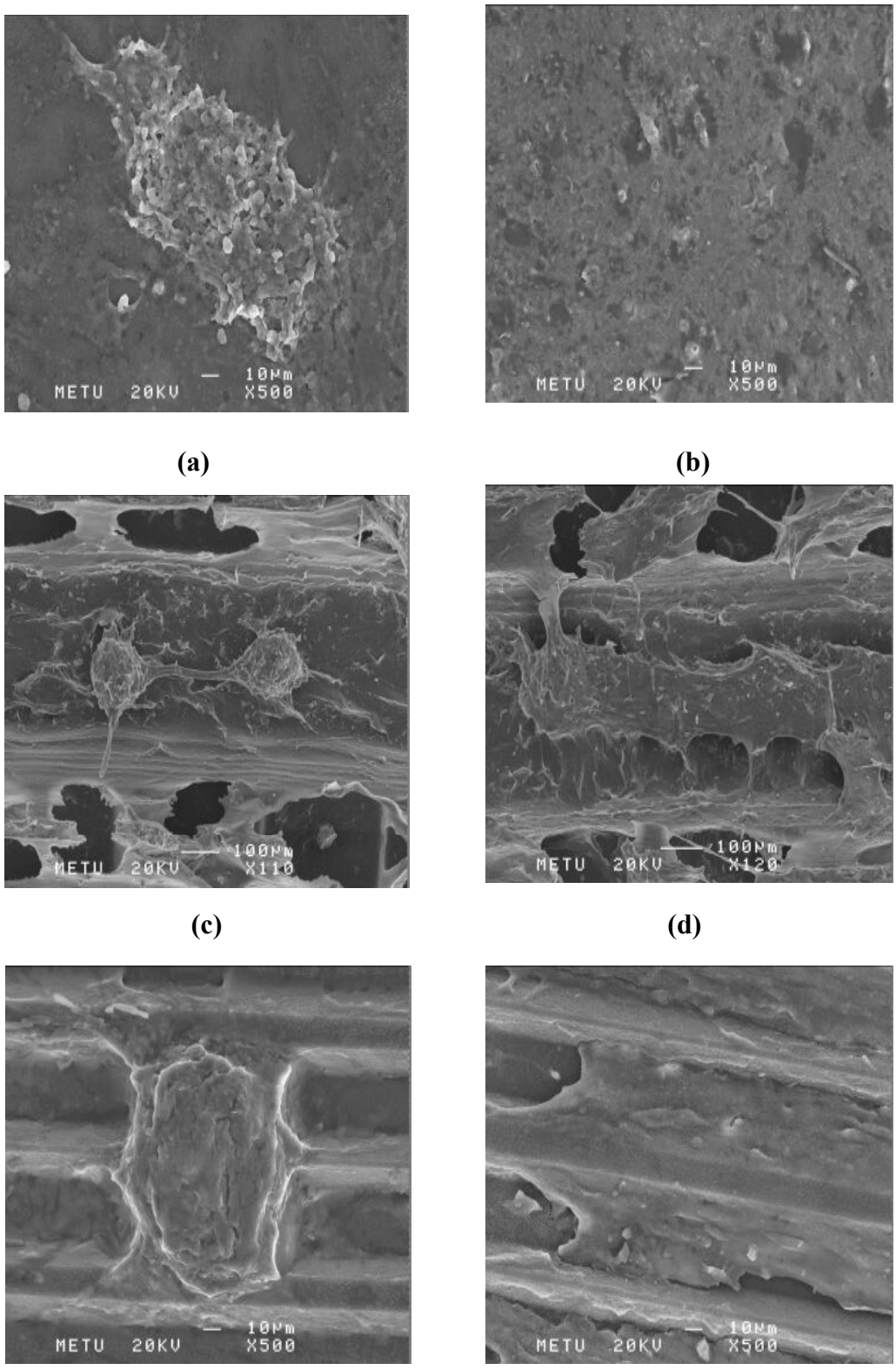

Figure 3.22. Scanning electron micrographs of cells on the films with different surface topography and chemistry, one week post-seeding, a) UNP, b) UNP Fb_a, c) MacP, d) MacP Fb_a, e) MP, and f) MP Fb_a

At the end of three weeks, cell movement towards a cell layer leaving an empty space or gap behind, was seen on the UNP film (Fig. 3.23.a). There was no change in cell organization on the MacP and MP films between the first and third weeks (Fig. 3.23. c and e). Small gap formations were observed within the homogeneous cell layers of UNP Fb_a and MP Fb_a samples, caused by cell movements to form bone nodules (Fig. 3.23.b and f). The other regions of the MP Fb_a samples, still contained the aligned cell layers. Both aligned and non-aligned single cells, which crossed the ridge to interact with other cells within a groove, were observed on the MP film (Fig. 3.23.e).

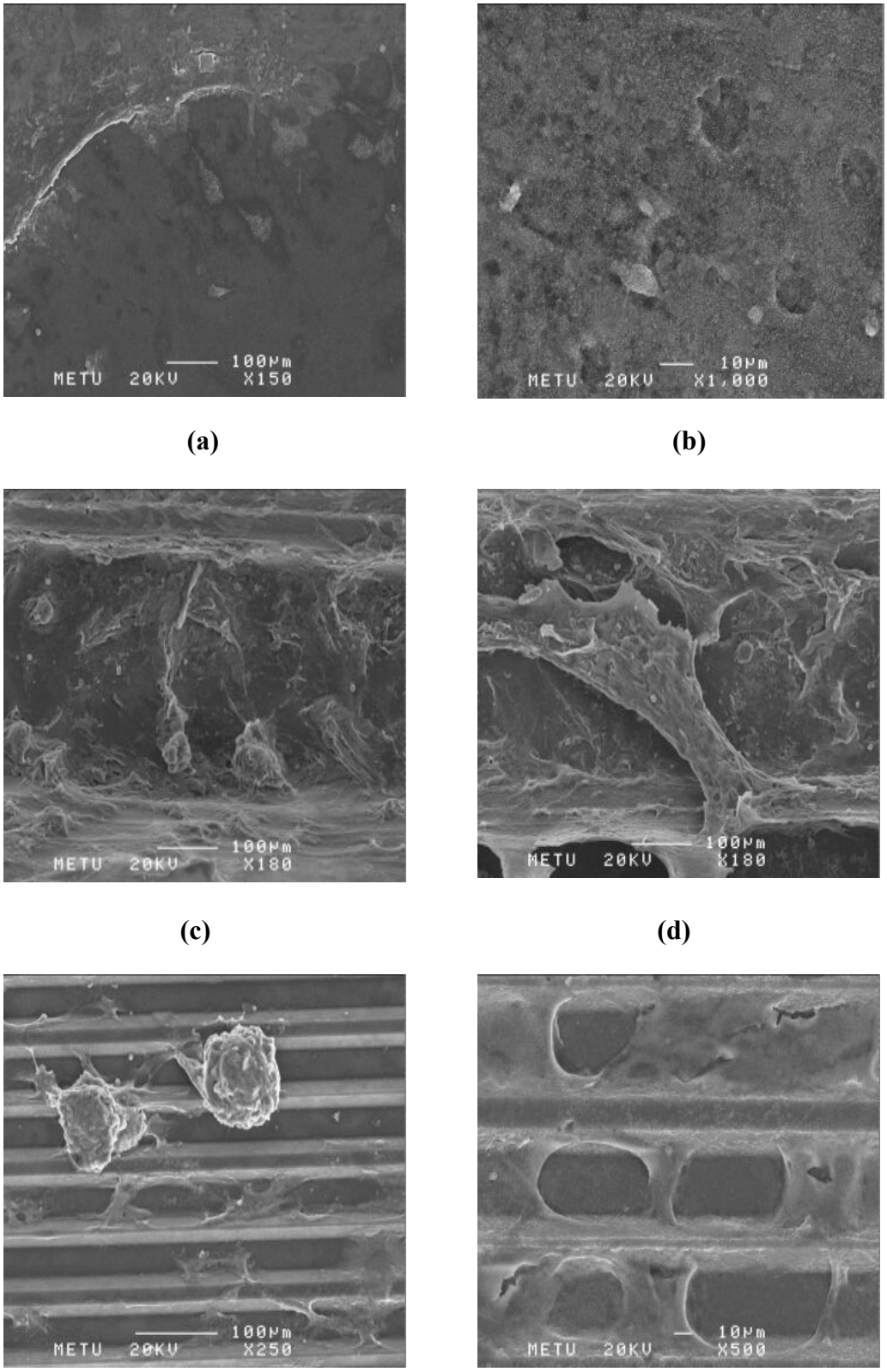

(a) **(b)**

(c) **(d)**

(e) **(f)**

Figure 3.23. Scanning electron micrographs of cells on the films with different surface topography and chemistry, three weeks post-seeding, a) UNP, b) UNP Fb_a, c) MacP, d) MacP Fb_a, e) MP, and f) MP Fb_a

Fig. 3.24.a shows that it is still possible to align the cells on the MP films, when they attach to the side walls of the grooves. It is possible to differentiate the lamellipodia of single cells and their contact sites with the side walls of the grooves in Fig. 3.24.b. It can be seen that a cell forming contact with opposite side walls of a groove may deviate from perfect alignment, since the groove width is larger than the size of an elongated osteoblast.

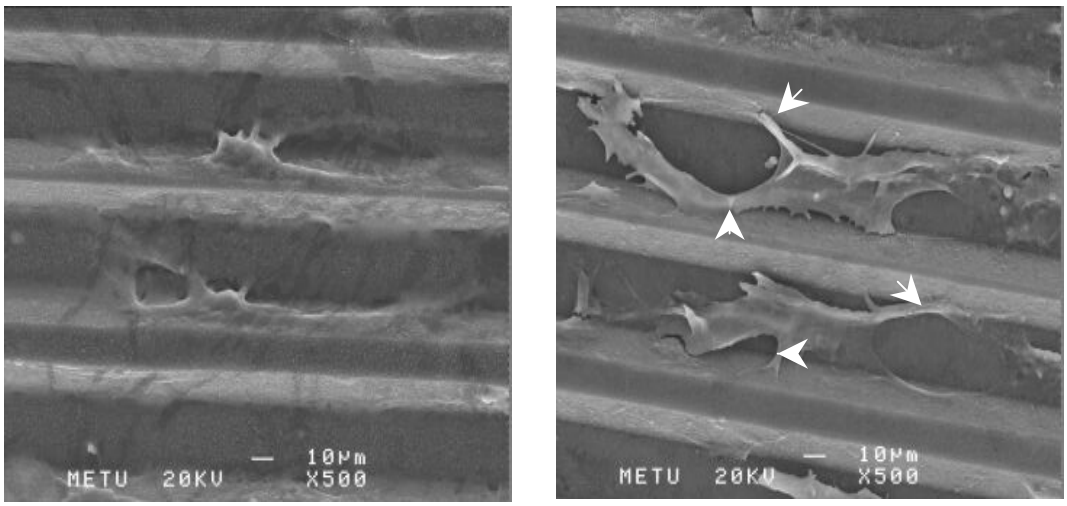

Figure 3.24. Scanning electron micrographs of single cells on a) MP, and b) MP Fb_a films. Arrow heads show the lamellipodia of the spread cells

To sum up, fluorescence and scanning electron microscopy revealed that fibrinogen had an invaluable role in achieving a homogeneous cell distribution on the polymeric surfaces and it served as an effective chemical cue to guide osteoblasts within the grooves of micropatterned films. Alignment of cells along the axis of the grooves with a mean deviation angle of 13.1 degrees was achieved on the MP Fb_a films. The cells on the MP and MacP films formed large cell aggregates, and those on the UNP and MP Fb_i films were distributed in patches, which were frequently

interconnected. Single cells attached on the side walls of the grooves of MP and MP Fb_i were found to be aligned along the groove axis. A very homogeneous cell distribution was obtained on the TCP control, UNP Fb_a and MacP Fb_a films with no preferred cell orientation direction. Bone nodule formation, which involved relocation of cells, was revealed on the TCP, unpatterned and micropatterned films, at the end of the third week. Cell relocations led to gap formations. The gaps were homogeneously scattered on TCP and were several in number on UNP Fb_a and MP Fb_a, one of them being large and central on the UNP Fb_a. At the end of first week, an osteoblast cell sheet was formed in the grooves of MacP Fb_a films that was connected to the smaller ones on the ridges.

CHAPTER 4

CONCLUSION

PHBV and PLA are two biodegradable polymers, natural and synthetic in origin, respectively, that are widely used in medical applications. A blend of PHBV (with 8% molar hydroxyvalerate) and P(L/DL)LA (70:30) was chosen to serve as a carrier for osteoblast cells in this study. The sharp features of the micropatterned template, produced by photolithography, were replicated successfully by this polymer blend, resulting in a polymer film with parallel microgrooves (ridge width 27 μm, groove width 2 and 12 μm alternating and groove depth 20 μm) and very a smooth texture. The carrier surfaces were chemically modified by fibrinogen (Fb) adsorption or covalent immobilization to promote cell adhesion on the hydrophobic carrier by either increasing the surface hydrophilicity or providing integrin binding sites, that is RGD amino acid sequences. In addition to that, Fb was also used to serve as a chemical cue for cell guidance on the patterned films. Increase in surface hydrophilicity was obtained as a result of Fb adsorption, however more hydrophobic surfaces were obtained with Fb covalent immobilization. Fb was immobilized on the micropatterned films via epichlorohydrin spacer with an expectation that a more uniform and stable Fb conformation is maintained for long time that will better support cell adhesion. Epichlorohydrin treatment partially digested one of the

polymers in the blend, although this did not affect the features of the micropattern. A homogeneous Fb immobilization was achieved throughout the micropatterned film surface that was revealed by Coomassie Brillant Blue staining.

Characterization of osteoblasts was carried out by microscopy. Osteoblasts spread on the glass coverslip surface exhibited a typical polygonal morphology. Microscopic observations revealed the presence of a non-osteoblastic cell type, probably osteoclast precursor or osteoclast, in the cell culture, suggesting that the cell isolation procedure is not totally exclusive to cell types other than mesenchymal stem cell lineage.

Biochemical and morphological characterization of osteoblasts seeded on the films with different microtopography and surface chemistry was done by ALP assay, tetracycline labelling of mineral deposited by osteoblasts, and fluorescence and scanning electron microscopy. MTS test was carried out to determine the cell growth on the films. Microscopic examination showed that cell alignment was achieved on the micropatterned films with adsorbed Fb, where cells were confined within the grooves due to selective adsorption of Fb, which served as a chemical cue. Cell distribution on the micropatterned films with covalent immobilized Fb was random due to homogeneous Fb immobilization throughout the film surface, unless the cells attached to the side walls of the grooves. No preferred cell orientation was observed on the unpatterned and macropatterned films, whose dimensions were too large when compared to the cell dimensions. Adsorbed Fb was found to be invaluable in homogeneous cell attachment and distribution on the films. Bone nodule formations were observed at the end of three weeks. Although adsorbed Fb better promoted cell proliferation, there was no significant difference among cell numbers on all the films,

at the end of three weeks. Presence of a micropattern on the surface made no difference in terms of cell proliferation, in long run. The mineralization on the samples was in vesicular form at the end of first week, and assumed a more crystalline appearance at the end of the third week. Generally, minerals were confined to the inner part of the nodules. The most homogeneous mineral deposition was observed on the micropatterned films with adsorbed Fb. In general, ALP activity, which was low on the first week and much higher on the third week, was obtained on all surfaces. A negative correlation was observed between the cell proliferation rate and ALP activity within a group, which is an indication of differentiated osteoblast phenotype. ALP specific activity was higher on the Fb adsorbed unpatterned and micropatterned films when compared to that on the TCP control. The highest ALP specific activity was obtained on the micropatterned films with adsorbed Fb, indicating the synergistic effect of the physical (micropattern) and chemical (adsorbed Fb) cues.

To conclude, this study revealed that the physical cue on the PHBV-P(L/DL)LA alone was not effective in guiding osteoblast cells, but use of both chemical and physical cues resulted in cell alignment along the axis of the grooves. Cell alignment led to a more homogeneous cell and mineral distribution on the film surface and better promoted osteoblast phenotype expression, as indicated by ALP specific activity, although had no effect on cell proliferation. Therefore, osteoblast guidance shows a great promise for development of more functional tissue- engineered bone constructs.

REFERENCES

Anderson H.C. Chapter 4: Matrix vesicles of cartilage and bone. In *The Biochemistry and Physiology of Bone vol IV Calcification and Physiology*. Ed: Bourne G.H., NY, 1976; pp. 135-157

Attawia M.A., Herbert K.M., Uhrich K.E., Langer R., Laurencin C.T. Proliferation, morphology, and protein expression by osteoblasts cultured on poly(anhydride-co-imides). *Appl Biomater* 1999; 48: 322-327

Barrera D.A., Zylstra E., Lansbury P.T., Langer R. Copolymerization and degradation of poly(lactic acid-co- lysine). *Macromolecules* 1995; 28: 425-432

Bennett S., Connolly K., Lee D.R., Jiang Y., Buck D., Hollinger J.O., Gruskin E.A. Initial biocompatibility studies of a novel degradable polymeric bone substitute that hardens in situ. *Bone* 1996; 19: 101S-7S

Bhatia S.N., Balis U.J., Yarmush M.L., Toner M. Effect of cell–cell interactions in preservation of cellular phenotype: cocultivation of hepatocytes and nonparenchymal cells *FASEB J* 1999; 13: 1883–1900

Bissel M.J., Hall H.G., Parry G. How does the extracellular matrix direct gene expression? *J Theor Bio* 1982; 99: 31-68

Bradford M.M. A rapid and sensitive method for the quantitation of microgram quantities of protein utilizing the principle of protein-dye binding. *Analytical Biochemistry* 1976; 72: 248-54

Bruder S.P.**,** Jaiswal N., Ricalton N.S., Mosca J.D., Kraus K.H., Kadiyala S. Mesenchymal stem cells in osteobiology and applied bone regeneration. *Clin Orthop* 1998; 355: S247-256

Brunette D.M., Kenner G.S., Gould T.R. Grooved titanium surfaces orient growth and migration of cells from human gingival explants. *J Dent Res* 1983; 62(10):1045

Buckwalter J.A., Glimcher M.J., Cooper R.R., Recker R. Bone Biology Part I: Structure, blood supply, cells, matrix, and mineralization. *J Bone Joint Surg* 1995; 77-A:1256-72

Buckwalter J.A., Glimcher M.J., Cooper R.R., Recker R. Bone Biology Part II: Formation, form, modeling, remodeling, and regulation of cell function. *J Bone Joint Surg* 1995; 77-A:1276-83

Burg K.J.L., Porter S., Kellam J.F. Biomaterial developments for bone tissue engineering. *Biomaterials* 2000; 21: 2347-59

Caplan A., Boyan B. Endochondral bone formation: the lineage cascade. In: *Bone*, *vol. 8*. Ed. Hall B. London: CRC Press, 1994; pp. 1-46

Chehroudi B., Brunette D.M., McDonnell D.M. The effects of micromachined surface on formation of bonelike tissue on subcutaneous implants as assessed by radiography, and computer image processing. *J Biomed Mater Res* 1997; 34: 279-290

Chen G., Ushida T., Tateishi T. Poly(DL-lactic-co-glycolic acid) sponge hybridized with collagen microsponges and deposited apatite particulates. *J Biomed Mater Res* 2001; 57: 8-14

Coelho M.J., Carbal A.T., Fernandes M.H. Human bone cell cultures in biocompatibility testing. Part I: osteoblastic differentiation of serially passaged human bone marrow cells cultured in α-MEM and in DMEM. *Biomaterials* 2000; 21: 1087-1094

Coelho M.J. and Fernandes M.H. Human bone cell cultures in biocompatibility testing. Part II: effect of ascorbic acid, β-glycerophosphate and dexamethasone on osteoblastic differentiation. *Biomaterials* 2000; 21: 1095-1102

Curtis A. and Rielhe M. Tissue Engineering: the biophysical background. *Phys Med Biol* 2001; 46: R47-R65

Curtis A. and Wilkinson C. Topographical control of cells. *Biomaterials* 1997; 18: 1573-83

Desai A.T. Micro- and nanoscale structures for tissue ngineering constructs. *Medical Eng & Phys* 2000;22:595-606

Deutsch J., Motlagh D., Russell B., Desai T.A. Fabrication of microtextured membranes for cardiac myocyte attachment and orientation. *J Biomed Mater Res Appl Biomater* 2000; 53(3): 267-75

Domb A.J., Amselem S., Langer R., Maniar M. Polyanhydrides as carriers of drugs. In *Biomedical Polymers*, NY: Hanser Publishers 1994; pp. 69-96

Dunn G.A., Heath J.P. A new hypothesis of contact guidance in tissue cells. *Exp Cell Res* 1976; 101: 1-14

Eisenbarth E., Linez P., Biehl V., Velten D., Breme J., Hildebrand H.F. Cell orientation and cytoskeleton organisation on ground titanium surfaces. *Biomolecular Engineering* 2002; 19: 233-237.

Folch A. and Toner M. Microengineering of cellular interactions. *Annu Rev Biomed Eng* 2000; 02: 227-256

Green-Martins M. The dynamics of cell-ECM interactions with implications for tissue engineering. In *Principles of Tissue Engineering*, Eds. Lanza R.P., Langer R., Chick W.L., Texas USA 1997; pp. 23-37

Goldstein A.S., Juarez T.M., Helmke C.D., Gustin M.C., Mikos A.G. Effect of convection on osteoblastic cell growth and function in biodegradable polymer foam scaffolds. *Biomaterials* 2001; 22: 1279-88

Gupta S., Kim S.K., Vemuru R.P., Aragona E., Yerneni P.R., Burk R.D., Rha C.K. Hepatocyte transplantation: an alternative system for evaluating cell survival and immunoisolation. *Int J Artif Organs* 1993; 16(3): 155-63

Hammerle C.H., Olah A.J., Schmid J., Fluckiger L., Gogolewski S., Winkler J.R. The biological effect of natural bone mineral on bone neoformation on the rabbit skull. *Clin Oral Implants Res* 1997; 8: 198-207

Hasenbein M.E., Andersen T.T., Bizios R. Micropatterned surfaces modified with select peptides promote exclusive interactions with osteoblasts. *Biomaterials* 2002; 23: 3937-3942

Healy K.E., Thomas C.H., Rezania A., Kim J.E., McKeown P.J., Lom B., Hockberger E.P. Kinetics of bone cell organization and mineralization on materials with patterned surface chemistry. *Biomaterials* 1996; 17: 195-208

Heller J., Sparer R.V., Zentner G.M. Poly(ortho esters) for the controlled delivery of therapeutic agents. *J Bioact Comper Polym* 1990; 3(2): 97-105

Hendren W.H., Reda E.F. Bladder mucosa graft for construction of male urethra. *J Pediatr Surgery* 1986; 21: 189-192

Holmes P.A. Applications of PHB- a microbially produced biodegradable thermoplastic. *Phys Technol* 1985; 16: 32-36

Ikari Y., Fujikawa K., Yee K.O., Schwartz S.M. Alpha(1)-proteinase inhibitor, alpha(1)-antichymotrypsin, or alpha(2)-macroglobulin is required for vascular smooth muscle cell spreading in three-dimensional fibrin gel. *J Biol Chem* 2000; 275 (17): 12799-805

Jiang Y., Jahagirdar B.N., Reinhardt R.L., Schwartz R.E., Keene C.D., Ortiz-Gonzalez X.R., Reyes M., Levnik T., Lund T., Blackstad M., Du J., Aldrich S., Lisberg A., Low W.C., Largaespada D.A., Verfaillie C.M. Pluripotency of mesenchymal stem cells derived from adult marrow. *Nature* 2002; 20 June : 1-9

Kane R.S., Takayama S., Ostuni E., Ingber D.E., Whitesides G.M. Patterning proteins and cells using soft lithography. *Biomaterials* 1999; 20: 2363-76

Khor E. and Lim L.Y. Implantable applications of chitin and chitosan. *Biomaterials* 2003; 24(13): 2339-49

Kim B-S., Mooney D.J. Development of biocompatible synthetic extracellular matrices for tissue engineering. *TIBTECH* 1998; 16: 224-230

Kim B-S., Baez C.E. Atala A., Biomaterials for tissue engineering. *World J Urol* 2000; 18: 2-9

Köse G.T. Ph.D. thesis, Middle East Technical University, Ankara, Turkey 2002

Lagasse E., Connors H., Al-Dhalimy M., Reitsma M., Dohse M., Osborne L., Wang X., Finegold M., Weissman I.L., Grompe M. Purified hematopoietic stem cells can differentiate into hepatocytes *in vivo*. *Nature Medicine* 2000; 6: 1229-1234

Langer R., and Vacanti J.P. Tissue engineering. *Science* 1993; 260: 920-925

Lee K.Y., and Mooney D.J. Hydrogels for tissue engineering. *Chemical Reviews* 2001; 101(7): 1869-79

Lopez G.P. Convenient methods for patterning the adhesion of mammalian cells to surfaces using self-assembled monolayers of alkanethiolates on gold. *J Am Chem Soc* 1993; 115: 5877

Marler J.J., Upton J., Langer R., Vacanti J.P. Transplantation of cells in matrices for tissue regeneration. *Adv Drug Del Rev* 1998; 33: 165-182

Matsuzaka K., Walboomers X.F., Ruijter J.E., Jansen J.A. The effect of poli-L-lactic acid with parallel surface micro groove on osteoblast-like cells in vitro. *Biomaterials* 1999; 20:1293-1301.

Meinhart J., Fussenegger M., Hobling W. Stabilization of fibrin-chondrocyte constructs for cartilage reconstruction. *Ann Plast Surg* 1999; 42(6): 673-8

Meinig R.P., Buesing C.M., Helm J., Gogolewski S. Regeneration of diaphyseal bone defects using resorbable poly(L/DL-lactide) and poly(D-lactide) membranes in the Yucatan pig model. *J Orthop Trauma* 1997; 11: 551-8

Miller C., Shanks H., Witt A., Rutkowski G.; Mallapragada S. Oriented Schwann cell growth on micropatterned biodegradable polimer substrates. *Biomaterials* 2001;22:1263-1269

Nebe B., Forster C., Pommerenka H., Fulda G., Behrend D., Bernewski U., Schmitz K-P., Rychly J. Structural alterations of adhesion mediating components in cells cultured on poly-β-hydroxy butyric acid. *Biomaterials* 2001; 22: 2425-2434

Orlic D., Kajstura J., Chimenti S., Jakoniuc I., Anderson S.M., Li B., Pickel J., McKay R., Nadal-Ginard B., Bodine D.M., Leri A., Anersa P. Bone marrow cells regenerate infarcted myocardium. *Nature* 2001; 410: 701-5

Pachence J.M. Collagen-based devices for soft tissue repair. *J Biomed Mater Res Appl Biomater* 1996; 33: 35-40

Pachence J.M. and Kohn J. Biodegradable polymers for tissue engineering. In *Principles of Tissue Engineering*, Eds. Lanza R.P., Langer R., Chick W.L., Texas USA 1997; pp273-286

Parfitt A.M. The cellular basis of bone remodeling: the quantum concept reexamined in light of recent advances in the cell biology of bone. *Calcif Tissue Int* 1984; 36: S37-45

Patel N., Padera R., Sanders G.H.W., Cannizzaro S.M., Davies M.C., Langer R., Roberts C.J., Tendler S.J.B., Williams P.M., Shakesheff K.M. Spacially controlled cell engineering on biodegradable polymer surfaces. *FASEB J* 1998; 12: 1447-1454

Peppas N.A. and Langer R. New challenges in biomaterials. *Science* 1994; 263: 1715-20

Perizzolo D., Lacefield W.R., Brunette D.M. Interaction between topography and coating in the formation of bone nodules in culture for hydroxyapatite- and titanium-coated micromachined surfaces. *J Biomed Mater Res* 2001; 56: 494-503.

Perka C., Spitzer R-S., Lindenhayn K., Sittinger M., Schultz O. Matrix-mixed culture: new methodology for chondrocyte culture and preparation of cartilage transplants. *J Biomed Mater Res* 2000; 49(3): 305-11

Peter S.J., Kim P., Yasko A.W., Yaszemski M.J., Mikos A.G. Cross-linking characteristics of an injectable poly(propylene fumarate)/β-tricalcium phosphate

paste and mechanical properties of the crosslinked composite for use as a biodegradable bone cement. *J Biomed Mater Res* 1999; 44: 314-21

Peter S.J., Lu L., Kim D.J., Mikos A.G. Marrow stromal osteoblast function on a poly(propylene fumarate)/β-tricalcium phosphate biodegradable orthopaedic composite. *Biomaterials* 2000; 21: 1207-1213

Petersen E.F., Spencer R.G.S., McFarland E.W. Microengineering neocartilage scaffolds. *Biotechnol Bioeng* 2002; 78: 802-805

Pins G.D., Toner M., Morgan J.R. Microfabrication of an analog of the basal lamina: biocompatible membranes with complex topographies. *FASEB J* 2000; 14: 593-602

Puelacher W.C., Vacanti J.P., Ferraro N.F., Schloo B., Vacanti C.A. Femoral shaft reconstruction using tissue-engineered growth of bone. *Int J Oral Maxillofac Surg* 1996; 25: 223-8

Risbud M.V., Sittinger M. Tissue engineering: advances in *in vitro* cartilage generation.*Trends in Biotechnology* 2002; 20(8): 351-6

Robey P.G., The biochemistry of bone. *Endocrinol Metab Clin North America* 1989; 18: 859-902

Rosen H.B., Chang J., Wnek G.E., Linhardt R.J., Langer R. Bioerodible polyanhydrides for controlled drug delivery. *Biomaterials* 1983; 4: 131-3

Saltzman W.M. Cell interactions with polymers. In *Principles of Tissue Engineering*, Eds. Lanza R.P., Langer R., Chick W.L., Texas USA 1997; pp225-236

Sam A.E., Nixon A.J. Chondrocyte–laden collagen scaffolds for resurfacing extensive articular cartilage defects. *Osteoarthritis Cartilage* 1995; 3: 47-59

Sanchez-Ramos J., Song S., Cardozo-Pelaez F., Hazzi C., Stedeford T., Willing A., Freeman T.B., Saporta S., Janssen W., Patel N., Cooper D.R., Sanberg P.R. Adult bone marrow stromal cells differentiate into neural cells *in vitro*. *Exp Neurol* 2000; 164: 247-256

Scotchford C.A., Ball M., Winkelmann M., Vörös J., Csucs C., Brunette D.M., Danuser G., Textor M. Chemically patterned, metal-oxide-based surfaces produced by photolithographic techniques for studying protein- and cell-interactions. II: Protein adsorption and early cell interactions. *Biomaterials* 2003; 24: 1147-1158

Sendil D., Gürsel I., Wise D., Hasırcı V. Antibiotic release from biodegradable PHBV microparticles. *J Control Rel* 1999; 59: 207-217

Sigma Catalog 2002/2003, Sigma-Aldrich Corporation , Deutschland Exp

Sikavitsas V.I., Temenoff J.S., Mikos A.G. Biomaterials and bone mechanotransduction. *Biomaterials* 2001; 22: 2581-2593

Silver F.H., Pins G. Cell growth on collagen: a review of tissue engineering using scaffolds containing extracellular matrix. *J Long-term Effects Med Implants* 1992; 2: 67-80

Stein G.S., and Lian J.B. Molecular mechanisms mediating proliferation/ differentiation interrelationships during progressive development of the osteoblast phenotype. *Endocrine Reviews* 1993; 14(4): 424-441

Suehiro K., Mizuguchi J., Nishiyama K., Iwanaga S., Farrell D.H., Ohtaki S. Fibrinogen binds to integrin alpha(5)beta(1) via the carboxyl-terminal RGD site of the Aalpha-chain. *J Biochem (Tokyo)* 2000; 128(4):705-10

Van de Graaff K.M. *Human Anatomy.* Fifth Ed., Weber State University, The McGraw-Hill Companies Inc. 1998; pp.136

Van der Walle G.A., de Koning G.J., Weusthuis R.A., Eggink G. Properties, modifications and applications of biopolyesters. *Adv Biochem Eng Biotechnol* 2001; 71: 263-291

Vlahos A., Yu P., Lucas C.E., Ledgerwood A.M. Effect of a composite membrane of chitosan and poloxamer gel on postoperative adhesive interactions. *Am Surg* 2001;67(1): 15-21

Vongchan P., Sajomsang W., Subyen D., Kongtawelert P. Anticoagulant activity of a sulfated chitosan. *Carbohydr Res* 2002; 337(13): 1239-42

Wang J.H.C., Grood E.S., Florer J., Wenstrup R. Alignment and proliferation of MC3T3-E1 osteoblasts in microgrooved silicone substrata subjected to cyclic stretching. *Journal of Biomechanics* 2000; 33: 729-735

Wilkinson C.D.W., Rielhe M., Wood M., Gallagher J., Curtis A.S.G. The use of materials patterned on a nano- and micro-metric scale in cellular engineering. *Mater Sci Eng* 2002; 19: 263-269

Williams S.F., Martin D.P., Horowitz D.M., Peoples O.P. PHA aplications: addressing the price performance issue I. Tissue engineering. *Inter J Biol Macrom* 1999; 25: 111-121

Wuthier R.E. A review of the primary mechanism of endochondral calcification with special emphasis on the role of cells, mitochondria and matrix vesicles. *Clin Orthop Rel Res* 1982; 169: 219-42

Yang X.B., Roach H.I., Clarke N.M.P., Howdle S.M., Quirk R., Shakesheff K.M., Oreffo R.O.C. Human osteoprogenitor growth and differentiation on synthetic biodegradable structures after surface modification. *Bone* 2001; 29: 523-531

Yang Y., Magnay J.L., Cooling L., El Haj A.J. Development of a 'mechano-active' scaffold for tissue engineering. *Biomaterials* 2002; 2119-26

Yaszemski M.J., Payne R.G., Hayes W.C., Langer R., Mikos A.G. Evolution of bone transplantation: molecular, cellular and tissue strategies to engineer human bone. *Biomaterials* 1996; 17: 175-85

Yaylaoglu M.B., Yildiz C., Korkusuz F., Hasirci V. A novel osteochondral implant. *Biomaterials* 1999; 20: 1513-20

Ye Q., Zund G., Benedikt P., Jockenhoevel S., Hoerstrup S.P., Sakyama S., Hubbell J.A., Turina M. Fibrin gel as a three dimensional matrix in cardiovascular tissue engineering. *Eur J Cardiothorac Surg* 2000; 17(5): 587-91

Young J.H., Teumer J., Kemp P.D., Parenteau N.L. Approaches to transplanting engineered cells and tissues. In *Principles of Tissue Engineering*, Eds. Lanza R.P., Langer R., Chick W.L., Texas USA 1997; pp297-305

Zhang Y.,Ni M., Zhang M., Ratner B. Calcium phosphate-chitosan composite scaffolds for bone tissue engineering. *Tissue Eng* 2003; 9(2): 337-45

Zhao K., Deng Y., Chen C.J., Chen G-Q. Polyhydroxyalkanoate (PHA) scaffolds with good mechanical properties and biocompatibility. *Biomaterials* 2003; 24: 1041-1045

Zinn M., Witholt B., Egli T. Occurrence, synthesis and medical applications of bacterial polyhydroxyalkanoate. *Adv Drug Del Rew* 2001; 53: 5-21

APPENDIX A

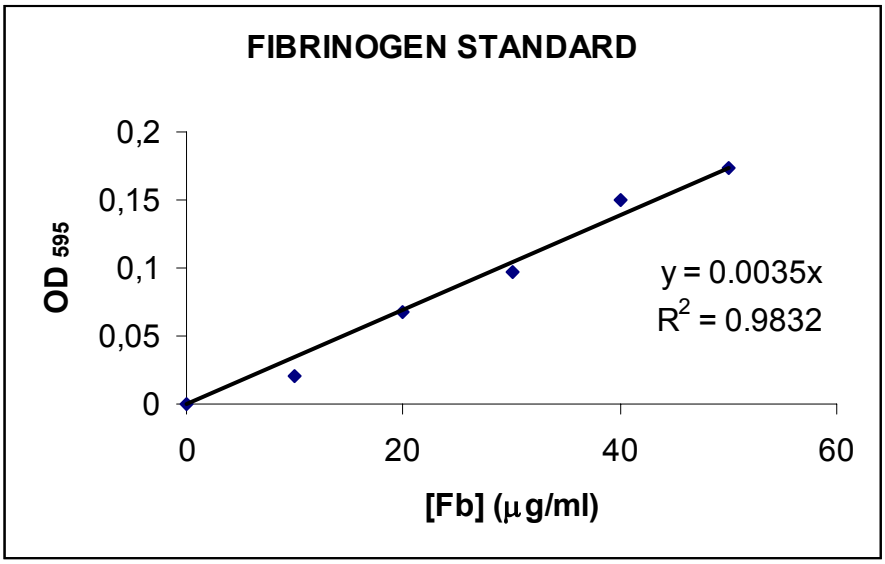

Figure A-1. Fibrinogen standard curve obtained with Bradford assay

APPENDIX B

Table B-1: Mean optical densities of different amounts of osteoblasts obtained with MTS assay (data of Fig. 3.9)

Number of Cells	Mean OD $_{490}$
5,000	0.026
10,000	0.122
15,000	0.199
30,000	0.365
40,000	0.489
50,000	0.592
75,000	0.914

Table B-2: Cell proliferation at the end of first week (data of Fig. 3.10)

Sample Type	OD $_{490}$	Cell Number*
UNP	0.209	17,400 ± 4,800
UNP Fb_a	0.198	16,500 ± 2,300
MP	0.132	11,000 ± 3,700
MP Fb_a	0.282	23,500 ± 400
MP Fb_i	0.135	11,300 ± 6,100
TCP	0.494	41,200 ± 1,100

*Initial Seeding: 20,000 cells per sample

Table B-3: Cell proliferation at the end of third week (data of Fig. 3.10)

Sample Type	OD_{490}	Cell Number*
UNP	**0.216**	**18,000 ± 8,200**
UNP Fb_a	**0.258**	**21,500 ± 500**
MP	**0.204**	**17,000 ± 2,200**
MP Fb_a	**0.257**	**21,400 ± 1,200**
MP Fb_i	**0.214**	**17,800 ± 6,900**
TCP	**0.606**	**50,500 ±0**

*Initial Seeding: 20,000 cells per sample

Table B-4: ALP activity of osteoblasts on the films at the end of first and third week (data of Fig. 3.11)

Sample Type	ALP Activity (μmole/min/sample ($x10^{-3}$))	
	1 week post seeding	3 weeks post seeding
UNP	**0.0367**	**0.1925**
UNP Fb_a	**0.1248**	**0.5926**
MP	**0.0395**	**0.1835**
MP Fb_a	**0.1707**	**0.9450**
MP Fb_i	**0.0275**	**0.1010**
TCP	**0.1405**	**0.9725**

Table B-5: ALP specific activity of osteoblasts on the filmsat the end of first and third week (data of Fig. 3.12)

Sample Type	ALP Specific Activity (μmole/min/cell ($x10^{-9}$))	
	1 week post seeding	3 weeks post seeding
UNP	**2.10**	**10.69**
UNP Fb_a	**7.56**	**27.60**
MP	**3.59**	**10.79**
MP Fb_a	**7.26**	**44.13**
MP Fb_i	**2.44**	**5.66**
TCP	**3.41**	**19.25**

APPENDIX C

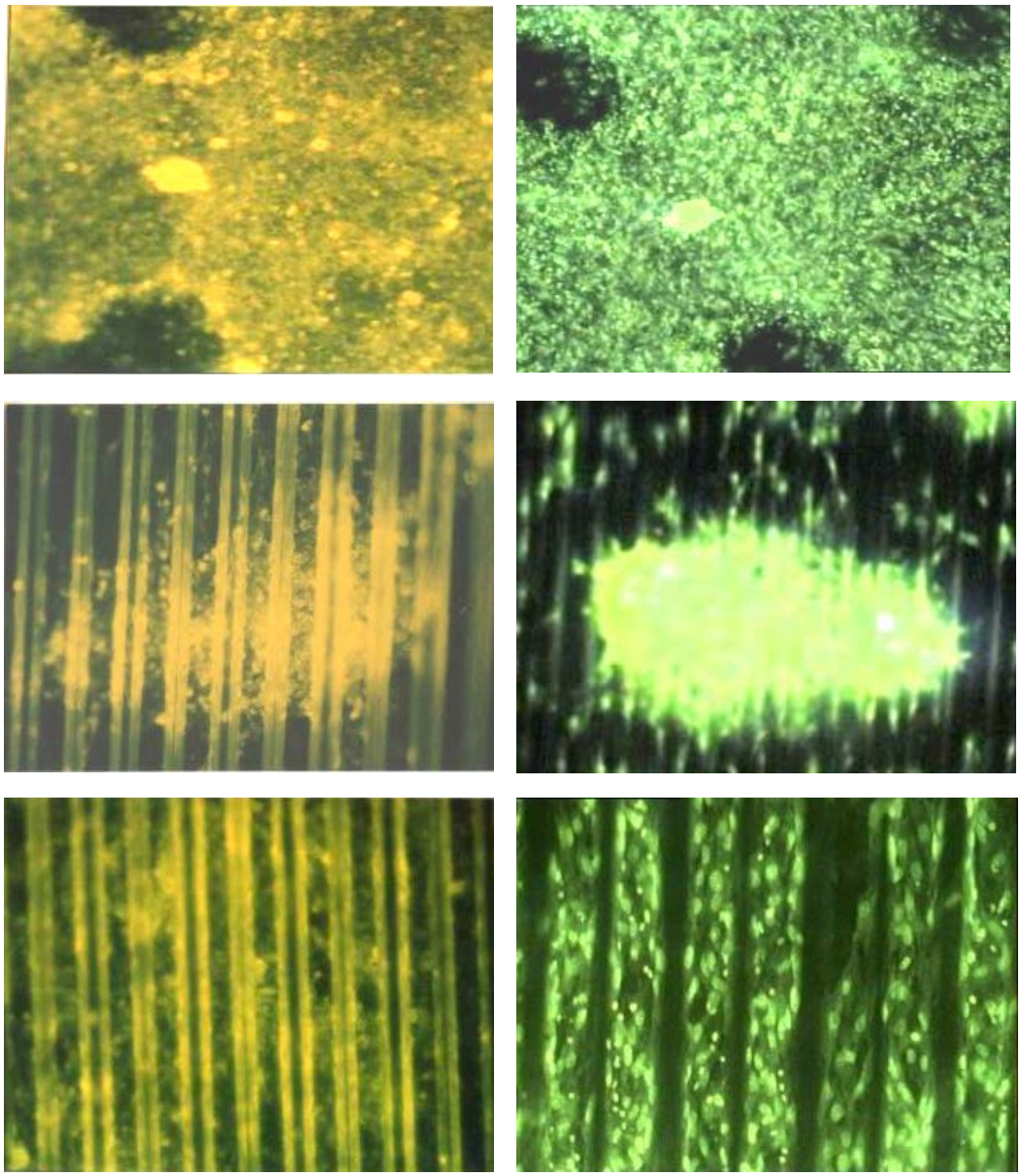

Figure C-1. Micrographs showing vesicular form of mineralization labelled with tetracycline (left) and cell distribution revealed by Acridine Orange staining (right) at the end of first week on the UNP Fb_a (top, x100), MP (middle, x200), and MP Fb_a (bottom, x 200) films.

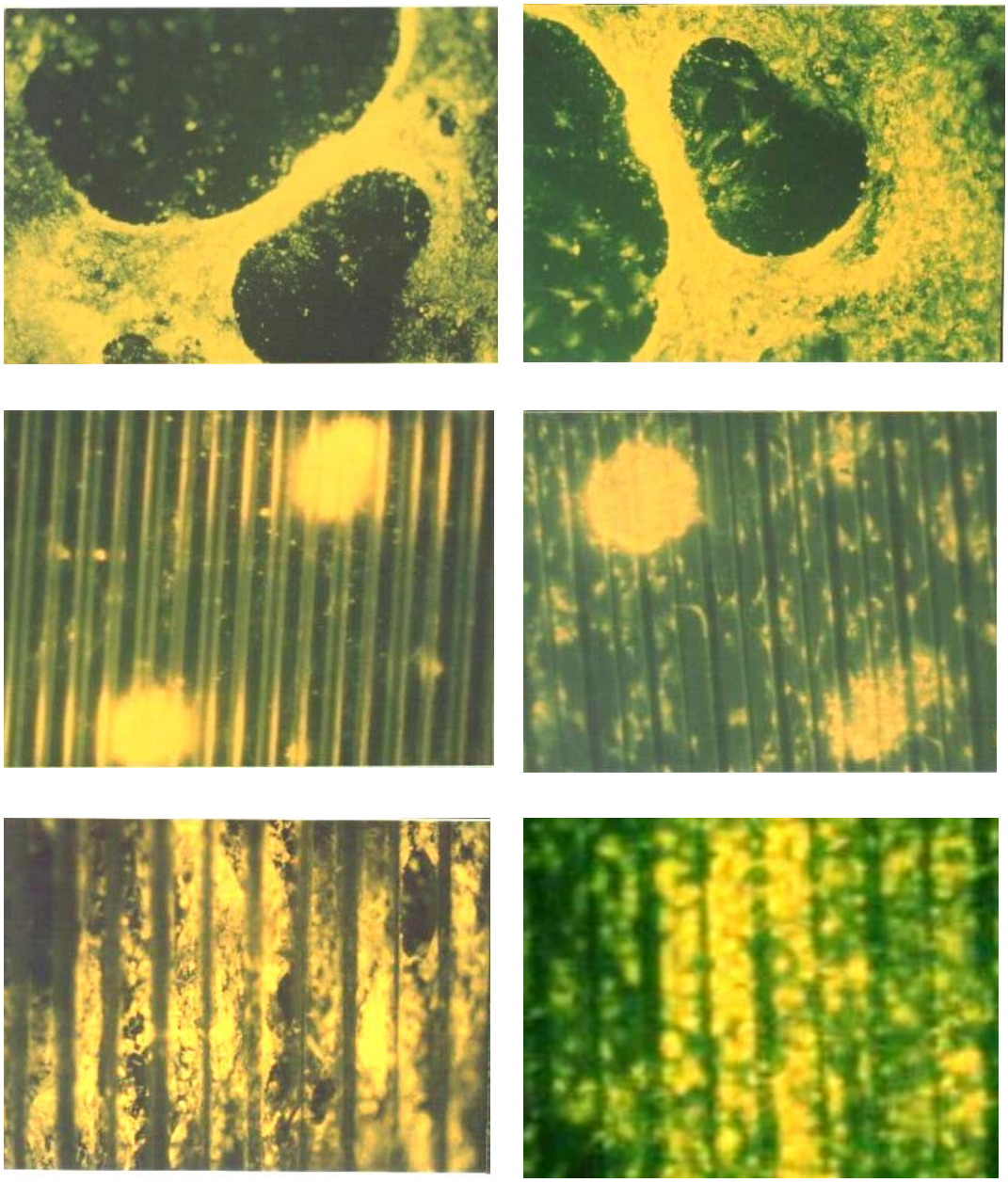

Figure C-2. Micrographs showing the more crystalline form of mineralization labelled with tetracycline (left) and cell distribution revealed by Acridine Orange staining (right) at the end of third week on the UNP Fb_a (top, x100), MP (middle, x100), and MP Fb_a (bottom, x 200) films.